Application of Shooting Method and Nonlinear Dynamical Techniques to Coupled Boundary Value problems in Fluid Mechanics and Heat Transfer

By

Yohannes Demiss

Computational Sciences Program
Addis Ababa University
Arat Kilo Campus

May, 2021
Addis Ababa, Ethiopia

Application of Shooting Method and Nonlinear Dynamical Techniques to Coupled Boundary Value problems in Fluid Mechanics and Heat Transfer

By

Yohannes Demiss

Thesis Submitted in Partial Fulfillment of the Requirement for the Degree of Master of Science in Computational Sciences at Addis Ababa University

Supervised by

Prof. Okey Oseloka Onyejekwe

May, 2021

Application of Shooting Method and Nonlinear Dynamical Techniques to Coupled Boundary Value problems in Fluid Mechanics and Heat Transfer

Yohannes Demiss

Supervisor

_____ _____

Prof. Okey Oseloka Onyejekwe Date

Chairman

_____ _____ _____

Dr. Solomon G. **Signature** **Date**

Approved by:

_____ _____ _____

Dr. Tsegaye **Signature** **Date**

_____ _____ _____

Dr. Manalebish Debalike **Signature** **Date**

Declaration

The Registrar (Academic)

Addis Ababa University

Dear Sir

I YOHANNES DEMISS BELETE, REG NO. GSR/0894/11, hereby declare that the dissertation entitled, Application of Shooting Method and Nonlinear Dynamical Techniques to Coupled Boundary Value problems in Fluid Mechanics and Heat Transfer is the result of my own investigation and research and that it has not been submitted in part or in full for any other degree or to any other University.

_____ _____

Yohannes Demiss Belete **Date**

Abstract

This thesis focused on a dynamical and numerical study of non-linear dynamics system of coupled boundary value problems for fluid mechanics and heat transfer. The study of heat transfer is a class of boundary layer theory and an integral part of natural convection flow. We used Runge-Kutta fourth order method with the help of a shooting-secant technique to solve numerically. We investigated the numerical solution of non-linear dynamics system of coupled boundary value problems for fluid mechanics and heat transfer and observed the Shooting- secant method results were accurate and generates numerical solutions that are stable and numerically acceptable. We also studied the dynamical solution of non-linear heat transfer equation. To this end, the study investigates coupled boundary value problems for fluid mechanics and heat transfer, which have different forms of non-linearity. And Falkner-Skan boundary layer viscous flow over a wedge was investigated including a nonslip and slip boundary condition and the result of Shooting-secant method was accurate and generates numerical solutions that are stable and physically reasonable. We also consider the magnetohydrodynamics viscous flow over a shrinking sheet for a closed form exact solution. The flow of magnetohaydrodynamics (MHD) over a shrinking sheet often varies significantly from the flow of MHD over a stretching sheet for Newtonian and non-Newtonian fluids and observed that the opposite value sign of the exact solution occurs only for mass suction and as the mass suction parameter increases, the wall shear stress for M= 1 increases. We also consider the two-dimensional magnitohydrodynamics (MHD) of the numerical and analytic solution boundary layer flow and heat transfer along an infinity porous hot horizontal continuous moving plate and observed the velocity profile in the flow region decreases as the magnetic parameters increase. Moreover, we investigate magnitohydrodynamics (MHD) convectional flow and entropy generation over an inclined stretching sheet. Increasing the magnetic parameter and Eckert number, increases entropy generation, while increasing the thermal convective parameter and dimensionless temperature function decreases entropy generation. A comparison with published results is presented.

Keywords: *Falkner-Skan equation,Shooting-secant method, viscous, velocity slip, Magnitohydrodynamics(MHD), Entropy. Dynamics system, phase plane analysis, eigenvalues.*

Acknowledgement

First I would like to express my profound gratitude to God Almighty and mother of God virgin Merry for providing me with good health, protection and knowledge throughout the study of this thesis.

I specially give thanks, Prof. Okey Oseloka Onyejekwe for always being there throughout the writing of this thesis, the consequent feedback which improved the thesis quality and guided and instructed me in the ways of computational research. Furthermore, he also demonstrated great patience by reading the most portions of this thesis. I also want to thank him for his style of computational and mathematical prose, which I have tried to adopt and emulate. God richly bless you for your advice, support and patience. Thank you again Prof.

I would like to thank Addis Ababa University Natural and Computational science teachers, staff members, Dr. Solomon Gizaw, Dr. Thilahun Abebaw, and Dr. Tomas W., my class mates, Senior and junior Computational science program students for a part played in my education. God Bless You all.

I also want to thank my father prof. Birhanu Gizaw and my special friend Beruk Minale many kind words of encouragement that always seemed appropriately timed. God Bless You.

I especially want to thank my mother for teaching me their love through working hard. I owe much… much to my wife Yordanos Lulu, for their patience, encouragement, and their gifts of silence when required. God Bless You all.

Yohannes Demiss Belete

PROF: "Always forgive your enemies - nothing annoys them so much." Oscar Wilde

Table of Content

Abstract i

Acknowledgement ii

Table of Content iii

List of Tables v

List of Figures vi

Chapter 1 Introduction 1

1.1. Background 1

1.2. Basic Concepts of Nonlinear Ordinary Differential Equations 5

1.2.1. Autonomous Equations and Stability 5

1.2.2. Phase Plane Analysis of Linear Systems 6

1.2.3. Non-linear Systems 8

1.2.4. Equilibrium Solution (Critical Point, or Stationary Point) 9

1.3. Statement of the problem 16

1.4. Objectives of the Thesis 17

1.4.1. General Objective 17

1.4.2. Specific Objectives 17

1.5. Methodology 18

1.5.1. Shooting Method 18

1.5.1.1. Reduction to Two IVP's: Linear Shooting Method 18

1.5.1.2. Shooting - Secant Method 18

1.5.1.3. Algorithms of Shooting - Secant Method 19

1.5.2. Pplane9 22

1.6. Organization the Thesis 24

Chapter 2 Numerical and Dynamical Analysis of Heat Transfer through a Rectangular Longitudinal Fin 26

2.1. Mathematical Formulation 26

2.2. Method of Solution: 28

2.3. Results and Discussion 28

2.3.1. Numerical Solutions 28

2.3.2. Reduction to Two IVP's: Dynamical system analysis 32

Chapter 3 Numerical Solution of the Falkner Skan Boundary Layer Viscous Flow over a Wedge: A Shooting Method Application 39
3.1. The Falkner Skan Equation for Numerical Solution by using Shooting Techniques 40
3.1.1. Mathematical formulation 41
3.1.2. Results and discussion 42
3.2. The Falkner-Skan Boundary Layer for Numerical Solution of Viscous Flow over a Wedge 47
3.2.1. Mathematical Formulation 47
3.2.2. Results and discussion 49
Chapter 4 The Effect of Velocity Slip Parameter on Boundary Layer Flow over a Static Wedge 57
4.1. Mathematical Formulation 57
4.2. Results and Discussion 59
Chapter 5 MHD viscous flow over a shrinking sheet for closed form Analytical solutions 63
5.1. Mathematical formulation 63
5.2. Results and discussion 65
Chapter 6 Numerically and Analytical Analysis of MHD boundary layer flow and heat transfer along an infinite porous hot horizontal continuous moving plate 69
6.1. Mathematical Formulation 69
6.2. Results and Discussion 72
Chapter 7 MHD Mixed Convection Flow and Entropy Generation over an Inclined Stretching Sheet 82
7.1. Mathematical Formulation 83
7.2. Results and Discussion 86
Chapter 8 Summary, Conclusion and Further Research 88
8.1. Summary 88
8.2. Conclusion 89
8.3. Further Research 91
Reference 92
Appendix: Publications 97

List of Tables

Table 1: Type of critical point of almost linear system 8

Table 2: Numerical values of $f(\eta), f'(\eta)$ and $f''(\eta)$ for $\beta = 0$ 43

Table 3: Numerical values of $f(\eta), f'(\eta)$ and $f''(\eta)$ for $\beta = 1$ 44

Table 4: Numerical values of $f(\eta), f'(\eta)$ and $f''(\eta)$ for $\beta = -0.1988$ 45

Table 5: Blasius flow profiles of eta value are from 0.0 to 8.8 and compare with B.D. Ganapol paper's result. 51

Table 6: Thermo-physical properties of fluid and nanoparticles [26] 52

Table 7: Values of $f''(0)$ for $\varphi = 0$ with $m = 2$ and $s = 0$ (impermeable surface) 52

Table 8: Values of $f''(0)$ for Cu nanoparticles with $m = 2$ and $s = 0.5$ 53

Table 9: Values of $f''(0)$ for cu-water with $m = 2$ and $s = 0.5$ 53

Table 10: Values of $f''(0)$ for cu-water when $\varphi = 0.1$ 55

Table 11: Values of $f''(0)$ when $\varphi = 0.1$ and $= -0.3$ 56

Table 12: Values of $f''(0)$ for different values of m when N = 0 59

Table 13: Shear stress coefficient for different values m, Values of velocity profiles, N 60

List of Figures

Figure 1: The window interface of pplane9 22

Figure 2: The result display of pplane9 23

Figure 3: Dimensionless temperature distribution in the fin parameters when $M = 0.1,\ \beta = 1\ \ and\ n = 1$ 29

Figure 4: Dimensionless temperature of the fin parameters with varying n when $M = \beta = 1.$ 29

Figure 5: Dimensionless the rate of temperature distribution in the fin parameters for varying n parameter when $M = \beta = 1.$ 30

Figure 6: Dimensionless temperature distribution in the fin parameters for varying thermo-geometric parameter when $n = \beta = 1.$ 30

Figure 7: Dimensionless rate of the temperature distribution in the fin for varying thermo-geometric parameter when $n = \beta = 1.$ 31

Figure 8: Dimensionless temperature distribution in the fin for varying values of non-linear parameters, when $n = M = 1.$ 31

Figure 9: Dimensionless the rate of the temperature distribution in the fin for varying values of β , when $n = M = 1.$ 32

Figure 10: Phase plane diagram for parameters $\mathrm{m} = 0.1,\ \mathrm{B} = 1$ and $\mathrm{n} = 1$ 35

Figure 11: Phase plane diagram for parameters $\mathrm{m} = 1, \mathrm{B} = 1$ and $\mathrm{n} = 1$ 36

Figure 12: Phase plane diagram for parameters $\mathrm{m} = 1,\ \mathrm{B} = 0$ and $\mathrm{n} = 1$ 37

Figure 13: Phase plane diagram for parameters for $\mathrm{m} = 1,\ \mathrm{B} = 1$ and $\mathrm{n} = 0$ 37

Figure 14: The velocity profile plot for different $\beta \in [-0.1988, 0)$ 46

Figure 15: The velocity profile plot for different $\beta \in [0, 2]$ 46

Figure 16: Velocity profile variation with α for Homann flow 49

Figure 17: The velocity profile of the Variation for $0 \le \alpha \le 1$ and $\beta = -0.1$ 50

Figure 18: Falkner-Skan functions variation 50

Figure 19: Velocity profiles for Cu nanoparticles when $m=2,\ \varphi=0.1,\ \lambda=-1.5$ and various values of $s=[0.5,\ 0.6,\ 0.7]$.....54

Figure 20: Variaton of $f''(0)$ with for Cu-water nanofluid and different values of $f_0=[-0.3,\ 0,\ 0.3]$ when $\varphi=0.1$ 54

Figure 21: Effect of m on the velocity when N = 1 60

Figure 22: Effects of on the velocity when N = -1. 61

Figure 23: Effects of $N(N\geq 0)$ on the velocity, when $\mathrm{m}=0.5$.....61

Figure 24: Effects of $N(N\leq 0)$ on the velocity, when m = 0.5 62

Figure 25: Velocity profiles at mass suction M = 2 under different parameters of $f'(0)$. 65

Figure 26: Velocity profiles at M = 1under different mass suction parameters. 66

Figure 27: Velocity profiles at M = 0.5 under different mass suction parameters. 66

Figure 28: Analytic solution of velocity profiles at M = 2 under different mass suction parameters. 67

Figure 29: Effect of α on the velocity profile for M = 0, Ec = 0.01, Pr = 1 and S = 0.1. 72

Figure 30: Effect of M on the velocity profile for $\alpha=0$, Ec = 0.01, Pr = 1 and S = 0.1. 73

Figure 31: Effect of M on the temperature profile for α = 0.5, Ec = 0.01, Pr = 1 and S = 0.2. 74

Figure 32: Effect of the prandtl number (Pr) on the temperature profile for α = 0.5, Ec = 0.01, S = 0.1 and M = 1. 75

Figure 33: Effect of Eckert number on the temperature profile for fixed values of α = 0.5, S = 0.1, Pr = 1 and M = 1. 75

Figure 34: Effect of heat source/sink (S) parameter on the temperature profile for α = 0, Ec = 0.01, Pr = 1 and M = 1. 76

Figure 35: The Numerical and analytical solution of temperature profile 77

Figure 36: The absolute error of temperature profile for Effect of magnetic parameter (M) on the velocity profile for $\alpha = 0$, Ec = 0.01, Pr = 1 and S = 0.1. 78

Figure 37: The 3D plot of analytic solution of velocity profile.....78

Figure 38: 3D plot of the absolute error of the numerical and analytic solution of temperature profile.....79

Figure 39: 3D plot for analytic solution of temperature profile 80

Figure 40: 3D plot for Absolute error for temperature profile 81

Figure 41: Variation of $\theta(\eta)$ with different value of magnetic parameter (M) and the value of the other constants are $\lambda = 1.2$, $Ec = 1$, $\alpha = \pi/4$ and $\Pr = 0.7$ 86

Figure 42: Variation of $f'(\eta)$ with different value of M and the value of the other constants are $\lambda = 1.2$, $Ec = 1$, $\alpha = \pi/4$ and $\Pr = 0.7$ 87

NOTATIONS

$\boldsymbol{k(\theta)}$	Dimensionless thermal condactivity
h(θ)	Heat transfer coefficient
M	Thermo-geometeric parameter
θ	Dimentionless temperature
λ	Dimentionless spatial variables
T_b	Dimentionless fin base temperature
m	Falkner-Skan equation constant (for chap. 3)
u & v	velocity components
ρ	Fluid density
p	Fluid pressure
N	Slip parameter
ψ	Stream function
σ	Electrical conductivity of the fluid
B	Magnetic field
m	Kenematic viscosity (for chap. 5)
p_r	Prandtl number
Ec	Eckart number
S	Heat sink/source
Nu	Nusselt number
Sk(C_f)	Skin friction
T_∞	Free stream temperatrure
C_p	Specific heat of fluid at constant pressure
α	Themal diffusivity
β	Thermal coefficient
τ_w	Shear stress
$\boldsymbol{q_w}$	Heat flux
$\boldsymbol{k}$	Thermal conductivity
ϕ	Viscous dissipation function
J	Current density
$\boldsymbol{B_e}$	Bejan number

Chapter 1
Introduction

1.1. Background

An equation containing the derivatives of one or more dependent variables, with respect to one or more independent variables, is said to be a differential equation (DE) [1]. If an equation contains only ordinary derivatives of one or more dependent variables with respect to a single independent variable it is said to be an ordinary differential equation (ODE) [1]. Ordinary differential equations are defined by the order of the highest derivative. If the highest derivative is first order the equation is referred as first order differential equation, if the highest derivative is second order the equation is referred as second order differential equation etc. Ordinary differential equations are only ordinary derivatives of the differential equations. [2] Differential equations are used much more extensively in science and engineering, and we shall therefore focus on them. Ordinary differential equations are categorized into linear and non-linear equations.

The ordinary differential equation:

$$F\left(t, y, y', \ldots, y^{(n)}\right) = 0 \tag{1.1}$$

is said to be linear if F is linear function of the variables $y, y', \ldots, y^{(n)}$ and the variables $y, y', \ldots, y^{(n)}$ are not linear then an equation is a Nonlinear equation.

Boundary Layer Concept

Initially boundary layer theory was developed mainly for the laminar flow of an incompressible fluid, where Stokes law of friction could be used for the viscous forces [3]. This area was later researched in very many pieces of work, so that today it can be considered to be fully understood. Later the theory was extended to the practically important turbulent incompressible boundary layer flows. Around 1890, O. Reynolds (1894) had already introduced the fundamentally important concept of apparent turbulent stresses, but this did not yet permit the theoretical treatment of turbulent flows.

The boundary layer concept was first introduced by a German scientist, Ludwig Prandtl (1875-1953) in 1904. [4] It found wide application in numerous problems of fluid dynamics and has provided a powerful implement for analysis of problem of fluid resistance. [5]

Flows of fluids with low viscosity values and thus very high Reynolds numbers occur in many technical applications. [6] A remarkable limitation of this limiting solution is that the no–slip situation is not satisfied, that is the velocities at the wall are not zero but are finite. The viscosity must be taken into explanation in implies that satisfy the no–slip condition. [7] This takes care of the velocity change from the limiting solution's finite value nearby to the wall to the value of zero directly at the wall. At large Reynolds numbers this change takes place in a thin layer close to the wall, called by L. Prandtl (1904) the boundary layer or frictional layer. [8] The boundary layer is thinner the smaller the viscosity then the number of Reynolds higher. [7]

From the basic definition of the boundary layer, the flows at high Reynolds numbers can be divided up into two unequally large regions. [4] In the main part of the flow region, the flow corresponds to the in viscous limiting solution and the viscosity can be neglected. This is called the in viscous outer flow. [7] The second region is the very thin boundary layer at the wall where the viscosity must be taken into interpretation. The main part of the flow region, the viscosity can be neglected, and the flow corresponds to the in viscous limiting solution. This is called the in viscous outer flow.

Fluid mechanics

Mechanics is concerned with the formulation and definition of entities such as **body, motion, force, power, work**; it deals with the fundamental laws connecting these entities. [9] Mechanics can be divided into several subfields according to different characterizations.

Fluid mechanics is a branch of continuous mechanics which study a relationship between motions, forces and statical situations in a continuous material. Fluid mechanics concern with the study of all under dynamics and statics conditions. The fluid mechanics studies involve many fields that have no clear boundaries between them. [8]

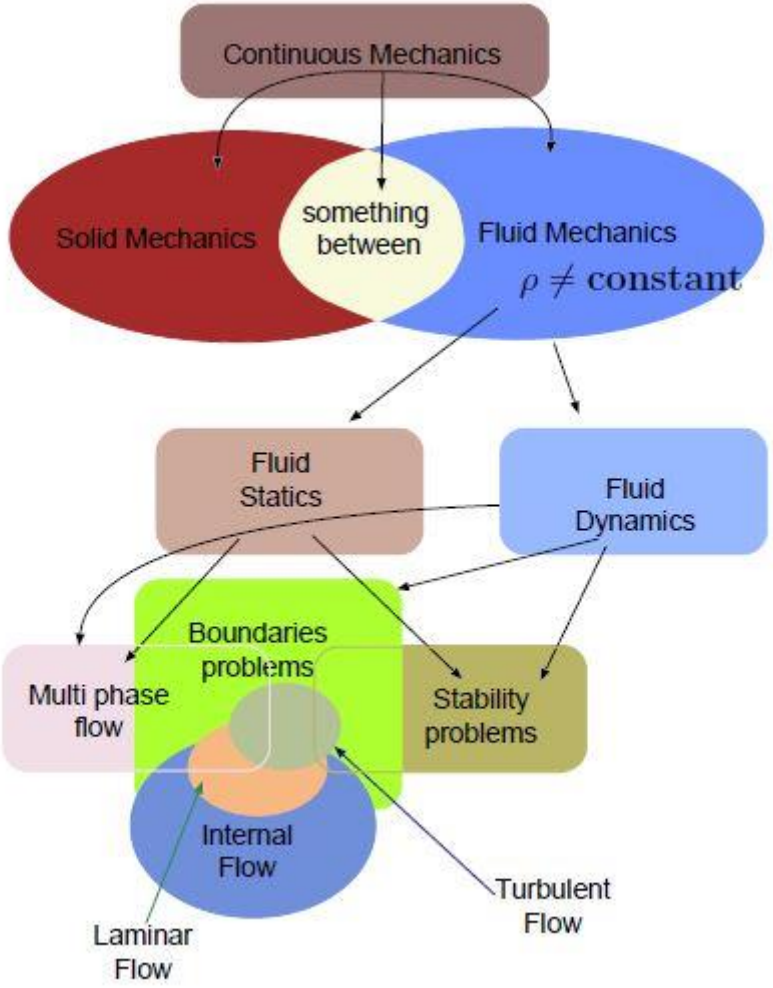

Figure 1: Diagram to explain part of relationships of fluid mechanics branches. [8]

At the end of the 19th century, fluid mechanics had split into two different directions which hardly had everything more in common. And the other was the science of theoretical hydrodynamics, originating from Euler's equations of motion and which had been advanced to great perfection. [3]

The major progress in fluid mechanics was made by Leonardo Da Vinci (1452-1519) who built the first chambered canal lock near Milan. [8] He also prepared numerous efforts developed certain concepts on the source of the forces and to study the flight. After his original work, the knowledge of fluid mechanics (hydraulic) progressively expanded speed by the contributions of Galileo, Torricelli, Euler, Newton, Bernoulli family, and D'Alembert. [8] At that phase experiment and theories had certain inconsistency. This fact was acknowledged by D'Alembert who stated that, "The theory of fluids must necessarily be based upon experiment." [8]

A main characteristic of recent research into fluid mechanics in overall and more exactly into the branch of boundary–layer theory is the near connection between theory and experiment. [3] The most critical advances have been achieved through a few important experiments together with theoretical considerations. Many years ago, A. Betz (1949) produced a review of the development of boundary–layer theory, with particular stress on the common fructification of theory and experiment. [3] Research into boundary layers, inspired by Prandtl from 1904, were, in the first 20 years up until Prandtl's Wilbur Wright memorial lecture at the Royal Aeronautical Society in London, (L. Prandtl (1927)) almost exclusively confined to Prandtl's institute in G¨ottingen. [3] Nowadays boundary–layer theory has spread over the entire world composed with other branches it systems one of the most significant pillars of fluid mechanics.

Dynamics

Kinetics or **dynamics** establish a connection between the forces acting on the body or between bodies and their motions. The methods of kinematics allow selections of the dynamically possible motions from all those which are kinematically in principle acceptable. [9]

Dynamics is an interdisciplinary subject today; it was originally a branch of physics. The subject began in the mid-1600s, when Newton invented differential equations, discovered his laws of motion and universal gravitation, and combined them to explain Kepler's laws of planetary motion. [10] Specifically, Newton solved the two-body problem the problem of calculating the motion of the earth around the sun, given the inverse-square law of gravitational attraction between them. Subsequent generations of mathematicians and physicists tried to extend Newton's analytical methods to the three-body problem but curiously this problem turned out to be much more difficult to solve. After decades of effort, it was eventually realized that the three-body problem was essentially impossible to solve, in the sense of obtaining explicit formulas for the motions of the three bodies. At this point the situation seemed hopeless. The breakthrough came with the work of Poincaré in the late 1800s. [10] He introduced a new point of view that emphasized qualitative rather than quantitative questions.

The study of heat transfer is a class of boundary layer theory and an integral part of natural convection flow. The heat transfer quantity is more depend on the fluid motion within the boundary layer. [11]

1.2. Basic Concepts of Nonlinear Ordinary Differential Equations

Nonlinear in linear ODE, the dependent function and all of its derivatives appear as linear terms. So, if *x* is the independent variable and y the dependent one, then the general ODE is

$$\sum_{n=0}^{N} a_n(x) y^{(n)}(x) = f(x) \tag{1.2}$$

Where $f(x)$ is a known function, $y^{(0)}(x) = y(x)$, and $y^{(0)}(x)(n>0)$ is the n^{th} derivative of *y*.

Note that all terms are linear in $y^{(n)}$. [12] [13] .

Systems of coupled second order and third order boundary value problems can be solved by shooting method by replacing each second order ordinary differential equation by two first ordinary differential equations and each third order ordinary differential equation by three first ordinary differential equations respectively, and solving the coupled systems of first order ordinary differential equations.

1.2.1. Autonomous Equations and Stability

Autonomous Equation: A differential equation where the independent variable does not explicitly appear in its expression [14]. It has the general form of

$$y' = f(y) \tag{1.3}$$

Examples:

$$y' = e^{2y} - y^3$$
$$y' = y^3 - 4y$$
$$y' = y^4 - 81 + \sin y$$

Every autonomous ODE is a separable equation. Because, assuming that $f(y) \neq 0$,

$$\frac{dy}{dt} = f(y) \quad \rightarrow \quad \frac{dy}{f(y)} = dt \quad \rightarrow \quad \int \frac{dy}{f(y)} = \int dt \tag{1.4}$$

Hence, we already know how to solve them. What we are interested now is to predict the behavior of an autonomous equation's solutions without solving it, by using its direction field.

1.2.2. Phase Plane Analysis of Linear Systems

Consider a systems of linear differential equations $\boldsymbol{x}' = \boldsymbol{A}\boldsymbol{x}$. Its *phase portrait* is a representative set of its solutions, plotted as parametric curves (with t as the parameter) on the Cartesian plane tracing the path of each particular solution $(x, y) = (x_1(t), x_2(t))$, $-\infty < t < \infty$. [15] Similar to a direction field, a phase portrait is a graphical tool to visualize how the solutions of a given system of differential equations would behave in the long run.

In this context, the Cartesian plane where the phase portrait resides is called the *phase plane*. The parametric curves traced by the solutions are sometimes also called their *trajectories* [16] [17].

The qualitative behavior of a function is often simpler to visualize from a graph than from an explicit or implicit expression of the function. In the case of systems the solution vector has the form

$$\boldsymbol{x}(t) = \begin{bmatrix} x_1(t) \\ x_2(t) \end{bmatrix} \tag{1.5}$$

Two functions define the solution vector. In this case one usually graphs each component of the solution vector and as functions of t. There is, however, another way to graph a 2-vector-valued function: plot the whole vector $x(t)$ at t on the plane . Each vector $x(t)$ is represented by its end point, while the whole solution x represents a line with arrows pointing in the direction of increasing t. Such a figure is called a phase diagram or phase portrait.

In the case that the solution vector $x(t)$ is interpreted as the position function of a particle moving in a plane at the time t, the curve given in the phase portrait is the trajectory of the particle. The arrows added to this trajectory indicate the motion of the particle as time increases.

Real Distinct Eigenvalues

The system $\boldsymbol{x}'(t) = A\boldsymbol{x}(t)$ in the case that matrix A has two real eigenvalues $\lambda_+ \neq \lambda_-$ .The case where both eigenvalues are non-zero. Two non-zero eigenvalues belong to one of the following cases:

(i) $\lambda_1 > \lambda_2 > 0$, both eigenvalues positive;

(ii) $\lambda_1 > 0 > \lambda_2$, one eigenvalue negative and the other positive;

(iii) $0 > \lambda_1 > \lambda_2$, both eigenvalues negative.

In a phase portrait the solution vector $\boldsymbol{x}(\mathrm{t})$ at t is displayed on the plane $[x_1;\ x_2]$

Complex Eigenvalues

A real-valued matrix may have complex-valued eigenvalues. These complex eigenvalues come in pairs, because the matrix is real-valued. If λ is one of these complex eigenvalues, then $\overline{\lambda}$ is also an eigenvalue. A usual notation is $\lambda = a \pm ib$ with $a, b \in R$. The same happens with their eigenvectors, which are written as $v = u + iw$, with $u, w \in R^n$ in the case of an $n \times n$ matrix. When the matrix is the coefficient matrix of a differential equation,

Almost (Locally) Linear Systems

Definition: A nonlinear system is almost linear at an isolated critical point $P = (x_0, y_0)$ if its linearization has an isolated critical point at the origin $(0,0)$.

Recall that the linearization (a linear system) has an isolated critical point at the origin if and only if both of its Eigen values are non-zero. The following Theorem states that almost linear critical points behave similarly to that of their linearization

Theorem: Let λ_1, λ_2 be the eigenvalues of the linearization of an almost linear system at a critical point $P = (x_0, y_0)$. Then the critical point P is identical in type to that of $(0,0)$ in its linearization, except in two cases:

- $\lambda_1 = \lambda_2$ The eigenvalues are repeated and real. The linearization has a node (proper or improper) at the origin, but the original almost linear system has either a node or a spiral point at P.
- $\lambda_1 = \overline{\lambda_2}$ The eigenvalues are pure imaginary. The linearization has a center at the origin, but the original almost linear system has either a center or a spiral.

In summary:

Table 1: Type of critical point of almost linear system

Eigenvalues of linearization	Type of critical point of almost linear system
Real, positive, unequal	Improper nodal source
Real, negative, unequal	Improper nodal sink
Real, opposite signs	Saddle point
Real, positive, equal	Nodal or spiral source
Real, negative, equal	Nodal or spiral sink
Complex, real part positive	Spiral source
Complex, real part negative	Spiral sink
Complex, real part zero	Center or Spiral source/sink

1.2.3. Non-linear Systems

Linearization

Definition: Suppose $P = (x_0, y_0)$ is an isolated critical point of the system

$$\begin{cases} \dfrac{dx}{dt} = f(x,y) \\ \dfrac{dy}{dt} = g(x,y) \end{cases} \tag{1.6}$$

And that *f* and *g* are differentiable at P. The linearization of the system at P is the linear system

$$\begin{cases} \dfrac{du}{dt} = f_x(p)u + f_y(p)v \\ \dfrac{dv}{dt} = g_x(p)u + g_y(p)v \end{cases} \tag{1.7}$$

Written in matrix format:

$$\begin{pmatrix} du/dt \\ dv/dt \end{pmatrix} = \begin{pmatrix} f_x(x_0, y_0) & f_y(x_0, y_0) \\ g_x(x_0, y_0) & g_y(x_0, y_0) \end{pmatrix} \begin{pmatrix} u \\ v \end{pmatrix} \tag{1.8}$$

Where, $\begin{pmatrix} f_x(x_0, y_0) & f_y(x_0, y_0) \\ g_x(x_0, y_0) & g_y(x_0, y_0) \end{pmatrix}$ the Jacobean matrix.

Limit Cycles, Competing Species, Chaos

Limit-Cycle: A limit-cycle on a plane or a two-dimensional manifold is a closed trajectory in phase space having the property that at least one other trajectory spirals into it either as time approaches infinity or as time approaches minus-infinity. Such behavior is exhibited in some nonlinear systems. In the case where all the neighboring trajectories approach the limit-cycle as time $t \to +\infty$, it is called a stable or attractive limit-cycle. If instead all neighboring trajectories approach it as time $t \to -\infty$, it is an unstable or non-attractive limit-cycle. In all other cases it is neither "stable" nor "unstable". [18]

Chaos The notion of "chaos" plays an important role in dynamical systems theory. A chaotic system is defined as a system that cannot be predicted within a given numerical accuracy. Once the starting point is known, the resulting trajectory can be calculated for all times. Chaotic behavior can arise nevertheless, due to an exponential sensitivity to the initial conditions [19].

1.2.4. Equilibrium Solution (Critical Point, or Stationary Point)

An equilibrium solution of the system $x' = Ax$ is a point (x_1, x_2) where $x' = 0$, that is, where $x_1' = 0 = x_2'$.

An equilibrium solution is a constant solution of the system, and is usually called a *critical point*. For a linear system $x' = Ax$, an equilibrium solution occurs at each solution of the system (of homogeneous algebraic equations) $Ax = 0$. As we have seen,

- If $\det(A) = 0$, then a system has exactly one solution, located at the origin.
- If $\det(A) \neq 0$, then there are infinitely many solutions.

For our purpose, and unless otherwise noted, we will only consider systems of linear differential equations whose coefficient matrix ***A*** has nonzero determinant. That is, we will only consider systems where the origin is the only critical point.

Equilibrium solutions (or critical points) occur whenever $y' = f(y) = 0$. That is, they are the roots of $f(y)$. [18] Any root c of $f(y)$ yields a constant solution $y = c$. (Verify that, if c is a root of $f(y)$, then $y = c$ is a solution of $y' = f(y)$). Equilibrium solutions are constant functions that satisfy the equation, i.e., they are the constant solutions of the differential equation.

Note: A matrix could only have zero as one of its eigenvalues if and only if its determinant is also zero. Therefore, since we limit ourselves to consider only those systems where $\det(\boldsymbol{A}) \neq 0$, we will not encounter in this section any matrix with zero as an eigenvalue

Classification of Critical Points

Similar to the earlier discussion on the equilibrium solutions of a single first order differential equation using the direction field, we will presently classify the critical points of various systems of first order linear differential equations by their *stability*. In addition, due to the truly two-dimensional nature of the parametric curves, we will also classify the *type* of those critical points by their shapes (or, rather, by the shape formed by the trajectories about each critical point). [15]

Given $\boldsymbol{x}' = \boldsymbol{A}\boldsymbol{x}$, where there is only one critical point, at (0,0):

Case I: Distinct real eigenvalues

The general solution is:

$$x(t) = c_1 e^{\lambda_1 t} v_1 + c_2 e^{\lambda_2 t} v_2 \tag{1.9}$$

1. When λ_1 and λ_2 are both positive, or are both negative

The phase portrait shows trajectories either moving away from the critical point to infinite-distant away (when $\lambda > 0$), or moving directly toward, and converge to the critical point (when $\lambda < 0$). The trajectories that are the eigenvectors move in straight lines. The rest of the trajectories move, initially when near the critical point, roughly in the same direction as the eigenvector of the eigenvalue with the smaller absolute value. Then, farther away, they would bend toward the direction of the eigenvector of the eigenvalue with the larger absolute value The trajectories either move away from the critical point to infinite-distant away (when λ are both positive), or move toward from infinite-distant out and eventually converge to the critical point (when λ are both negative). [15]

This type of critical point is called a *node*. It is *asymptotically stable* if λ are both negative, *unstable* if λ are both positive.

2. When λ_1 and λ_2 have opposite signs (say $\lambda_1 > 0$ and $\lambda_2 < 0$)

In this type of phase portrait, the trajectories given by the eigenvectors of the negative eigenvalue initially start at infinite-distant away, move toward and eventually converge at the critical point. The trajectories that represent the eigenvectors of the positive eigenvalue move in exactly the opposite way: Starts at the critical point then diverge to infinite-distant out. Every other trajectory starts at infinite-distant away, moves toward but never converges to the critical point, before changing direction and moves back to infinite-distant away. All the while it would roughly follow the two sets of eigenvectors.

This type of critical point is called a *saddlepoint*. It is always *unstable*. [15]

Case II: Repeated real eigenvalue

3. When there are two linearly independent eigenvectors v_1 *and* v_2

The general solution is

$$x(t) = c_1 e^{\lambda t} v_1 + c_2 e^{\lambda t} v_2 = e^{\lambda t}\left(c_1 v_1 + c_2 v_2\right) \tag{1.10}$$

Every nonzero solution traces a straight-line trajectory, in the direction given by the vector $c_1 v_1 + c_2 v_2$. The phase portrait thus has a distinct star-burst shape. The trajectories either move directly away from the critical point to infinite-distant away (when $\lambda > 0$), or move directly toward, and converge to the critical point (when $\lambda < 0$). [18]. This type of critical point is called a *propernode* (or a *starl point*). It is *asymptotically stable* if $\lambda < 0$, *unstable* if $\lambda > 0$.

Note: For 2×2 systems of linear differential equations, this will occur if, and only if, when the coefficient matrix ***A*** is a constant multiple of the identity matrix:

$$A = \alpha \begin{bmatrix} 1 & 0 \\ 0 & 1 \end{bmatrix} = \begin{bmatrix} \alpha & 0 \\ 0 & \alpha \end{bmatrix} \tag{1.11}$$

Where α = any nonzero constant.

4. When there is only one linearly independent eigenvector v.

Then the general solution is:

$$x = c_1 v e^{\lambda t} + c_2 (v t e^{\lambda t} + \eta e^{\lambda t}) \tag{1.12}$$

The phase portrait shares characteristics with that of a node. With only one eigenvector, it is a degenerated-looking node that is a cross between a node and a spiral point. The trajectories either all diverge away from the critical point to infinite-distant away (when $\lambda > 0$), or all converge to the critical point (when $\lambda < 0$) [18].

This type of critical point is called an *improper node*. It is *asymptotically stable* if $\lambda < 0$, *unstable* if $\lambda > 0$.

Case III: Complex conjugate eigenvalues

The general solution is:

$$x(t) = e^{\alpha t}[c_1(u\cos\beta t - w\sin\beta t) + c_2(u\sin\beta t + w\cos\beta t)] \qquad (1.13)$$

5. When the real part λ is zero.

In this case the trajectories neither converge to the critical point nor move to infinite distant away. Rather, they stay in constant, elliptical (or, rarely, circular) orbits.

This type of critical point is called a *center*. It has a unique stability classification shared by no other: *stable* (or *neutrally stable*). It is **NOT** asymptotically stable and one should not confuse them [15]

6. When the real part λ is nonzero.

The trajectories still retain the elliptical traces as in the previous case. However, with each revolution, their distances from the critical point grow/decay exponentially according to the term $e^{\lambda t}$ [18]. Therefore, the phase portrait shows trajectories that spiral away from the critical point to infinite-distant away (when $\lambda > 0$). Or trajectories that spiral toward, and converge to the critical point (when $\lambda < 0$). [15].

This type of critical point is called a *spiralpoint*. It is *asymptotically stable* if $\lambda < 0$, it is *unstable* if $\lambda > 0$.

Summary of Stability Classification

Asymptotically stable – All trajectories of its solutions converge to the critical point as $t \to \infty$. A critical point is asymptotically stable if all of A's eigenvalues are negative, or have negative real part for complex eigenvalues [15].

Unstable – All trajectories (or all but a few, in the case of a saddle point) start out at the critical point at $t \to -\infty$, then move away to infinitely distant out as $t \to -\infty$. A critical point is unstable if at least one of A's eigenvalues is positive, or has positive real part for complex eigenvalues [15].

Stable (or neutrally stable) – Each trajectory move about the critical point within a finite range of distance. It never moves out to infinitely distant, nor (unlike in the case of asymptotically stable) does it ever go to the critical point. A critical point is stable if A's eigenvalues are purely imaginary. [15]

In short, as *t* increases, if all (or almost all) trajectories

1. Converge to the critical point → ***asymptotically stable***,
2. Move away from the critical point to infinitely far away → ***unstable***,
3. Stay in a fixed orbit within a finite (i.e., bounded) range of distance away from the critical point → ***stable (or neutrally stable).***

Nonhomogeneous Linear Systems with Constant Coefficients

Now let us consider the nonhomogeneous system

$$x' = Ax + b \qquad .(1.14)$$

Where b is a constant vector. The system above is explicitly: [20]

$$x_1' = a\,x_1 + b\,x_2 + g_1 \qquad (1.15.a)$$

$$x_2' = c\,x_1 + d\,x_2 + g_2 \qquad (1.15.b)$$

As before, we can find the critical point by setting $x_1' = x_2' = 0$ and solve the resulting nonhomogeneous system of algebraic equations [14]. The origin will no longer be a critical point, since the zero vectors is never a solution of a nonhomogeneous linear system. Instead, the unique critical point (as long as A has nonzero determinant, there remains exactly one critical point) will be located at the solution of the system of algebraic equations:

$$0 = a\,x_1 + b\,x_2 + g_1 \qquad (1.16.a)$$

$$0 = c\,x_1 + d\,x_2 + g_2 \qquad (1.16.b)$$

Once we have found the critical point, say it is the point $(x_1, x_2) = (\alpha, \beta)$, it then could be moved to (0, 0) via the translations $x_1 = x_1 - \alpha$ and $x_2 = x_2 - \beta$. The result after the translation would be the homogeneous linear system $x' = Ax$. The two systems (before and after the translations) have the same coefficient matrix. Their respective critical points will also have identical type and stability classification. Therefore, to determine the type and stability of the critical point of the given nonhomogeneous system, all we need to do is to disregard b, then take its coefficient matrix A and use its eigenvalues for the determination, in exactly the same way as we would do with the corresponding homogeneous system of equations.

Note: Here is the formal justification of our ability to discard the vector b when determining the type and stability of the critical point of the nonhomogeneous system $x' = Ax + b.$

Suppose $(x_1, x_2) = (\alpha, \beta)$ is the critical point of the system. That is

$$0 = a\alpha + b\beta + g_1 \tag{1.17.a}$$

$$0 = c\alpha + d\beta + g_2 \tag{1.17.b}$$

Now apply the translations $X_1 = x_1 - \alpha$ and $X_2 = x_2 - \beta$.

We see that $x_1 = X_1 + \alpha,\ x_2 = X_2 + \beta,\ X_1' = x_1',$ and $X_2' = x_2'$.

Substitute them into the system x′ = Ax + b:

$$\begin{aligned} x_1' &= X_1' = ax_1 + bx_2 + g_1 = a(X_1 + \alpha) + b(X_2 + \beta) + g_1 \\ &= aX_1 + bX_2 + (a\alpha + b\beta + g_1) = aX_1 + bX_2 \end{aligned} \tag{1.18.a}$$

$$\begin{aligned} x_2' = X_2' &= cx_1 + dx_2 + g_2 = c(X_1 + \alpha) + d(X_2 + \beta) + g_2 \\ &= cX_1 + dX_2 + (c\alpha + d\beta + g_2) = cX_1 + dX_2 \end{aligned} \tag{1.18.b}$$

That is, with the new variables x_1 and x_2 the given system has become [21]

$$\begin{aligned} x_1' &= ax_1 + bx_2 \\ x_2' &= cx_1 + dx_2 \end{aligned} \tag{1.19}$$

Notice it has the form $x' = Ax$. That is, it is a homogeneous system (with the critical point at the origin) whose coefficient matrix is exactly A, the same as the original system's. Hence, b could be disregarded, and a determination of the type and stability of the critical point of the system (with or without the translations) could be based solely on the coefficient matrix A.

In this thesis focus on qualitative analysis and numerical techniques for trial general non-homogeneous boundary value problems with a single independent variable. The two well-known numerical techniques are shooting method and finite difference method. Now the thesis is try to demonstrate the application of shooting method only for different nonlinear boundary value problems.

1.3. Statement of the problem

Recently, numerical solution to nonlinear dynamical of coupled boundary value problems in fluid mechanics and heat transfer, have studied by many researchers and scholars. Among these C.Herly [22] studied in titled by Asymptotic and Dynamical Analyses of Heat Transfer through a Rectangular Longitudinal Fin, Muatazz Abdolhadi Bashir, Mustafa Mamatand and Ilyani Abdullah [23] were conducted on Velocity Slip Effect on Falkner-Skan Boundary Layer Flow over a Static Wedge, Tiegang Fange and Ji Zhang [24] were also studied in titled Closed-form exact solutions of MHD viscous flow over a shrinking sheet, Anuj Kumar Jhankal [25] were studied MHD boundary layer and heat transfer along an infinite porous hot horizontal continuous moving plate and Mohammad Mehdi Keshtkar and Mohammad Mehdi Keshtkar [26] studied on Numerical Solution for the Falkner-Skan Boundary Layer Viscous Flow over a Wedge.

C.Herly [22] used dynamical analysis in her report. Tiegang Fange and Ji Zhang [24] using the homotopy analysis method, On the other hand Muatazz Abdolhadi Bashir, Mustafa Mamatand and Ilyani Abdullah [23], and Anuj Kumar Jhankal [25] and Mohammad Mehdi Keshtkar and Mohammad Mehdi Keshtkar [26] using an implicit finite difference method; respectively used implicit finite difference method for their numerical analysis. As discussed above all these studies did not use shooting-secant method, and then we are demonstrating the shooting-secant method is a powerful approximation method for non-linear BVPs. Thus, this thesis conducted on dynamical and numerical solution of non-linear dynamics of coupled boundary value problems by applying shooting-secant method. To this end, the study investigates coupled boundary value problems for fluid mechanics and heat transfer, which have different forms of non-linearity.

The Shooting- secant method were used for in space discretization to solve non-linear dynamical of coupled boundary value problems. The issues of convergence also dealt in order to distinguish valid results and an eigenvalue and phase plane analysis of fixed points were used to determine the convergence dynamics of the systems.

1.4. Objectives of the Thesis

1.4.1. General Objective

The general objective of this thesis is a dynamical and applying shooting-scant method for numerical study of non-linear dynamics system of coupled boundary value problems for fluid mechanics and heat transfer. To this end the specific objectives were presented as followed:

1.4.2. Specific Objectives

1. **To find the Numerical solutions and dynamical analysis of a heat transfer Equations**

In this proposed work, shooting-secant method is chosen for finding the numerical solutions of nonlinear dynamical coupled boundary value problems subject to specified boundary conditions. An eigenvalue and phase plane analysis was used for dynamical analysis of a heat transfer equations.

2. **To find the numerical solution of boundary layer viscous flow over a wage by Falkner-Skan equations**

Shooting-secant method is chosen for finding numerical solutions of boundary layer viscous flow over a wage by Falkner-Skan equation subject to specified initial and boundary conditions.

3. **To find the numerical solution for the effect of velocity slip problems**

In the work reported here in, shooting-secant method is implemented to determine numerically the velocity slip parameter on boundary layer fallow with Falkner-Skan equation.

4. **To find the numerical solutions of MHD viscous problems**

Shooting-secant method is used to find the numerical solutions of MHD viscous flow over a shrinking sheet.

1.5. Methodology

The numerical solution to nonlinear dynamical of coupled boundary value problems in fluid mechanics and heat transfer, we used to approaches. Such as for numerical analysis we use shooting-secant method and the phase portraits will be developed in MATLAB using a program known as pplane9 cited [27]. All the simulations would be done using MATLAB version 9.4.0. The methods are briefly describe in the following:

1.5.1. Shooting Method

Shooting is an iterative approach, is employed to vary the assumed initial conditions on one boundary until the boundary conditions on the other boundary are satisfied. The initial-value problem is solved, and the solution at the other boundary is compared to the known boundary conditions on that boundary [28].

The Shooting Method is essentially an iterative application of numerical integration techniques used for IVPs. It is easy to apply in most cases, but it is not appropriate for solving BVPs with more than one independent variable.

1.5.1.1. Reduction to Two IVP's: Linear Shooting Method

Linear shooting method takes the advantages of well-known numerical solution methods for IVPs. However, some IVPs with rapidly growing nature can be unstable although the BVP itself may be well posed and stable. [29]

Finding the solution of a linear boundary problem is assisted by the linear structure of the equation and the use of two special initial value problems.

1.5.1.2. Shooting - Secant Method

For the Shooting method, we consider the problem; assume the following ordinary differential equation are given: then

$$y'' = f(x, y, y') \tag{1.20}$$

$$y(a) = A, \tag{1.21.a}$$

$$y'(a) = t, \tag{1.21.b}$$

We let

$$m(t) = f(b;t) - B \tag{1.22}$$

Where $f(b;t)$ is the solution to using the value t. we wish to find a zero of $m(t)$ to solve the boundary value problem. In this case we use the secant method to locate the zero. We make successive approximations using the iteration:

$$x_{n+1} = x_n - \frac{x_n - x_{n-1}}{f(x_n) - f(x_{n-1})} f(x_n) \tag{1.23}$$

We need two guess to start the process, then we just proceed until the iterations converge.

Note: In the technical literature, the various Boundary conditions (BCs) are often referred to as [30]

- Dirichlet BC: $B(y, y') \to B(y)$ only a function of y
- Neumann BC: $B(y, y') \to B(y')$ only related to the derivative of y
- Robin BC: $B(y, y') \to B(y')$ function of both y and y' (mixed BC)

Runge-Kutta Methods

The idea of Ringe-Kutta methods is to use combinations of compositions of the right-side function of the equation to approximate the derivative terms to a required order. The resulting Runge-Kutta methods are among the most popular methods in solving initial value problems [31].

1.5.1.3. Algorithms of Shooting - Secant Method

Consider the following ODEs system

For Boundary value problems one need to satisfy conditions at up to *n* points.

Input: Endpoints *a* and *b*; Boundary conditions and number of subintervals *N*.

Steps 1: Rewrite as two or more order ODEs (as we need)

Assumes the ***second order ODEs***

$$\begin{aligned} \frac{dy}{dx} &= z; & y(a) &= 0 \\ \frac{dz}{dx} &= f(x, y, z); & y(b) &= y_b \end{aligned} \tag{1.24}$$

Assumes ***the third order ODEs***

$$\begin{aligned} \frac{dy}{dx} &= z; & y(a) &= 0 \\ \frac{dz}{dx} &= p; & y(b) &= y_b \\ \frac{dp}{dx} &= f(x, y, z, p); & y(y_b) &= z_b \end{aligned} \tag{1.25}$$

Steps 2: We need conditions (an initial value), and guess which our bullet is very necessary. The guess value is at the beginning or at the end boundaries of $z\left(i.e.\ z(a)\ \ or\ z(b)\right)$.

Apply the shooting-secant methods of the above Equations(1.24)

Steps 3: Using Runge-Kutta 4 method we obtain the solution of the end value $\left(i.e.\ y(b)\right)$

$$\text{Set: } x_n = a + (n-1)h, \qquad n = 1, 2, \ldots \tag{1.26}$$

For the second order ODEs

$$\begin{aligned} k_{11} &= hf(x_n, y_n, z_n), \\ k_{12} &= hg(x_n, y_n, z_n) \\ k_{21} &= hf\left(x_n + \frac{1}{2}h, y_n + \frac{1}{2}k_{11}, z_n + \frac{1}{2}k_{12}\right), \\ k_{22} &= hg\left(x_n + \frac{1}{2}h, y_n + \frac{1}{2}k_{11}, z_n + \frac{1}{2}k_{12}\right) \\ k_{31} &= hf\left(x_n + \frac{1}{2}h, y_n + \frac{1}{2}k_{21}, z_n + \frac{1}{2}k_{22}\right), \\ k_{32} &= hg\left(x_n + \frac{1}{2}h, y_n + \frac{1}{2}k_{21}, z_n + \frac{1}{2}k_{22}\right) \\ k_{41} &= hf(x_n + h, y_n + k_{31}, z_n + k_{32}), \\ k_{42} &= hg(x_n + h, y_n + k_{31}, z_n + k_{32}) \end{aligned} \tag{1.27}$$

Then compute the above Rk4 (1.27) the ODEs

$$y_{n+1} = y_n + \frac{1}{6}(k_{11} + 2k_{21} + 2k_{31} + k_{41}) \tag{1.28.a}$$

$$z_{n+1} = z_n + \frac{1}{6}(k_{12} + 2k_{22} + 2k_{32} + k_{42}) \tag{1.28.b}$$

For the third order ODEs

$$
\begin{aligned}
k_{11} &= hf\left(x_n, y_n, z_n, p_n\right)\\
k_{12} &= hg\left(x_n, y_n, z_n, p_n\right),\\
k_{13} &= hr\left(x_n, y_n, z_n, p_n\right)\\
k_{21} &= hf\left(x_n+\frac{1}{2}h, y_n+\frac{1}{2}k_{11}, z_n+\frac{1}{2}k_{12}, P_n+\frac{1}{2}k_{13}\right)\\
k_{22} &= hg\left(x_n+\frac{1}{2}h, y_n+\frac{1}{2}k_{11}, z_n+\frac{1}{2}k_{12}, p_n+\frac{1}{2}k_{13}\right),\\
k_{23} &= hr\left(x_n+\frac{1}{2}h, y_n+\frac{1}{2}k_{11}, z_n+\frac{1}{2}k_{12}, p_n+\frac{1}{2}k_{13}\right)\\
k_{31} &= hf\left(x_n+\frac{1}{2}h, y_n+\frac{1}{2}k_{21}, z_n+\frac{1}{2}k_{22}, p_n+\frac{1}{2}k_{23}\right)\\
k_{32} &= hg\left(x_n+\frac{1}{2}h, y_n+\frac{1}{2}k_{21}, z_n+\frac{1}{2}k_{22}, p_n+\frac{1}{2}k_{23}\right),\\
k_{33} &= hr\left(x_n+\frac{1}{2}h, y_n+\frac{1}{2}k_{21}, z_n+\frac{1}{2}k_{22}, p_n+\frac{1}{2}k_{23}\right)\\
k_{41} &= hf\left(x_n+h, y_n+k_{31}, z_n+k_{32}, p_n+k_{33}\right)\\
k_{42} &= hg\left(x_n+h, y_n+k_{31}, z_n+k_{32}, p_n+k_{33}\right),\\
k_{43} &= hr\left(x_n+h, y_n+k_{31}, z_n+k_{32}, p_n+k_{33}\right)
\end{aligned}
\tag{1.29}
$$

Then compute the above Rk4 the ODEs

$$y_{n+1} = y_n + \frac{1}{6}\left(k_{11} + 2(k_{21}+k_{31}) + k_{41}\right) \tag{1.30.a}$$

$$z_{n+1} = z_n + \frac{1}{6}\left(k_{12} + 2(k_{22}+k_{32}) + k_{42}\right) \tag{1.30.b}$$

$$p_{n+1} = p_n + \frac{1}{6}\left(k_{13} + 2(k_{23}+k_{33}) + k_{43}\right) \tag{1.30.c}$$

Remark: For the three ODEs or the above expand the equation RK4.

Step 4: Check an acceptable tolerance. $\varepsilon \le \varepsilon_s$

Step 5: If not use the secant method for the next guess. Repeat to the above steps.

Step 6: stop the process.

1.5.2. Pplane9

To see Pplane in action, enter pplane9 at the MATLAB prompt. A new window will appear with the label PPLANE9 Setup. Figure 1 shows how this window looks on PC running windows. The appearing might differ slightly depending on your computer, but the functionality will be the same on all operating systems.

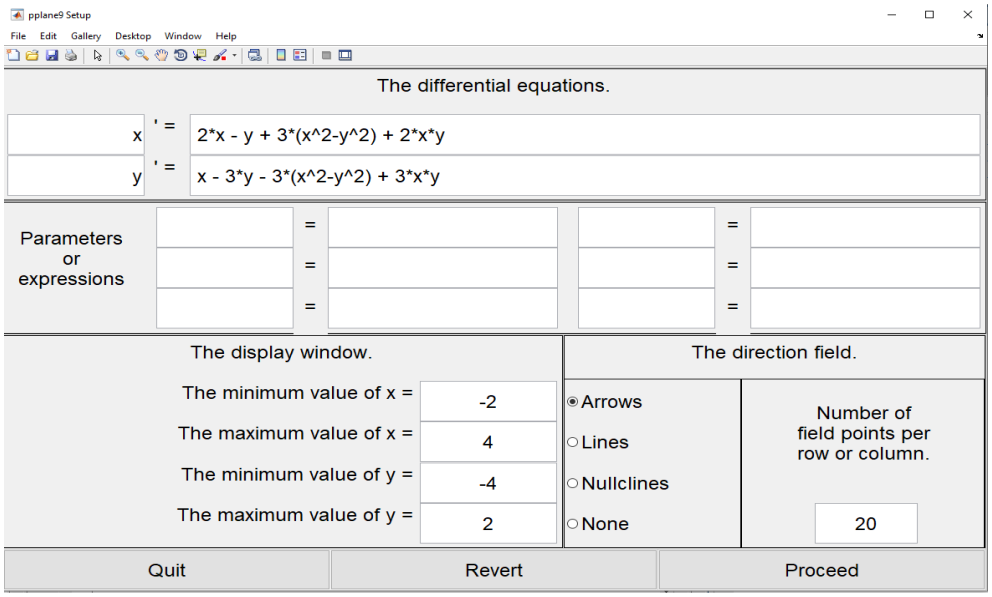

Figure 1: The window interface of pplane9

You will notice that there is a rather complicated autonomous system already entered in the upper part of PPLANE9 Setup window, in the form $x' = f(x, y)$ and $y' = g(x, y)$. There is middle section for entering parameters and expressions, although none are entered at the moment. There is another section for describing a "display window", and yet another for defining what kind of field is to be used. There are three buttons at the bottom of the window and several menus across the top.

The most prominent feature of the PPLANE9 Display window is a rectangle label with the variable x on the bottom, and the variable y on the left. The dimensions of this rectangle are slightly larger than the rectangle specified in the PPLANE9 Setup window in order to accommodate the extra space needed by the vectors in the field. Inside this rectangle the PPLANE9 Display window shows the vector field for the system defined in the PPLANE9 Setup window. At each point (x, y) of a grid of points, there is drown a small arrow. The direction of the vector is the same as that of

$F(x) = [f(x, y), g(x, y)]^T$, entered as different equations in the PPLANE9 setup window, and the length varies with the magnitude of $F(x, y)$. The vector must be tangent to any solution curve through (x, y). Simply said, the PPLANE9 Display window display window displays the phase plane for the polar system.

There are two buttons on the PPLANE9 Display window with the labels **Quit** and **Print.** There are several menus. Finally, below the vector field there is a small Cursor position window, and a larger message window through which pplane9 will communicate with the user. At this time it should contain the single word "Ready", indicated that it is ready to follow orders.

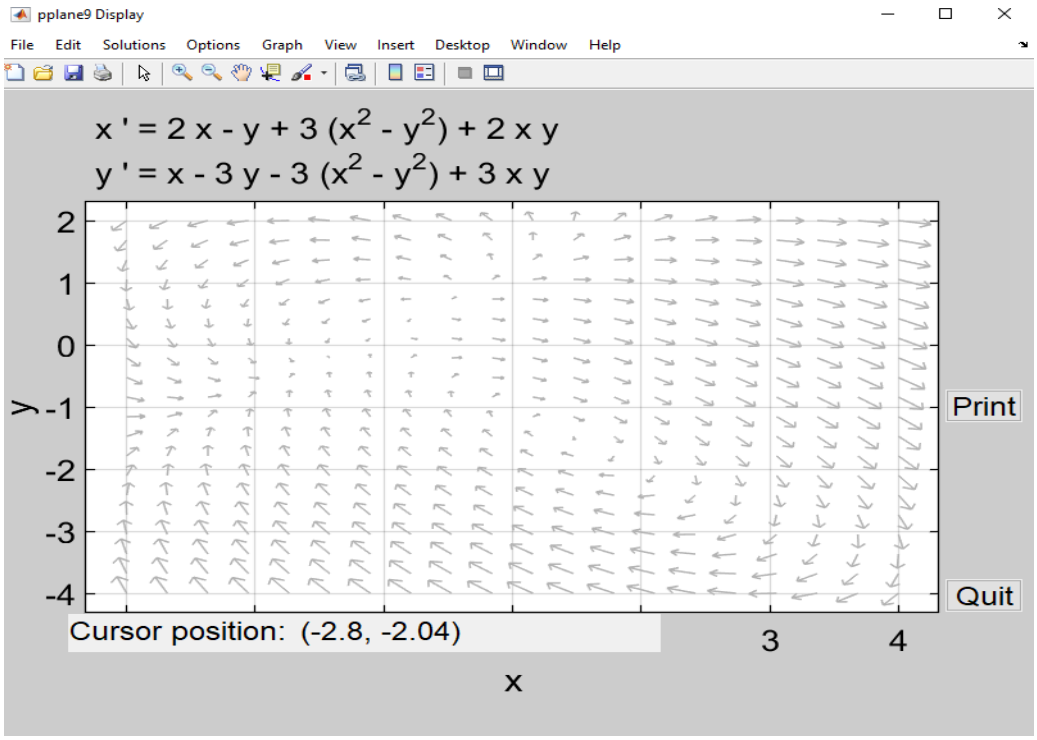

Figure 2: The result display of pplane9

To compare and plot a solution curve from an initial point, move the mouse to that point, using the cursor position window to improve your accuracy, and click the mouse button. The solution will be computed and plotted, first in the direction in which the dependent variable is increasing like Figure 3. Notice that the solution curves all seem to start and stop in the same two points, and that the message window indicates that these are equilibrium points.

If you open the **options** menu, you will see several ways of modifying how solutions are computed and plotted. The solution direction can be chosen by choosing **Options →Solution direction →Back**. Sometimes it is desirable to indicate where the computation of a solution curve is started. This can be effected by selecting **Options →Mark initial points.**

1.6. Organization the Thesis

This thesis is organized in to eight chapters. The first chapter deals about background, basic concepts of nonlinear ODEs, statement of the problem, objective of the this thesis and methodology.

In Chapter 2, deals about the Numerical and Dynamical Analysis of Heat Transfer through a Rectangular Longitudinal Fin: We have many mathematical models which describe heat transfer in fins with boundary conditions and obtain the solution such equations numerically and analytically alike. In this chapter contain to qualitative analysis and numerical technique for the fin problem. Moreover, investigate the stability of a dynamic system and identify the effect of the different value of the thermo-geometric parameter. And also, observe the effect of the various exponents of the problem.

In Chapter 3, Numerical solution of the Falkner-Skan boundary layer viscous flow over a wedge using a shooting method application. The numerical solution of Boundary Layer Viscous Flow over a Wedge is investigated. A numerical solution of Boundary Layer Viscous Flow over a Wedge is conducted and furthers the effect of the nonlinear by the Falkner-Skan equations. Also in it the comparison between the Blasius equation result with the previous work.

In Chapter 4, deals about the velocity slip parameter for boundary layer flow over a static wedge. The problem of the Falkner-Skan boundary layer flow past a wedge considering the velocity slips condition. It investigated, the effect of velocity slip boundary, which is the boundary is increases the velocity profile is decreases.

In Chapter 5, provides the shrink sheet of a magnitohydrodynamics. Solutions of a closed-form exact by a steady, two-dimensional laminar flow over a continuously shrinking sheet in a quiescent fluid.

In Chapter 6, deals about MHD boundary layer flow and heat transfer along an infinite porous hot horizontal continuous moving plate. In this chapter compare the numerical and the analytical solution of a about MHD boundary layer. And also check the errors, which are absolute error and relative errors of a problem.

In Chapter 7, contain the magnitohydrodynamic Mixed Convection Flow and Entropy Generation over an Inclined Stretching Sheet. The flow behavior that is find the velocity profile and temperature distribution (first law investigation) in the boundary layer district was comprehend. In addition, to comprehend the vitality misfortunes during the boundary layer flow, it bodes well to play out a second law investigation. Entropy creation is the proportion of irreversibility in the heat transfer issues.

The last chapter, Chapter 8, includes summary, conclusions and recommendations for further study.

Chapter 2

Numerical and Dynamical Analysis of Heat Transfer through a Rectangular Longitudinal Fin

The temperature profile in a longitudinal rectangular fin attached to a stationary base surface. The basic definition of Fin is extended surfaces used to enhance the heat dissipation from a hot surface [22] [32]. Fins are different importance let as in refrigeration, air-conditioning, air-cooled craft engines, and the cooling of computer processors and oil carrying pipe lines. There are many mathematical models which describe heat transfer in fins with boundary conditions and obtain the solution such equations numerically and analytically alike. For engineering applications and physical phenomena thermal conductivity of a fin is assumed to be linearly enthusiastic about temperature [33]. We've got chosen the thermal conductivity as a linear function of the temperature and therefore the heat transfer coefficient as a nonlinear function of the temperature [34]. The most effective heat transfer improvement can be done by using fins as elements for heat transfer surface extension [35].

2.1. Mathematical Formulation

The energy balance for a longitudinal fin is given by an ordinary differential equation (ODE) as follow

$$A_c \frac{d}{dX}\left[k(T)\frac{dT}{dX}\right] = PH(T)(T - T_a) + q(T), \qquad 0 \le X \le L \tag{2.1}$$

Where K and H are the non-uniform thermal conductivity and heat transfer coefficient both of which depend on the temperature. The boundary conditions are

$$\begin{aligned} x &= 0, \qquad \frac{dT}{dx} = 0 \\ x &= L, \qquad T = T_b \end{aligned} \tag{2.2}$$

The heat transfer coefficient may be given as the power law

$$H(T) = h_b\left(\frac{T - T_a}{T_b - T_a}\right)^n \tag{2.3}$$

As done for most industrial applications. As such may be written as the following:

$$K(T) = k_a\left[1+\lambda(T-T_a)\right] \tag{2.4}$$

On introducing the following dimensionless variables:

$$\begin{aligned} x &= \frac{X}{L}; \quad \theta = \frac{T-T_a}{T_b-T_a}; \quad h = \frac{H}{h_0}; \\ k &= \frac{K}{k_a}; \quad M^2 = \frac{ph_bL^2}{A_ck_a}; \end{aligned} \tag{2.5}$$

It allows (2.1) to be reduced to the following non dimensional ordinarily differential equations:

$$\frac{d}{dx}\left[k(\theta)\frac{d\theta}{dx}\right] = M^2\theta h(\theta), \qquad 0 \le x \le 1 \tag{2.6}$$

In (2.6) θ is defined as the dimensionless temperature and x as the dimensionless spatial variable, where $k(\theta)$ is the dimensionless thermal conductivity, $h(\theta)$ is the heat transfer coefficient, and M is termed the thermo-geometric parameter. In the dimensionless variables the heat transfer coefficient is chosen as $h(\theta) = \theta^n$ with n termed as the exponent. The thermal conductivity coefficient can be written in dimensionless variables as $k(\theta) = 1+\beta\theta$ with $\beta = \lambda(T_b - T_a)$, where T_b is the dimensionless fin base temperature. From these choices of $k(\theta)$ and $h(\theta)$, we obtain the one-dimensional nonlinear heat condition equation:

$$\frac{d}{dx}\left[(1+\beta\theta)\frac{d\theta}{dx}\right] = M^2\theta^{n+1}, \qquad 0 \le x \le 1 \tag{2.7}$$

The dimensionless boundary conditions become

$$\begin{aligned} \left.\frac{d\theta}{dx}\right|_{x=0} &= 0 \\ \theta(1) &= 1 \end{aligned} \tag{2.8}$$

2.2. Method of Solution:

The above non-linear equation (2.7) has a numerical method of solution. In this work, a simple and a powerful approximate method of a solution the Shooting-secant method is used. The Shooting Method is essentially an iterative application of numerical integration techniques used for IVPs. The boundary conditions on one side of the given interval are used as initial conditions [36].

Reduction to Two IVP's: Linear Shooting Method for Numerical solution

Finding the solution of a linear boundary problem is assisted by the linear structure of the equation and the use of two special initial value problems. Therefore, from equation (2.7). Let

$$y_1 = \frac{d\theta}{dx}; \quad \text{With } \theta(0) = ? \text{ and } \theta(1) = 1 \tag{2.9}$$

Therefore; $\theta(0)$ **is the bullet, and** $\theta(1) = 1$ **is the target.**

$$y_2 = \frac{dy_1}{dx} = \frac{d^2\theta}{dx^2} = \frac{-\beta(\theta')^2 + M^2\theta^{n+1}}{1+\beta\theta}, \quad with\ \theta'(0) = 0 \tag{2.10}$$

2.3. Results and Discussion

This section presents and discusses the numerical solution results and dynamical system analysis.

2.3.1. Numerical Solutions

The results are demonstrated that a high thermal conductivity implies that energy can be conducted more easily as expected. The dimensionless temperature distribution rises monotonically along fin length for all various thermogeometric, thermal conductivity and convective heat transfer parameters. When the value of the thermogeometric parameter M maximize, the more heat converted from the fin through its length and the more thermal energy is efficiently transferred into environment through the fin length [37]. In condition of negligible heat loss from the fin tip (insulted tip) to the environment, the fin temperature decreases along the fin length. Also, and the temperature decreasing rate is the same around the fin base area.

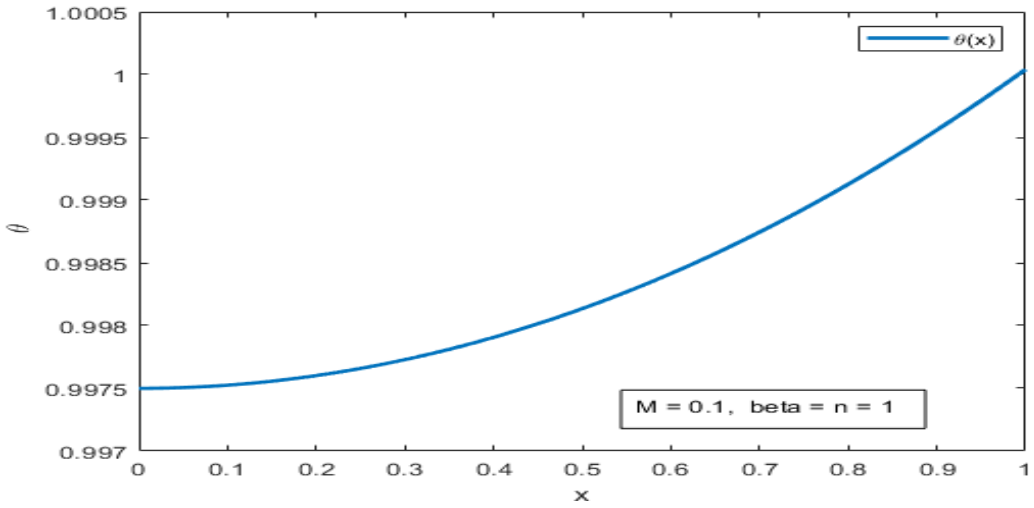

Figure 3: Dimensionless temperature distribution in the fin parameters when $M = 0.1,\ \beta = 1\ \ and\ n = 1$

From Figure 3, the numerical solution of temperature that the length of the fin has a proportional with the thermogeometric parameter. Let us $M << \in$, where $\in = 1/M$, we found an asymptotic solution which plotted has a maximum temperature at the fin tip.

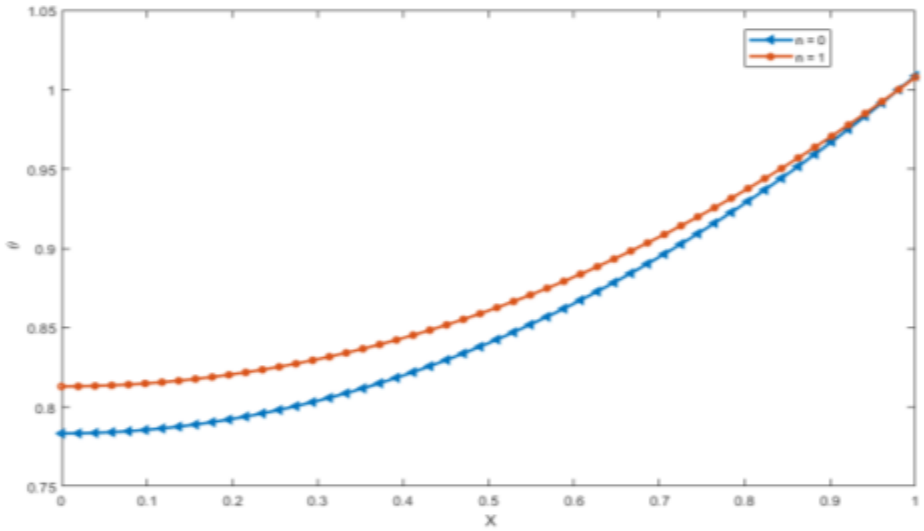

Figure 4: Dimensionless temperature of the fin parameters with varying n when $M = \beta = 1.$

As shows Figure 4, the dimensionless temperature distribution rises monotonically from the fin tip to the fin base for the different parameter of thermogeometric value. As thermogeometric parameter is increase when the heat transfer coefficient to be pronounced on the temperature slop and temperature dependent convective. This implies that the prediction efficiency and temperature fin based on dependent by

temperature results in the fin material and significant reductions in the size and weight of the heat transfer material since reduced the surface area.

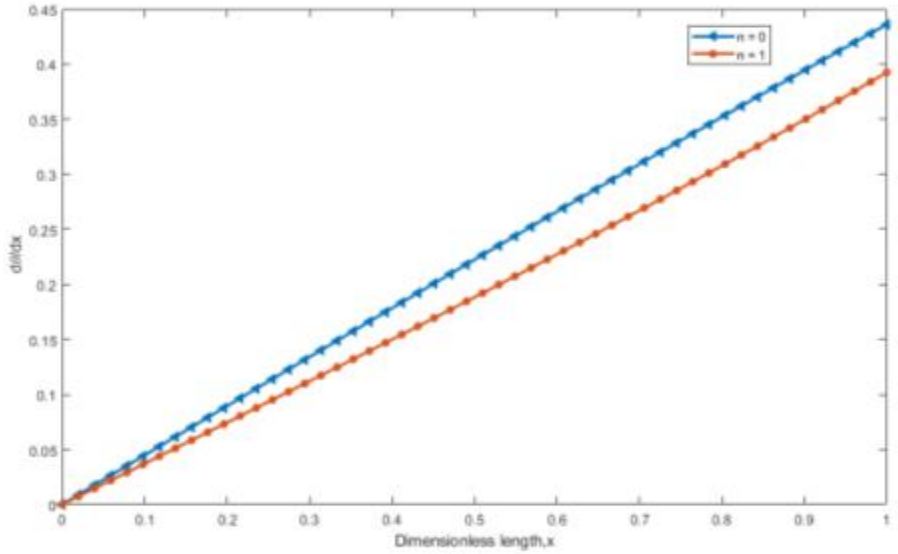

Figure 5: Dimensionless the rate of temperature distribution in the fin parameters for varying n parameter when $M = \beta = 1.$

As shows Figure 5, the rate of the dimensionless temperature distribution rises monotonically from the fin tip to the fin base for the different parameter of thermogeometric value. As thermogeometric parameter is increase when the heat transfer coefficient to be pronounced on the temperature slop and temperature dependent convective.

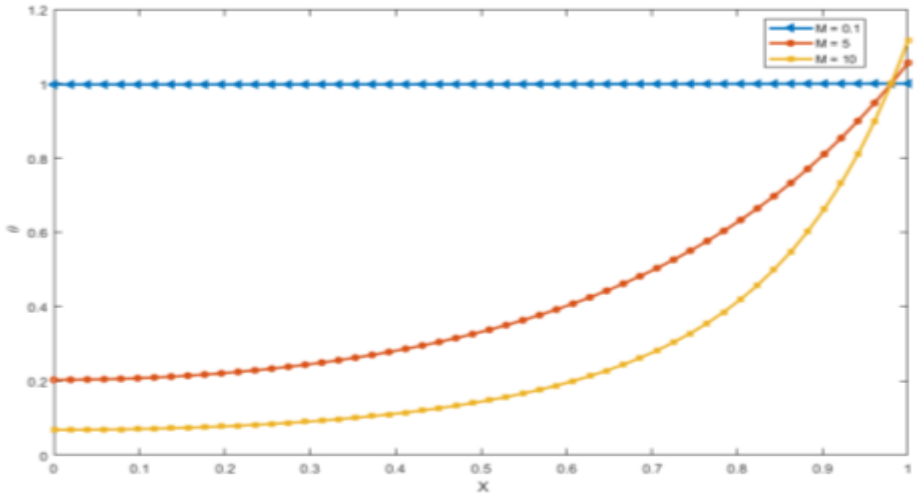

Figure 6: Dimensionless temperature distribution in the fin parameters for varying thermo-geometric parameter when $n = \beta = 1.$

As Figure 6, the dimensionless temperature distribution in the fin parameters for different value thermo-geometric parameter are increases. In this figure the two parameters such as n and β are fixed. The thermo-geometric parameter value maximum the temperature distribution is decreases.

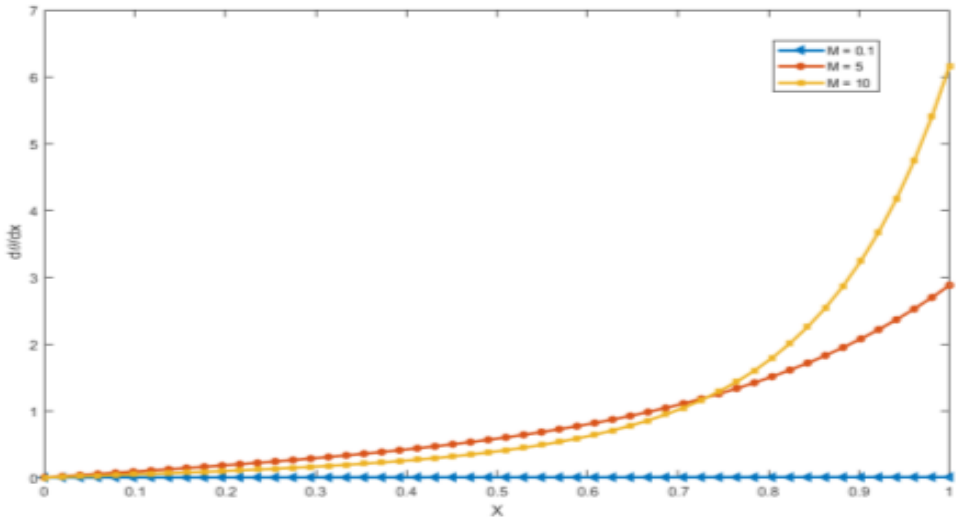

Figure 7: Dimensionless rate of the temperature distribution in the fin for varying thermo-geometric parameter when $n = \beta = 1.$

As Figure 7, the dimensionless temperature rate distribution in the fin parameters for different value thermo-geometric parameter all are start from 0 and increases. In this figure the two parameters such as n and β are fixed.

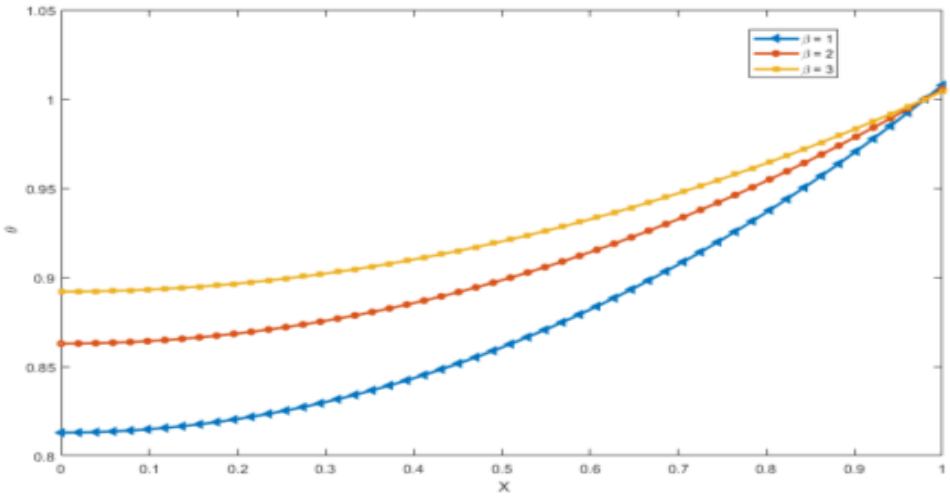

Figure 8: Dimensionless temperature distribution in the fin for varying values of non-linear parameters, when $n = M = 1.$

As Figure 8, the dimensionless temperature distribution in the fin parameters for different value non-linear parameter are increases. In this figure the two parameters

such as n and M are fixed. The non-linear parameter value maximum the temperature distribution is increases.

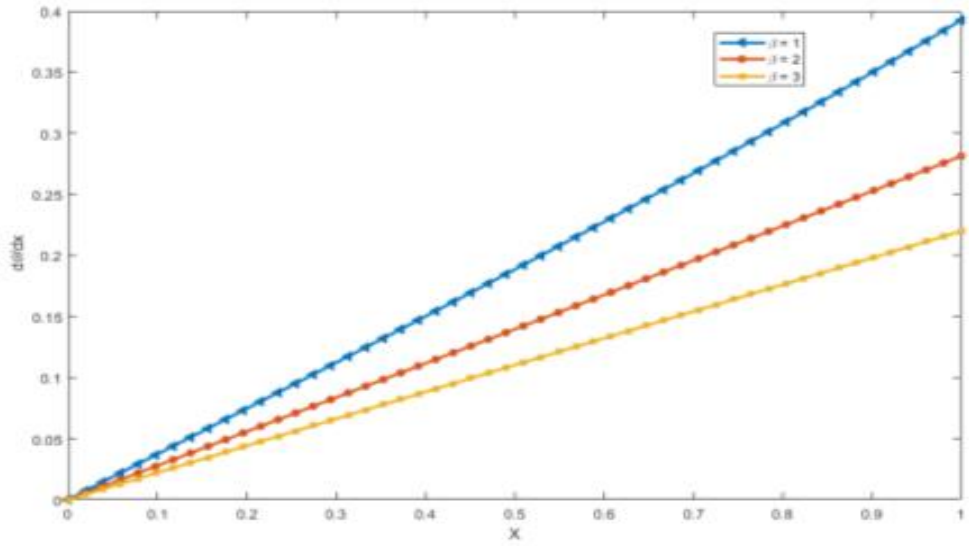

Figure 9: Dimensionless the rate of the temperature distribution in the fin for varying values of β , when $n = M = 1$.

As Figure 9, the dimensionless temperature rate distribution in the fin parameters for different value non-linear parameter all are start from 0 and increases. In this figure the two parameters such as n and M are fixed. The non-linear parameter value maximum the temperature distribution is increases.

2.3.2. Reduction to Two IVP's: Dynamical system analysis

The process of the method is described as follows. Based on equation (2.8) and boundary values, rewriting equation (2.7), the governing equation, as a system of first-order ordinary differential equations through the transformations

$$\begin{aligned} \theta(x) &= u(x), \quad \text{and} \\ v(x) &= d\theta / dx \end{aligned} \tag{2.11}$$

such that

$$d^2\theta / dx^2 = v(du / d\theta) \tag{2.12}$$

.

This gives the following system: From equation (2.7) for $0 \le x \le 1$

$$\frac{d^2\theta}{dx^2} + \beta\theta\frac{d^2\theta}{dx^2} + \beta\left(\frac{d^2\theta}{dx^2}\right) = M^2\theta^{n+1} \tag{2.13}$$

$$\frac{d^2\theta}{dx^2}(1+\beta\theta) + \beta\left(\frac{d^2\theta}{dx^2}\right) = M^2\theta^{n+1} \tag{2.14}$$

$$\frac{d^2\theta}{dx^2} = \frac{1}{(1+\beta\theta)}\left(M^2\theta^{n+1} - \beta\left(\frac{d^2\theta}{dx^2}\right)\right) \tag{2.15}$$

$$(1+\beta\theta)\frac{d^2\theta}{dx^2} = M^2\theta^{n+1} - \beta\left(\frac{d^2\theta}{dx^2}\right) \tag{2.16}$$

$$(1+\beta\theta)\frac{d}{dx}\left(\frac{d\theta}{dx}\right) = M^2\theta^{n+1} - \beta\left(\frac{d^2\theta}{dx^2}\right) \tag{2.17}$$

Then, from the assumption equation (2.11),

$$(1+\beta u)v\frac{du}{d\theta} = M^2u^{n+1} - \beta v^2 \tag{2.18}$$

Hence,

$$\begin{aligned} \frac{dv}{dx} &= M^2u^{n+1} - \beta v^2 \\ \frac{du}{dx} &= v(1+\beta u) \end{aligned} \tag{2.19}$$

With $u(1) = 1$ and $v(0) = 0$.

Now, uses equation (2.19) find the equilibrium points:

$$\begin{aligned} \frac{dv}{dx} = 0 \quad &\Rightarrow M^2u^{n+1} - \beta v^2 = 0 \\ \frac{du}{dx} = 0 \quad &\Rightarrow v(1+\beta u) = 0 \end{aligned} \tag{2.20}$$

Thus, obtain the following equilibrium points:

$$\begin{aligned} e_1 &= (0,0), \\ e_2 &= \left(-\frac{1}{\beta}, -\frac{M(-1)^{\frac{n+1}{2}}}{\beta^{\frac{n+1}{2}}} \right), \quad and \\ e_3 &= \left(-\frac{1}{\beta}, \frac{M(-1)^{\frac{n+1}{2}}}{\beta^{\frac{n+1}{2}}} \right) \end{aligned} \tag{2.21}$$

The Jacobian matrix J for the system (2.19) is given by

$$\begin{aligned} J(u_1, v_1) &= \begin{bmatrix} \frac{d}{du}\left(v(1+\beta u)\right) & \frac{d}{dv}\left(v(1+\beta u)\right) \\ \frac{d}{du}\left(M^2 u^{n+1} - \beta v^2\right) & \frac{d}{dv}\left(M^2 u^{n+1} - \beta v^2\right) \end{bmatrix} \\ &= \begin{bmatrix} \beta v & 1+u\beta \\ M^2(n+1)u^n & -2\beta v \end{bmatrix} \end{aligned} \tag{2.22}$$

To be able to a phase plane analysis of the relevant equation, to linearise the system. The calculation of the Jacobian (2.22), where the elements in J need to be linear with respect to v and u. From the Jacobian (2.22) for the equilibirum points given the above (2.21). To begin with, the equilibrum points $e_1 = (0,0)$ which produces the following Jacobian equation:

$$J(u_1, v_1) = \begin{bmatrix} 0 & 1 \\ 0 & 0 \end{bmatrix} \tag{2.23}$$

This in turn produces the eigenvalues

$$\lambda_1^{(1)} = 0, \qquad \lambda_2^{(1)} = 0 \tag{2.24}$$

The second equilibrum points, evaluating J at e_2 produces the following:

$$J(u_2, v_2) = \begin{bmatrix} -M(-1)^{(n+1)/2}\beta^{(-n/2)} & 0 \\ M^2(n+1)\beta^{-n} & 2M(-1)^{(n+1)/2}\beta^{(-n/2)} \end{bmatrix} \tag{2.25}$$

with eigenvalues

$$\begin{aligned} \lambda_1^{(2)} &= -M(-1)^{(n+1)/2}\beta^{-n/2} \\ \lambda_2^{(2)} &= 2M(-1)^{(n+1)/2}\beta^{-n/2} \end{aligned} \tag{2.26}$$

From the third equilibrum points, valuating J at e_3 produces the following:

$$J(u_3, v_3) = \begin{bmatrix} M(-1)^{(n+1)/2}\beta^{(-n/2)} & 0 \\ M^2(n+1)(-\beta)^{-n} & -2M(-1)^{(n+1)/2}\beta^{(-n/2)} \end{bmatrix} \tag{2.28}$$

with eigenvalues

$$\begin{aligned} \lambda_1^{(3)} &= -2M(-1)^{(n+1)/2}\beta^{-n/2} \\ \lambda_2^{(3)} &= M(-1)^{(n+1)/2}\beta^{-n/2} \end{aligned} \tag{2.30}$$

For these two equilibrium points we observe the eigenvalues with no zero and purely imaginary.

In all figures, we have three equilibrium points with pure real Eigenvalues. This makes it very straight forward that we do not have an imaginary component for the Eigenvalues of the system. Moreover, in all situations visited here, all equilibrium points are unstable saddle type, at best a center.

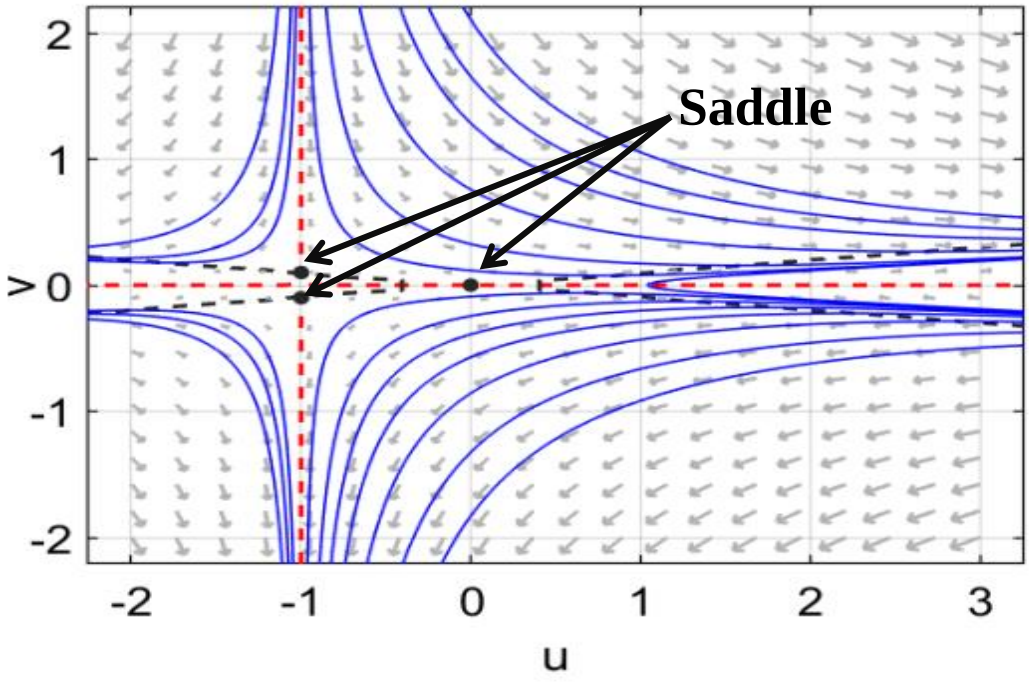

Figure 10: Phase plane diagram for parameters $\mathrm{m} = 0.1,\ \mathrm{B} = 1$ and $\mathrm{n} = 1$

From Figure 10, we can see that that we have three equilibrium points at $(-1,\ 0.1)$, $(-1,\ -0.1), (0,\ 0)$. Its corresponding Eigenvalues are $(-0.2,\ 0.1), (0.2,\ -0.1)$ and $(-0.0065,\ 0.0065)$ respectively which can be understood that all the three points are unstable saddle node.

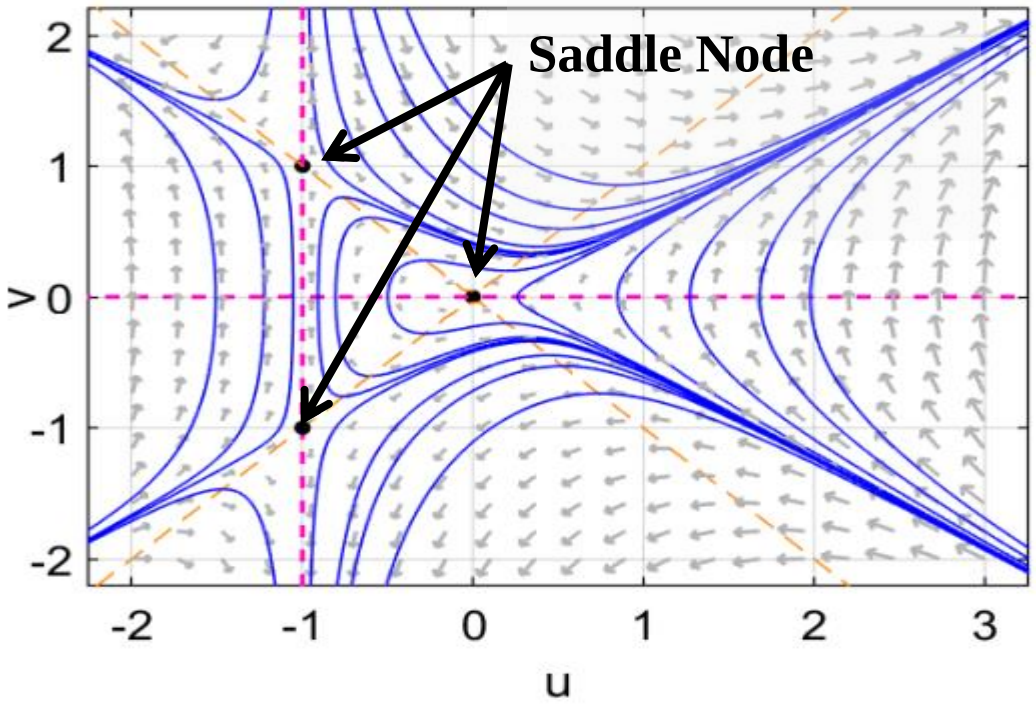

Figure 11: Phase plane diagram for parameters $\mathrm{m}=1, \mathrm{B}=1$ and $\mathrm{n}=1$

From Figure 11, we can see that we have three equilibrium points at $(-1,-1), (-1,1)$ and $(0,0)$. The corresponding Eigenvalues are $(-2,1)$, $(2,-1)$ and $(-5\times10^{-7}+0.015i, -5\times10^{-7}-0.015i)$. Which can be understood that the first two are unstable saddle node and the last is a stable node.

In Figure 12 below, we can see that that we have only one equilibrium points at (0, 0). Its corresponding Eigenvalues are $(0.0347\ i,\ -0.0347\ i)$ which can be understood the equilibrium point is neutrally stable, since the real part of the eigenvalue is zero.

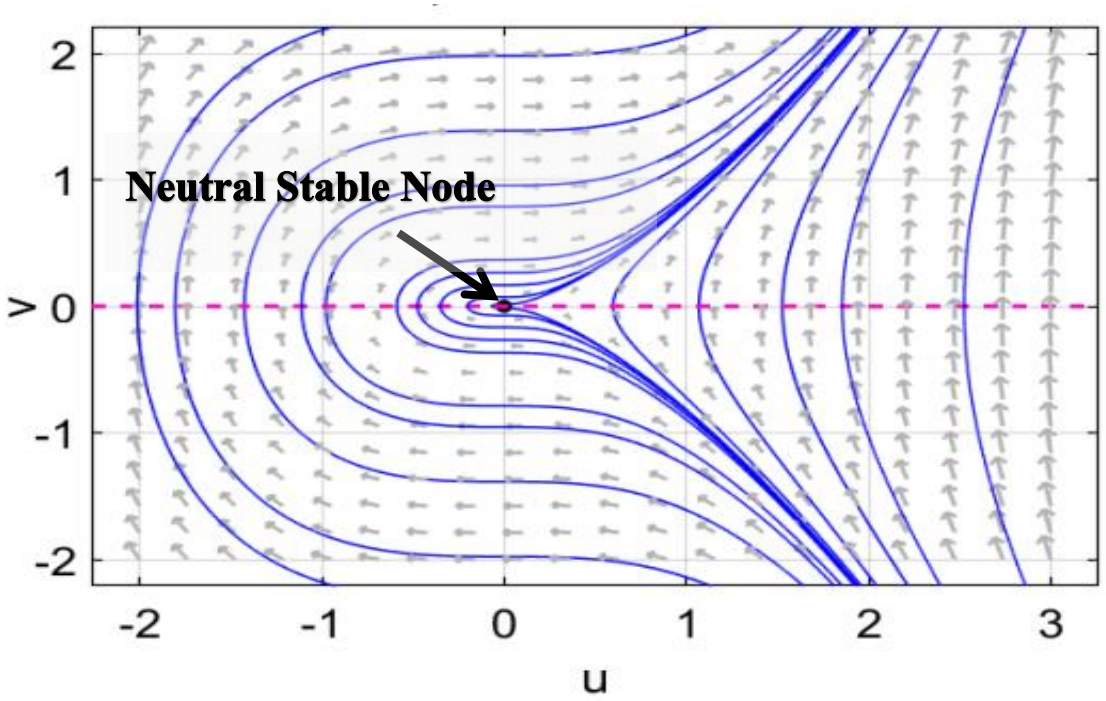

Figure 12: Phase plane diagram for parameters $m=1,\ B=0$ and $n=1$

Below in Figure 13, we can see that that we have only one equilibrium points at $(0,0)$. Its corresponding Eigenvalues are $(-1,1)$ which can be understood the equilibrium point is unstable saddle point, since the real parts of the eigenvalues are $+1$ and -1.

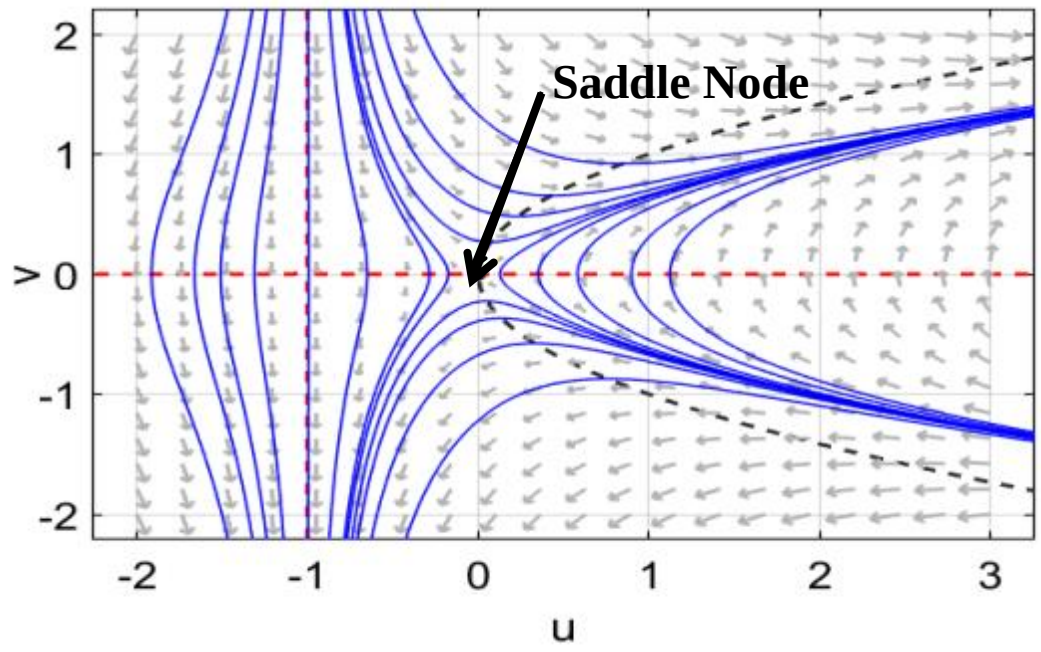

Figure 13: Phase plane diagram for parameters for $m=1,\ B=1$ and $n=0$

Therefore, we can classify the transition from figure 10 to figure 13 as a Subcritical Pitchfork Bifurcation, since one unstable node is distributed to two unstable and one stable node.

Generally, In figures 10 to 13, we tried to show how the property of the fin varies for different values of M. It can be seen that for Figure 10, for M = 0.1, equilibrium points are very close altogether. For M=1, the points starts scattering and we now have three equilibrium points. As we further increased the M value to 10, the points scattered further. Here, all equilibrium points are unstable.

In Figure 12, we tried to vary the parameter β (thermal conductivity coefficient) to 0, we obtained a natural center. This confirms that when the conduction parameter is zero, the conduction is inhibited so the sections throughout the system tend to remain somehow constant, because convection will be the only mode of heat transfer. In addition, in Figure 13, we set the n parameter to zero or m=1. Since n is used to describe the character of heat transfer, and when n=0, it is a constant heat transfer, we have a stable center on our phase diagram.

We summarize the chapter, from the numerical and the dynamical analysis of the above nonlinear problem, an investigation of such solutions is important given the prevalence of the many parameters whose impact and relationship with one another has yet to be fully understood. It's the aim of asymptotic solutions to reveal the dominant physical mechanisms of the model. In Harley and Moitsheki [38] and Moitsheki and Harley [38], the impact of the thermogeometric parameter was small values of M that there looked as if it would be unstable heat transfer within the fin and discussed with regards to its proportionality to the length of the fin, L. This was thought to be associated with the very fact that $M \propto L$. an asymptotic solution to the steady heat transfer in a very rectangular longitudinal fin allows us to validate this relationship and more firmly establish the importance of the length of the fin. A phase space analysis was conducted in Harley and Moitsheki [38], however, to not the extent conducted here. During this work, the analysis in [38] is improved upon and also the behavior, particularly the tip of the fin, more meticulously investigated and documented. This dynamical analysis also functions as a method of investigating the effect of the thermo-geometric parameter [18].

Chapter 3

Numerical Solution of the Falkner Skan Boundary Layer Viscous Flow over a Wedge: A Shooting Method Application

The Falkner-Skan equation, originally derived in 1931, Falkner and Skan (1931), is of central importance to the fluid mechanics of wall-bounded viscous flows. It is derived from the two-dimensional incompressible Navier-Stokes equations for a one-sided bounded flow using a similarity analysis and its solution describes the form of an external laminar boundary layer in the presence of an adverse or favorable stream wise pressure gradient. Although the apparent simplicity of the Falkner-Skan equation (a one-dimensional ordinary differential equation) solving it accurately can be fraught with difficulty; these problems mainly stem from its non-linearity and third-degree order. There are some examples of analytical solutions to the Falkner-Skan equations for special cases but most studies have focused either on demonstrating a solution's existence and uniqueness or finding a numerical/computational solution for particular boundary-layer conditions [39].

Results for solution existence and uniqueness to the Falkner- Skan equation can be found in Rosenhead (1963), Weyl (1942), Hartman (1972) and Tam (1970). In some of these works, ranges of validity for the boundary-layer parameters and similarity variable are established. More recently, Yang (2008) presents a non-existence result that places upper and lower bounds on, in essence, the non-dimensional wall shear stress. However, despite the amount of effort dedicated to this problem, this two- point boundary value problem still lacks a general closed-form solution, and as such, numerical treatments are the most common and valuable route for its study and solution [39].

The boundary layer theory unmistakably explains the consistent state flow more than a level plate at zero event point which is perceived as Blasius flow [26]. The Falkner–Skan condition was introduced by Falkner and Skan. Falkner and Skan built up an investigation about viscous fluid lowered the flow more than a static wedge. They extended a comparability change that can be used to lessen the restricted differential boundary layer conditions to a nonlinear third-order typical differential equation and after that clarified it numerically. It is notable that customary heat transfer fluids, for

example, mineral oil, water, and ethylene glycol have, all in all, helpless heat transfer properties contrasted with those of most solids [26]. A creative method of improving the heat transfer of fluids is to suspend little strong particles in the fluids. This new sort of liquids named as "nanofluids" was presented in 1995 by Choi [40]. The term nanofluid is utilized to depict a solid liquid blend which comprises of base fluid with low volume part of high conductivity solid nanoparticles.

3.1. The Falkner Skan Equation for Numerical Solution by using Shooting Techniques

In fluid dynamics, the Falkner–Skan boundary layer (named after V. M. Falkner and Sylvia W. Skan) describes the steady two-dimensional laminar boundary layer that forms on a wedge, which is a flow in which the plate is not parallel to the flow [41]. It is a generalization of the Blasius boundary layer.

The **Falkner–Skan boundary** equation is:

$$f'''+ ff''+\frac{2m}{m+1}(1- f'^{2}) = 0 \tag{3.1}$$

$$\text{with} \quad f(0) = f'(0) = 0 \qquad and \qquad f'(1) = 1 \tag{3.2}$$

To solve the Falkner-Skan problem, that is a third-order nonlinear ordinary differential equation, we rewrite the equation to three first-order ordinary differential equations. We then have three so-called initial value problems which can be solved. The Falkner-Skan problem is rewritten in such a way that is an equation involving only a first-derivative:

$$\frac{df}{d\eta} = f', \qquad with \quad f(0) = 0 \tag{3.3.a}$$

$$\frac{df'}{d\eta} = f'', \qquad with \quad f'(0) = 0 \quad and \quad f'(1) = 1 \tag{3.3.b}$$

$$\frac{df''}{d\eta} = -\frac{1}{2} ff'', \qquad with \quad f''(0) = ? \tag{3.3.c}$$

3.1.1. Mathematical formulation

Now in this particular problem modify a little bit of the first Falkner-Skan equation (3.1)

The governing equation is: Falkner Skan Equation. Then, $\beta = 2m/m+1$

$$\frac{\partial^3 f}{\partial \eta^3} + f\frac{\partial^2 f}{\partial \eta^2} + \beta\left[1-\left(\frac{\partial f}{\partial \eta}\right)^2\right] = 0 \tag{3.3}$$

With the boundary conditions:

$$\begin{aligned} f(0) &= 0 \\ f'(0) &= 0 \\ f'(\eta = \infty) &= 1 \end{aligned} \tag{3.4}$$

The differential equation (3.3) is the other form of Falkner-Skan equation [42].

Reduction of equation (3.3) to a first order system:

To solve the Falkner-Skan equation numerically, equation (3.3) is reduced to a first order system by introducing the three auxiliary variables.

$$f = u_1 \frac{\partial f}{\partial \eta} = u_2 \quad and \quad \frac{\partial^2 f}{\partial \eta^2} = u_3, \tag{3.5}$$

So that we have the following system three coupled ODE's

$$f_1(\eta, u_1, u_2, u_3) = u_1' = u_2 \tag{3.6.a}$$

$$f_2(\eta, u_1, u_2, u_3) = u_2' = u_3 \tag{3.6.b}$$

$$f_3(\eta, u_1, u_2, u_3) = u_3' = -u_1 u_3 - \beta\left(1-u_2^2\right) \tag{3.6.c}$$

The first order system can be written more compactly using vector notation

$$\frac{\partial f}{\partial \eta} = f_1(\eta, u_1, u_2, u_3) \tag{3.7}$$

Thus it is written as:

$$\begin{bmatrix} f_1 \\ f_2 \\ f_3 \end{bmatrix} = \begin{bmatrix} u_2 \\ u_3 \\ -u_1 u_3 - \beta\left(1-u_2^2\right) \end{bmatrix} \tag{3.8}$$

The boundary conditions are:

$$\begin{aligned} u_1(0) &= 0 \\ u_2(0) &= 0 \\ u_2(\eta = \infty) &= 1 \end{aligned} \tag{3.9}$$

Where $\eta = \infty$ is the unknown free boundary used to truncate the semi-infinite interval to a finite one which is to be determining as the part of the procedure. In addition, an initial condition on the second derivatives is introduced to apply the shooting method:

$$\frac{\partial^2 f}{\partial \eta^2} = \alpha; \qquad at \quad \eta = 0 \tag{3.10}$$

Where α is the shooting angle.

3.1.2. Results and discussion

In this section, the output results of equation (3.8) with the given boundary conditions are presented in tabular and graphs.

Below in Table 2, the output of table to is the comparison of Summiya Parveen works and this thesis output for $\beta = 0$. The table is display the result of $f(\eta)$, $f'(\eta)$ and $f''(\eta)$ for four decimal places are very close each other. That is, the present thesis shooting-secant method for a Falkner-Skan equation is a good approximation.

Table 2: Numerical values of $f(\eta), f'(\eta)$ and $f''(\eta)$ for $\beta = 0$

η	$f(\eta)$		$f'(\eta)$		$f''(\eta)$	
	Summiya [43]	**Present result**	Summiya [43]	**Present result**	Summiya [43]	**Present result**
0.0	0	0	0	0	0.4696	0.469700
0.2	0.009391	0.009394	0.093905	0.093925	0.469306	0.469406
0.4	0.037549	0.037558	0.87605	0.187645	0.467254	0.467353
0.6	0.084386	0.084405	0.280575	0.280635	0.461734	0.461831
0.8	0.149674	0.149708	0.371963	0.372041	0.451190	0.451282
1.0	0.232990	0.233042	0.460633	0.460728	0.434379	0.434465
1.2	0.333657	0.333730	0.545246	0.545358	0.410565	0.410641
1.4	0.450724	0.450821	0.624386	0.624511	0.379692	0.379757
1.6	0.582956	0.583080	0.696700	0.696836	0.342487	0.342538
1.8	0.728872	0.729024	0.761057	0.761202	0.300445	0.300482
2.0	0.886797	0.886979	0.816695	0.816845	0.255669	0.255693
2.2	1.054947	1.055160	0.863304	0.863457	0.210580	0.210592
2.4	1.231528	1.231772	0.901065	0.901219	0.167560	0.167563
2.6	1.414824	1.415100	0.930601	0.930754	0.128613	0.128610
2.8	1.603284	1.603591	0.952875	0.953026	0.095113	0.095108
3.0	1.795568	1.795906	0.969055	0.969202	0.067710	0.067705
3.2	1.990581	1.990949	0.980365	0.980510	0.046370	0.046368
3.4	2.187467	2.187866	0.987970	0.988113	0.030535	0.030535
3.6	2.385590	2.386018	0.992888	0.993029	0.019329	0.019332
3.8	2.584499	2.584955	0.995944	0.996084	0.011759	0.011764
4.0	2.783886	2.784372	0.997770	0.997909	0.006874	0.006880
4.2	2.983555	2.984069	0.998818	0.998957	0.003861	0.003867
4.4	3.183383	3.183925	0.999397	0.999536	0.002084	0.002089
4.6	3.383296	3.383866	0.999703	0.999843	0.001081	0.001085
4.8	3.583254	3.583853	0.999859	0.999999	0.000538	0.000542
5.0	3.783235	3.783861	0.999936	1.000076	0.000248	0.000260

From Table 3 below, the output of table to is the comparison of Summiya Parveen works and this thesis output for $\beta =$ 1. The table indicates the results for $f(\eta), f'(\eta)$ and $f''(\eta)$ are not similar to his results and this thesis results.

Table 3: Numerical values of $f(\eta), f'(\eta)$ and $f''(\eta)$ for $\beta = 1$

η	$f(\eta)$		$f'(\eta)$		$f''(\eta)$	
	Summiya [43]	**Present result**	Summiya [43]	**Present result**	Summiya [43]	**Present result**
0.00	0.000000	0.000000	0.000000	0.000000	0.332060	1.232590
0.20	0.006640	0.023330	0.066410	0.226610	0.331990	1.034460
0.40	0.026560	0.088070	0.132770	0.414460	0.331470	0.846340
0.60	0.059740	0.186720	0.198940	0.566280	0.330080	0.675200
0.80	0.106110	0.312450	0.264710	0.685940	0.327390	0.525170
1.00	0.165570	0.459260	0.329780	0.777870	0.323010	0.398060
1.20	0.237950	0.622060	0.393780	0.846680	0.316590	0.293830
1.40	0.322980	0.796690	0.456260	0.896820	0.307870	0.211070
1.60	0.420320	0.979830	0.516760	0.932370	0.296670	0.147430
1.80	0.529520	1.168910	0.574760	0.956870	0.282930	0.100050
2.00	0.650030	1.362040	0.629770	0.973260	0.266750	0.065920
2.20	0.781200	1.557840	0.681310	0.983910	0.248350	0.042140
2.40	0.922300	1.755350	0.728990	0.990630	0.228090	0.026120
2.60	1.072510	1.953920	0.772460	0.994730	0.206460	0.015710
2.80	1.230980	2.153140	0.811510	0.997160	0.184010	0.009160
3.00	1.396820	2.352720	0.846050	0.998560	0.161360	0.005190
3.20	1.569100	2.552520	0.876090	0.999340	0.139130	0.002880
3.40	1.746960	2.752440	0.901770	0.999770	0.117880	0.001570
3.60	1.929530	2.952420	0.923330	1.000010	0.098090	0.000860
3.80	2.116040	3.152430	0.941120	1.000140	0.080130	0.000500

In Table 4,here below, the output of table to is the comparison of Summiya Parveen works and this thesis output for β = -0.1988. The table is display the result of $f(\eta), f'(\eta)$ and $f''(\eta)$ for three decimal places are very close each other. That is, the present thesis shooting-secant method for a Falkner-Skan equation is a good approximation.

Table 4: Numerical values of $f(\eta)$, $f'(\eta)$ and $f''(\eta)$ for $\beta = -0.1988$

η	$f(\eta)$		$f'(\eta)$		$f''(\eta)$	
	Summiya [43]	**Present result**	Summiya [43]	**Present result**	Summiya [43]	**Present result**
0.0	0.000000	0	0.000000	0	0.008416	0.010771
0.2	0.000433	0.000480	0.005659	0.006130	0.048175	0.050530
0.4	0.002794	0.002982	0.019268	0.020210	0.087908	0.090260
0.6	0.008670	0.009093	0.040814	0.042225	0.127512	0.129852
0.8	0.019646	0.020398	0.070249	0.072126	0.166740	0.169049
1.0	0.037288	0.038462	0.107456	0.109789	0.205139	0.207383
1.2	0.063131	0.064816	0.152203	0.154974	0.241999	0.244131
1.4	0.098646	0.100926	0.204087	0.207269	0.276324	0.278277
1.6	0.145201	0.148155	0.262479	0.266026	0.306832	0.308524
1.8	0.204011	0.207707	0.326465	0.330318	0.332012	0.333350
2.0	0.276079	0.280569	0.394820	0.398897	0.350241	0.351132
2.2	0.362128	0.367448	0.465995	0.470198	0.359983	0.360342
2.4	0.462544	0.468708	0.538165	0.542382	0.360032	0.359802
2.6	0.577326	0.584325	0.609319	0.613429	0.349788	0.348956
2.8	0.706066	0.7138677	0.677407	0.681293	0.329487	0.328092
3.0	0.847956	0.856503	0.740520	0.744078	0.300318	0.298454
3.2	1.001840	1.011055	0.797079	0.800230	0.264364	0.262173
3.4	1.166280	1.1760815	0.845994	0.848688	0.224361	0.222013
3.6	1.339969	1.3499852	0.886753	0.888976	0.183301	0.180967
3.8	1.520440	1.531134	0.919431	0.921202	0.143987	0.141818
4.0	1.706960	1.717969	0.944613	0.945976	0.108648	0.106751
4.2	1.089785	1.909093	0.963249	0.964266	0.078699	0.077133
4.4	2.091900	2.103322	0.976488	0.977225	0.054699	0.053474
4.6	2.288816	2.299709	0.985511	0.986036	0.036472	0.035562
4.8	2.485900	2.497535	0.991411	0.991782	0.023327	0.022683
5.0	2.684590	2.696281	0.995113	0.995377	0.014311	0.013875
5.2	2.883850	2.895592	0.997340	0.997533	0.008421	0.008139
5.4	3.083460	3.095235	0.998625	0.998774	0.004753	0.004577
5.6	3.283260	3.295066	0.999337	0.999458	0.002573	0.002466
5.8	3.483170	3.494998	0.999715	0.999819	0.001335	0.00127
6.0	3.683130	3.694982	0.999907	1.000001	0.000663	0.000624
6.2	3.883120	3.894993	1.000000	1.000089	0.00314	0.000290

.

As using shooting-secant method with applying RK4 method for the boundary value problem of a nonlinear third order differential equations on semi-finite intervals. We successfully compute the Falkner-Skan equation.

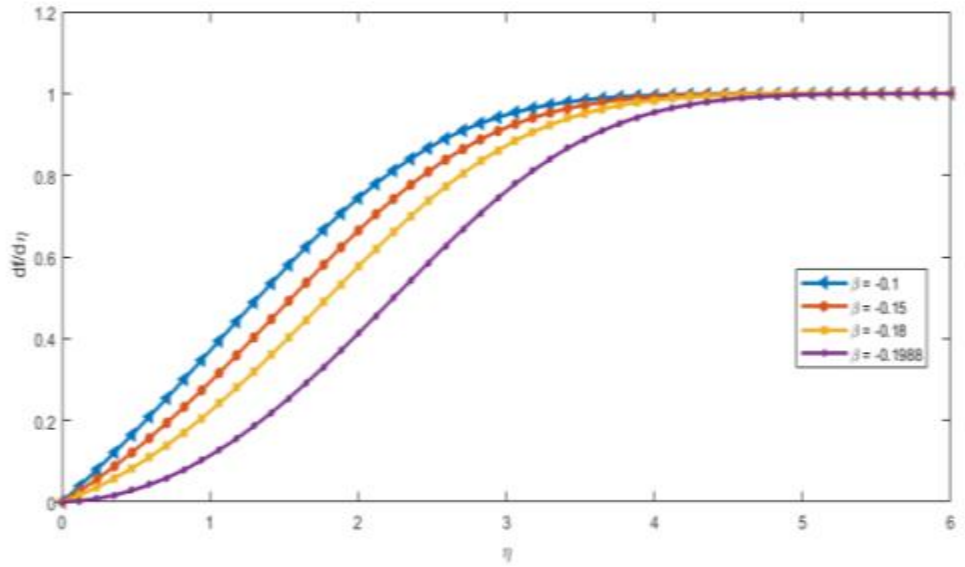

Figure 14: The velocity profile plot for different $\beta \in [-0.1988, 0)$

As Figure 14, the velocity profile for different value of Beta is satisfy the boundary conditions. The beta value is beginning from negative to zero. From this the eta value after 4 is the velocity profile is overlapping each other.

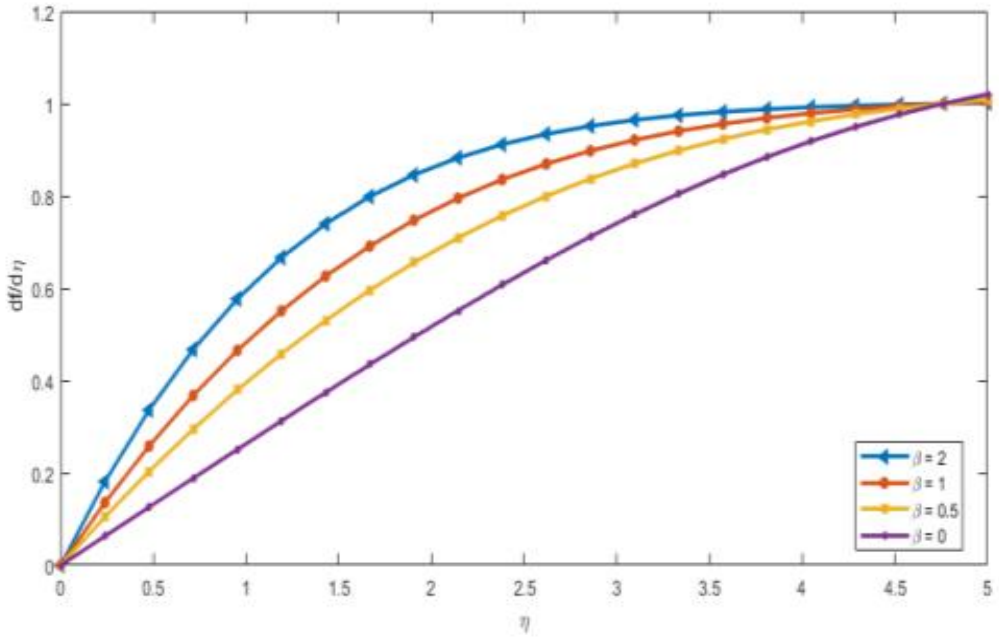

Figure 15: The velocity profile plot for different $\beta \in [0, 2]$

As Figure 15, the velocity profile for different value of Beta is satisfy the boundary conditions. The beta values are positive that is from zero to two. From this the eta value after 4.5 is the velocity profile is overlapping each other.

3.2. The Falkner-Skan Boundary Layer for Numerical Solution of Viscous Flow over a Wedge

The impacts of nanoparticle volume fraction, the kind of nanoparticles, the convective boundary, and the thermal conductivity on the heat move attributes are examined. It is discovered that the heat transfer rate at the surface increments with expanding nanoparticle volume fraction while it diminishes with the convective boundary. In addition, the heat transfer rate at the surface of Ag -water nanofluid is lower than that at the surface of Cu -water nanofluid despite the fact that the thermal conductivity of Cu is lower than that of Ag [26].

3.2.1. Mathematical Formulation

Flow over the top of a wedge can be modeled as an external flow $U(x)$ with a pressure gradient given by the in viscid flow solution. The angle of the wedge is given as $\beta\pi$.

The external flow velocity and pressure gradients are given by:

$$U\left(x\right)=bx^{m} \tag{3.11}$$

$$\frac{\partial p}{\partial x}=-\rho U\left(x\right)\frac{dU\left(x\right)}{dx}=-m\rho b^{2}x-2m-1 \tag{3.12}$$

Where U is the external velocity, P is the pressure, ρ is the density, and x is the position along the wedge. The coefficient b is a function of the flow geometry. As long as the boundary layer is relatively thin, the external flow, and the pressure gradient will be independent of the thickness of the boundary layer. The exponent m is a function of the angle β :

$$m=\frac{\beta}{2-\beta} \tag{3.13}$$

The flow near the wedge will be governed by the boundary-layer equations. The equation for continuity is identical to the flat-plate case:

$$\frac{\partial u}{\partial x}+\frac{\partial v}{\partial y}=0 \tag{3.14}$$

For steady flow in a boundary layer, the *x*-momentum equation is given by:

$$u\frac{\partial u}{\partial x}+v\frac{\partial u}{\partial y}=-\frac{1}{\rho}\frac{dp(x)}{dx}+v\frac{\partial^2 u}{\partial y^2} \tag{3.15}$$

Where u is the x velocity, v is the y velocity, and v is the kinematic viscosity.

These equations can then be transformed, using the non-dimensionalizations and then non-dimensional stream functions developed by Falkner and Skan [41]. These non-dimensionalizations are similar to, but not identical to, those used by Blasius. A non-dimensional flow coordinate η is formed by combining x and y with the other flow variables:

$$\eta = y\sqrt{\frac{m+1}{2}\frac{b}{v}}x^{\frac{m-1}{2}} \tag{3.16}$$

A non-dimensional stream function $f(\eta)$ is found from dimensional stream function ψ :

$$\psi(x,y)=\sqrt{\frac{2bv}{m+1}}x^{\frac{m+1}{2}}f(\eta) \tag{3.17}$$

The non-dimensional velocities are given as:

$$u^{*}=\frac{u}{U(x)}=f'(\eta) \tag{3.18.a}$$

$$v^{*}=\frac{v}{\sqrt{\frac{2}{m+1}vbx^{m-1}}}=\left[f(\eta)-\frac{m-1}{m+1}\eta f'(\eta)\right] \tag{3.18.b}$$

A governing equation for f can be found by substituting these non-dimensional terms into the x-momentum equation:

$$f'''(\eta)+\beta_0 f(\eta)f''(\eta)+\beta\left(1-f'(\eta)^2\right)=0\,,\qquad \eta\in[0,\infty) \tag{3.19}$$

For the no-slip case, the boundary conditions are:

$$u^*(y=0)=0 \rightarrow f'(\eta=0)=0 \tag{3.20.a}$$

$$v^*(y=0)=0 \rightarrow f(\eta=0)=0 \tag{3.20.b}$$

$$u^*(y\rightarrow\infty)=1 \rightarrow f'(\eta\rightarrow\infty)=1 \tag{3.20.c}$$

3.2.2. Results and discussion

The iterative method is existing for the boundary value problems of a discussion of nonlinear third-order differential equation on semi-infinite intervals. The boundary value problem on an infinite interval is transformed to a free boundary problem on a finite interval, using the boundary formulation. This is then solved by nonlinear shooting. We are comparing the results with the previous work B.D. Ganpol's [44] variation of velocity profile with α namely the shooting angle $f''(0)$ for Homann flow in Figure 16.

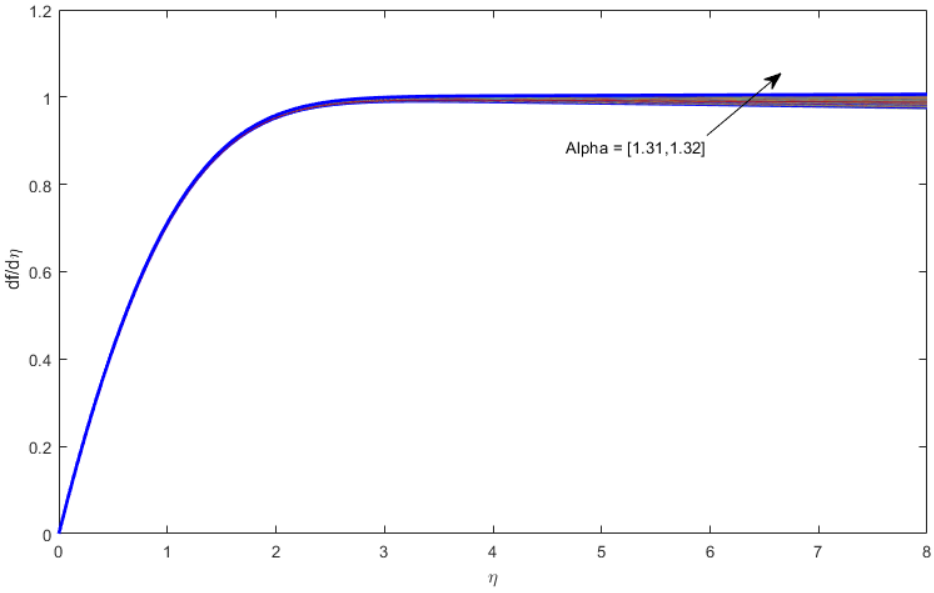

Figure 16: Velocity profile variation with α for Homann flow

From Figure 16, the true for all the physically relevant determine is $\beta > 0$. That is value of β is $\beta_0 = 2$ and $\beta = 1$. The asymptotic velocity profile the numerically positive β for the α value is decrease. Also B.D. Ganapol [44] submitted variation of the velocity profile for $\beta = -0.1$ according to Figure17.

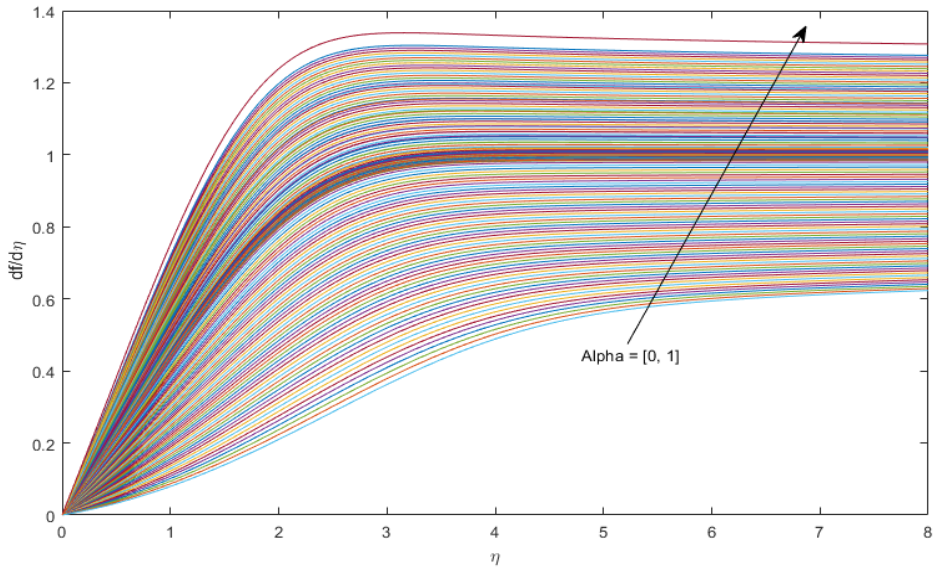

Figure 17: The velocity profile of the Variation for $0 \le \alpha \le 1$ and $\beta = -0.1$

As Figure 17 indicates the velocity profile for this figure is plots for iteration. The value of α is between 0 and 1 and the value of beta is negative.

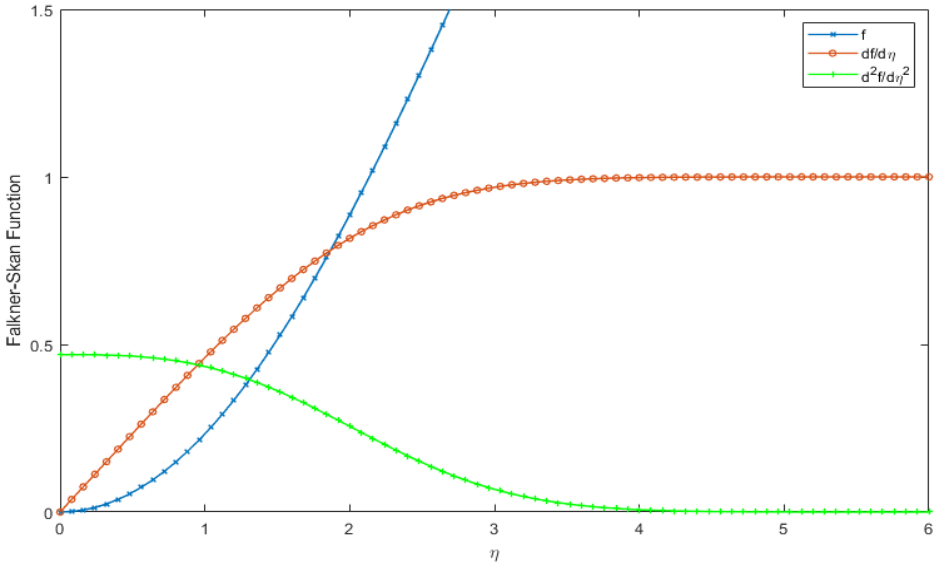

Figure 18: Falkner-Skan functions variation

As Figure 18, the plot is known Falkner-Skan equation(3.1) of $f(\eta), f'(\eta)$ and $f''(\eta)$. This plots are the Falner-Skan equation for the $f(\eta), f'(\eta)$ and $f''(\eta)$, with the given boundary conditions.

The following table 5, compares the results obtained by B.D. Ganapol [44] Blasius flow profiles with the results obtained by the present method. From this table we

observed that the present results and the previous author's results are the same. That is the shooting-Secant method is a power full numerical method for approximate solution.

Table 5: Blasius flow profiles of eta value are from 0.0 to 8.8 and compare with B.D. Ganapol paper's result.

η	f		f'		f''	
	Ganapol [44]	**Present result**	**Ganapol** [44]	**Present result**	**Ganapol** [44]	**Present result**
0.0	0.00000000E+00	0.00000000e+00	0.000000E+00	0.0000000e+00	3.320573362E-01	3.320581523106653e-01
0.4	2.655988402E-02	2.656024294e-02	1.327641608E-01	1.327644842888765e-01	3.314698442E-01	3.314706663748230e-01
1.0	1.655717258E-01	1.655728431644791e-01	3.297800312E-01	3.297807866344531e-01	3.230071167E-01	3.230079297469711e-01
1.4	3.229815738E-01	3.229832969248536e-01	4.562617647E-01	4.562627332141478e-01	3.078653918E-01	3.078661664594144e-01
2.0	6.500243699E-01	6.500270469675202e-01	6.297657365E-01	6.297668831002603e-01	2.667515457E-01	2.667521997494688e-01
2.4	9.222901256E-01	9.222934364289904e-01	7.289819351E-01	7.289831193212341e-01	2.280917607E-01	2.280923048863939e-01
3.0	1.396808231E+00	1.396812531103267e+00	8.460444437E-01	8.460455876192247e-01	1.613603195E-01	1.613607429113598e-01
3.4	1.746950094E+00	1.746955125583579e+00	9.017612214E-01	9.017622629669844e-01	1.178762461E-01	1.178767141805685e-01
4.0	2.305746418E+00	2.305752642191260e+00	9.555182298E-01	9.555190041482240e-01	6.423412109E-02	6.423496949180482e-02
4.4	2.692360938E+00	2.692367943587843e+00	9.758708321E-01	9.758714181394009e-01	3.897261085E-02	3.897385839244390e-02
5.0	3.283273665E+00	3.283281695239100e+00	9.915419002E-01	9.915423640658988e-01	1.590679869E-02	1.590850961157098e-02
5.4	3.680919063E+00	3.680927661192650e+00	9.961553040E-01	9.961558422565102e-01	7.927659815E-03	7.929403085885717e-03
6.0	4.279620923E+00	4.279630273301652e+00	9.989728724E-01	9.989736797275167e-01	2.402039844E-03	2.403408609700753e-03
6.4	4.679356615E+00	4.679366454024485e+00	9.996117017E-01	9.996127063974518e-01	9.806151170E-04	9.816013303256071e-04
7.0	5.279238811E+00	5.279249410241051e+00	9.999216041E-01	9.999228302407683e-01	2.201689553E-04	2.206480293178852e-04
7.4	5.679220147E+00	5.679231277063972e+00	9.999754577E-01	9.999767692205621e-01	7.359298339E-05	7.384918026412033e-05
8.0	6.279213431E+00	6.279225380382528e+00	9.999962745E-01	9.999976467894631e-01	1.224092624E-05	1.232256388324610e-05
8.4	6.679212609E+00	6.679225112875630e+00	9.999990369E-01	1.000000424387817e+00	3.349939753E-06	3.383350100340170e-06
8.8	7.079212403E+00	7.079225463769060e+00	9.999997695E-01	1.000001163247565e+00	8.462841214E-07	8.586419674311345e-07

In this table 6, the thermo-physical properties of fluid and nanoparticles are given.

Table 6: Thermo-physical properties of fluid and nanoparticles [26]

	Physical properties		Fluid phase(water)
	Cu	Ag	
C_p(J/kg K)	385	235	4179
ρ(kg/m^3)	8933	10500	997.1
k(W/mK)	400	429	0.613

The governing equation is:

$$\frac{1}{(1-\phi)^{2.5}\left(1-\phi+\frac{\phi\rho_s}{\rho_f}\right)} f'''+mff''+1-f'^2=0 \tag{3.21}$$

$$f(0)=s,\quad f'(0)=\lambda,\quad f'(\eta\to\infty)\to 1 \tag{3.22}$$

Here, s is the suction $(s>0)$ parameter, $\lambda=c/a$ is the stretching $(\lambda>0)$ or shrinking $(\lambda<0)$ parameter and φ is the nanoparticle volume fraction, ρ_f is the reference density of the fluid fraction, ρ_s is the reference density of the solid fraction. Values of $f''(0)$ for $\varphi=0$ with m = 2 and s = 0 (impermeable surface) evaluated as Table 6.

Table 7: Values of $f''(0)$ for $\varphi=0$ with *m* = 2 and *s* = 0 (impermeable surface)

λ	$f''(0)$	
	Mohammad Mehdi Keshtkar [26]	Present result
1	0	0
0.5	0.78032	0.78033307
0.2	1.13374	1.13377650
0.1	1.22911	1.229157428
0	1.311938	1.312002398
- 0.25	1.45664	1.45680972
- 0.5	1.49001	1.49052754
- 0.75	1.35284	1.35512458
- 0.95	0.94690	0.96929056
- 0.9945	0.64502	0.75530412
- 0.99945	0.500204	0.71868981
- 1	0.319476	0.71428664

We obtained this table (Values of $f''(0)$ for $\varphi = 0$ with $m = 2$ and $s = 0$) according to Table 7.

Table 8: Values of $f''(0)$ for Cu nanoparticles with $m = 2$ and $s = 0.5$

λ	$f''(0)$			
	$\varphi = 0$		$\varphi = 0.1$	
	Keshtkar [26]	Present result	Keshtkar [26]	Present result
1	0	0	0	0
0.5	1.1031	1.1033	1.3690	1.3691
0.2	1.6614	1.6618	2.0716	2.0717
0.1	1.8279	1.8284	2.2835	2.2836
0	1.9839	1.9845	2.4833	2.4834
- 0.25	2.3229	2.3241	2.9255	2.9258
- 0.5	2.5785	2.5807	3.2747	3.2752
- 0.75	2.7298	2.7344	3.5102	3.5112
- 1	2.7373	2.7481	3.5954	3.5979
- 1.2	2.6361 (0.4403)	2.6018	3.5042 (0.44002)	3.5101
- 1.25	1.08223 (0.5672)	2.5302	3.4483 (0.5634)	3.4559
- 1.3	2.3858 (0.7150)	2.4370	3.3736 (0.6974)	3.3839

That we calculate values of $f''(0)$ for this case(cu-water nanofluid , m=2 & s=0.5) as Table 8.

Table 9: Values of $f''(0)$ for cu-water with $m = 2$ and $s = 0.5$

λ	$f''(0)$					
	$\varphi = 0$		$\varphi = 0.1$		$\varphi = 0.2$	
	Mohammad Mehdi Keshtkar [26]	Present result	Mohammad Mehdi Keshtkar [26]	Present result	Mohammad Mehdi Keshtkar [26]	Present result
1	0.02	0	0.02	0	0.02	0
0.5	1.1	1.1031	1.38	1.3690	1.44	1.4386
0.2	1.66	1.6614	2.08	2.0716	2.2	2.1792
0.1	1.82	1.8279	2.28	2.2835	2.4	2.4031
0	1.98	1.9839	2.48	2.4833	2.62	2.6146
- 0.25	2.32	2.3229	2.92	2.9255	3.08	3.0846
- 0.5	2.58	2.5785	3.28	3.2747	3.44	3.4594
- 0.75	2.74	2.7298	3.5	3.5102	3.72	3.7182
- 1	2.72	2.7373	3.58	3.5955	3.84	3.8256

They draw velocity profiles *f(η)* for Cu nanoparticles when $m=2,\ \varphi=0.1,\ \lambda=-1.5$ and various values of *s* as table 9.

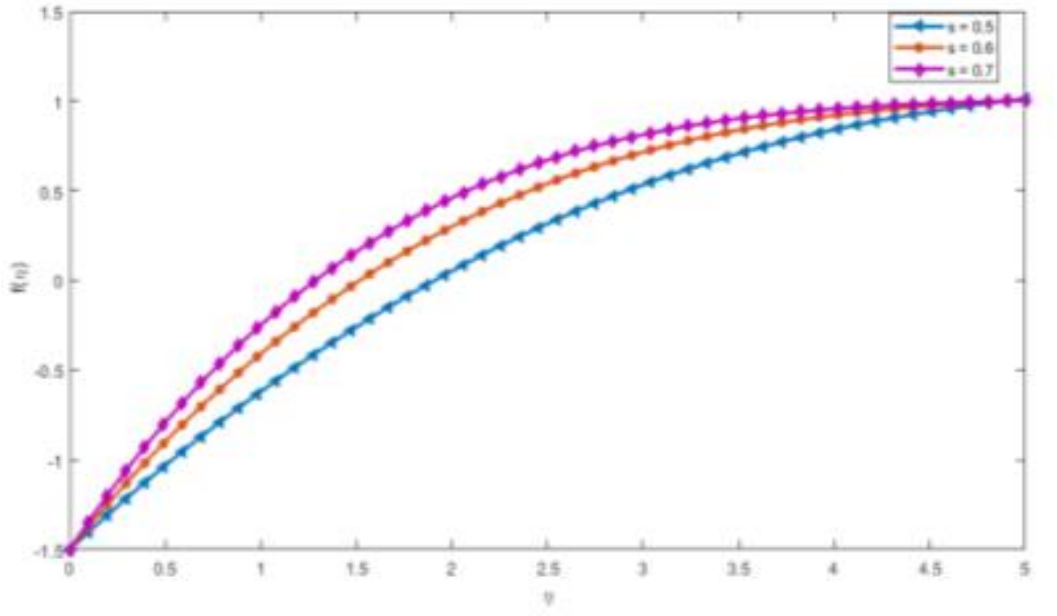

.

Figure 19: Velocity profiles for Cu nanoparticles when $m=2,\ \varphi=0.1,\ \lambda=-1.5$ and various values of $s=[0.5,\ 0.6,\ 0.7]$.

We obtain one of these velocity profile (for s=0.5) as Figure 19. In this figure as expected the velocity profile approach to number 1.

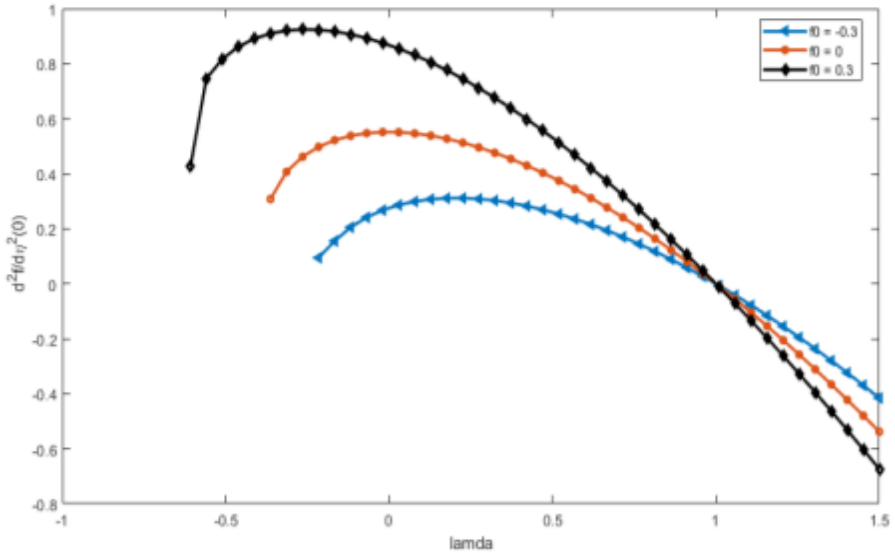

Figure 20: Variaton of $f''(0)$ with for Cu-water nanofluid and different values of $f_0=[-0.3,\ 0,\ 0.3]$ when $\varphi=0.1$

As figure 20, Variation of $f''(0)$ with φ for Cu-water nanofluid and different values of f_0 when $\varphi = 0.1$ in this paper is given.

We obtained this variation as Table7. In this table, variation of $f''(0)$ with φ for Cu-water nanofluid and different values of f_0 when $\varphi = 0.1$ are given

Table 10: Values of $f''(0)$ for cu-water when $\varphi = 0.1$

λ	$f''(0)$					
	$f_0 = -0.3$		$f_0 = 0$		$f_0 = 0.3$	
	Mohammad Mehdi Keshtkar [26]	Present result	Mohammad Mehdi Keshtkar [26]	Present result	Mohammad Mehdi Keshtkar [26]	Present result
-0.5					0.25	0.8250
0	0.3	0.27412	0.55	0.5520	0.87	0.8675
0.5	0.27	0.25978	0.4	0.3866	0.52	0.5307
1	0.02	-0.0001	0.02	-0.0005	0.02	0.0002
1.5	-0.42	-0.4158	-0.52	-0.5377	-0.67	-0.6732

As table 10, the results of Mohammad Mehdi Keshtkar **[26]** and our results are almost the same. This implies that our shooting-Secant method his method that is implicit finite difference method results outputs are much closed. But the $f''(0)$ when $\varphi = 0.1$and $= -0.3$ at $\lambda = 1$ the present result is varies. However, our result are satisfy the given condition.

Table 11: Values of $f''(0)$ when $\varphi = 0.1 \text{and} = -0.3$

λ	$f''(0)$	
	Mohammad Mehdi Keshtkar [26]	Present result
-0.2	0.1	0.1475
0	0.27	0.2656
0.2	0.3	0.2947
0.4	0.27	0.2722
0.6	0.2	0.2052
0.8	0.12	0.1248
1	0.02	0.0002
1.2	-0.12	-0.1160

As table 11, we obtained variation of $f''(0)$ with λ. The comparison of Mohammad Mehdi Keshtkar [26] work and the thesis results are much closed.

Generally, For investigate the unknown boundary for the shooting angle is used secant's method. The Runge-Kutta fourth order method used for the initial values problems arise during shooting. Finally, this thesis is successfully computing several cases of the Falkner-Skan equation. The error tolerance is 10^{-5}, that is the computing is good accuracy.

Flow over a wedge was investigated including a nonslip and slip boundary condition. This problem was solved for compared with Nano fluid and Newtonian fluid. Moreover the problem of required convection boundary layer flow close the stagnation point on a porous stretching/shrinking surface in a Nano fluid is considered in theory.

Chapter 4

The Effect of Velocity Slip Parameter on Boundary Layer Flow over a Static Wedge

The boundary layer theory particularly clarifies the consistent state flow more than a level plate at zero angles which is perceived as Blasius [23] flow. The Falkner-Skan condition was offered by Falkner-Skan. As its name offers, the Falkner-Skan condition was introduced by Falkner and Skan. They are built up investigation about viscous fluid lower the more than a static wedge.

The problem of the Falkner-Skan boundary layer flow past a wedge considering the velocity slips condition [45]. It is discovered that as the velocity slip boundary increases, the speed profile is decreases and the skin contact and warmth move diminished while the mass exchange is expanded [23]. Expanding the warm slip boundary causes diminishes in the warmth and mass exchange rates.

4.1. Mathematical Formulation

Falkner-Skan boundary layer flow past a static wedge is considering a steady two-dimensional. We consider the effects of slip condition; let as the velocity of the free stream is $u_e = U_\infty x^m$, we consider a Cartesian coordinate system (x, y), where x and y are the coordinates measured along the surface of the wedge and normal to it, respectively. Under the above conditions, the partial differential equations governing [23] the problem and the corresponding boundary conditions are:

$$\frac{\partial u}{\partial x} + \frac{\partial v}{\partial y} = 0 \tag{4.1}$$

$$u\frac{\partial u}{\partial x} + v\frac{\partial u}{\partial y} = u_e\frac{\partial u_e}{\partial x} + v\frac{\partial^2 v}{\partial y^2} \tag{4.2}$$

Subject to the boundary conditions,

$$y = 0, \quad u = N_1(x)v\frac{\partial u}{\partial y}, \quad v = 0, \quad y \to \infty, \; u \to u_e(x) \tag{4.3}$$

Hear u and v are the velocity components along x, y axis, ρ is the fluid density, v is the kinematic viscosity, N the slip parameter.

We now introduce the following relations for u and v as follows:

$$u = \frac{\partial \psi}{\partial y}, \quad v = -\frac{\partial \psi}{\partial x} \tag{4.4}$$

Where ψ is the stream function, then equation(4.1) holds and equation (4.2) transforms to the following equation:

$$\psi_x \psi_{xy} - \psi_x \psi_{yy} = u_e \frac{du_e}{dx} + v\psi_{yyy} \tag{4.5}$$

and the boundary conditions(4.3) become,

$$y = 0, \psi_y = N_1 v \psi_{yy}, \quad \psi_x = 0, \quad \psi_y = u_e(x) \tag{4.6}$$

To transform equation (4.5) to an ordinary differential equation, we introduce the following scaling transformation,

$$x^* = \lambda^{\varepsilon c_1} x, \quad y^* = \lambda^{\varepsilon c_2} y, \quad \psi^* = \lambda^{\varepsilon c_3} \psi \tag{4.7}$$

Where c's are constants. Therefore, equation (4.5) will remains invariant under the group of transformations (4.7) if,

$$c_2 = \frac{1}{2}(1-m)c_1, \quad c_3 = \frac{1}{2}(1+m)c_1 \tag{4.8}$$

The characteristics equations are,

$$\frac{dx}{c_1 x} = \frac{dy}{\frac{1}{2}(1-m)c_1 y} = \frac{d\psi}{\frac{1}{2}(1+m)c_1 \psi} \tag{4.9}$$

Solving the above equations we the following similarity transformations,

$$\eta = x^{\frac{1-m}{2}} y, \quad \psi = x^{\frac{1+m}{2}} f(\eta) \tag{4.10}$$

Substituting from(4.10) into (4.5) and (4.6), we get,

$$vf''' + \frac{m+1}{2} ff'' - m(f')^2 + mU_\infty^2 = 0 \tag{4.11}$$

Where prime is the derivative with respect to η. The boundary conditions become,

$$f(0) = 0, \quad f'(0) = vN_1(x) x^{(m+1)/2} f''(0), \quad f'(\infty) \to U_\infty \tag{4.12}$$

We introduce the following dimensionless independent variable

$$\eta = \sqrt{\frac{U_\infty (m+1)}{2v}} \eta \tag{4.13}$$

Also, form of the boundary condition $N_1(x) = \sqrt{2}N \Big/ \sqrt{vU_\infty (m+1)x^{m+1}}$ Where N is the constant velocity slip parameter. Then using(4.13), equation (4.11) become,

$$f''' + ff'' + \frac{2m}{m+1}\left[1-(f')^2\right] = 0 \tag{4.14}$$

and the corresponding boundary conditions (4.12) become,

$$f(0) = 0, \quad f'(0) = Nf''(0), \quad f'(\infty) = 1 \tag{4.15}$$

4.2. Results and Discussion

In this section, the output results are presented in tabular and graphs.

Table 13, we are comparing the result with the previous works which is our method is Shooting-Secant method and the previous works method is infinite difference methods. From the output the present result and the previous results are much closed. Then we observed that our method is a powerful approximation. The previous works was obtained by Yacob in (2011) [46] and Muatazz Abdolhadi Bashir, Mustafa Mamat and Ilyani Abdullah, [23] with the present results for $N = 0$.

Table 12: Values of $f''(0)$ for different values of m when N = 0

m	Yacob [46]	Bashir, et.al [23]	Present result
0	0.4996	0.46960007	0.4696197
1/11	0.6550	0.65499372	0.6549966
0.2	0.8021	0.80212560	0.8021264
1/3	0.9277	0.92768004	0.9276800
0.5	1.0389	1.03890348	1.0389027
1	1.2326	1.23258764	1.2325847

Table 12 results indicate that there is the similar agreement between the present results and the result obtained by Yacob [46] and Bashir, et.al [23].

Table 13: Shear stress coefficient for different values m, Values of velocity profiles, N

m	N	$f'(0)$		$f''(0)$	
		Bashir, [23]	**Present result**	**Bashir,** [23]	**Present result**
0.2	0.1	0.0767407205	0.0767407822	0.7674072052	0.7674078229
	0.4	0.2642342882	0.2642344263	0.6605857204	0.6605860658
	0.7	0.3973701457	0.3973700112	0.5676716367	0.5676714446
	1	0.4929949612	0.4929947535	0.4929949612	0.4929947535
0.5	0.1	0.0972083207	0.0972082324	0.9720832067	0.9720823240
	0.4	0.3164097033	0.3164093173	0.7910242584	0.7910232934
	0.7	0.4577470706	0.4590850123	0.6539243866	0.6558357319
	1	0.5531097083	0.5542858104	0.5531097083	0.5542858104
0.8	0.1	0.1083608791	0.1087773668	1.0836087909	1.0877736681
	0.4	0.3429196697	0.3436481552	0.8572991742	0.8591203880
	0.7	0.4870643731	0.4877406623	0.6958062472	0.6967723748
	1	0.5814728292	0.5877410108	0.5814728292	0.5877410108
1.5	0.1	0.1218758371	0.1219371633	1.2187583709	1.2193716335
	0.4	0.3733379099	0.3734356041	0.9333447747	0.9335890103
	0.7	0.5196006099	0.5198874198	0.7422865856	0.7426963141
	1	0.6123133420	0.6123865337	0.6123133420	0.6123865337

Table 13, Shown that the wall share stresses and constant velocity slip parameter (N) are inversely proportional. That is, when the wall share stress decreases with the slip parameter increases with m. And also the wall velocity increases with an increase in m and N .

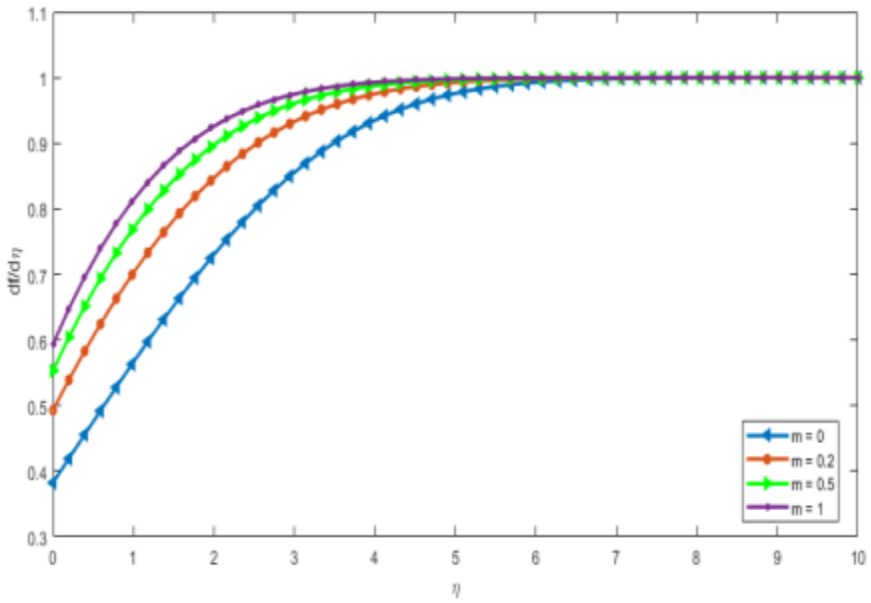

Figure 21: Effect of m on the velocity when N = 1

As Figure 22, the velocity profiles are affected by the parameter m. And the velocity profile is increasing as well as the effect of the power law parameter is increase.

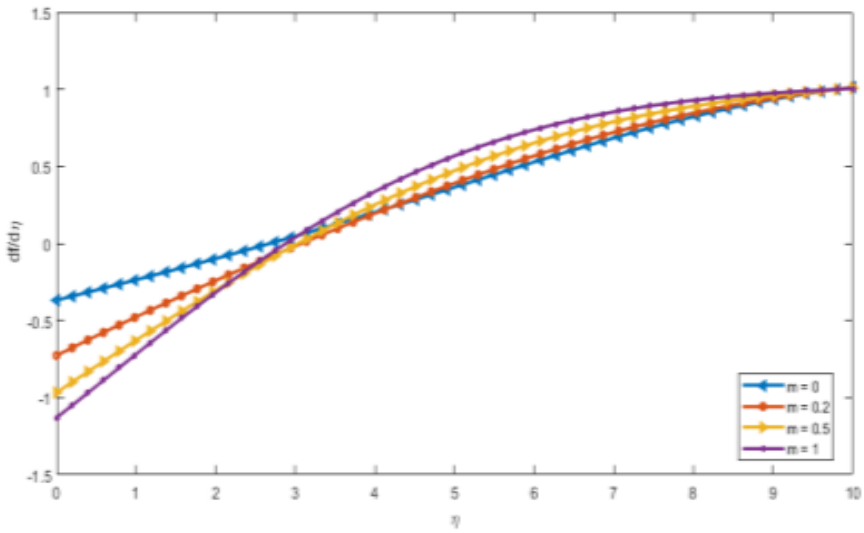

Figure 22: Effects of on the velocity when N = -1.

As figure 23, we observe the effect of the different value of m and the fixed value of the constant velocity slip parameter. Then, the value of m is maximizing as dimensionless independent variable increases, the Falkner-Skan boundary layer flow past a static wedge.

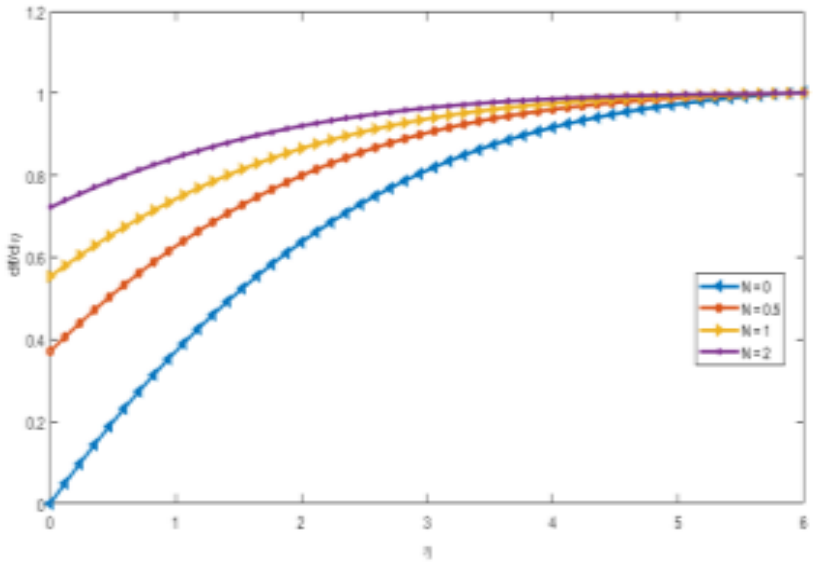

Figure 23: Effects of $N(N \geq 0)$ on the velocity, when $\mathrm{m} = 0.5$.

As Figure 24, the effect of the velocity slips for $N \geq 0$ at $\mathrm{m} = 0.5$. From this plot we observe the constant velocity slip varies but the Falkner-Skan boundary layer flow past a static wedge. The boundary layer is 1.

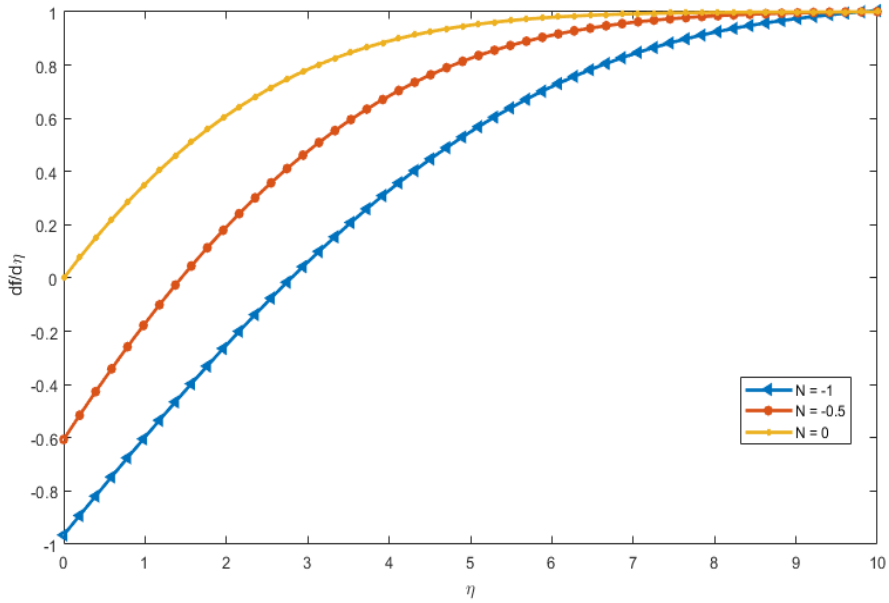

Figure 24: Effects of $N(N \leq 0)$ on the velocity, when m = 0.5

From Figure 25, the plots are demonstrate the effect of different value of the constant velocity parameters. The flow static wedge is affected by the constant velocity parameters. That is the slip parameter is less than zero and preserves the boundary layer.

We summarize this chapter as, the effect of velocity slip parameter on boundary layer flow over a static wedge. For this work we compared the result with the previous work Yacob's and Muatazz Abdolhadi Bashir papers. We observed the solution of the numerical solution was accurate. By means of ascending transformations, the ordinary differential equation governs the problem. The effect of the velocity slip for an ordinary differential equation on the Falkner-Skan boundary layer flow past a wedge has transformed. Additional, using shooting-secant method, which shows the increase of the slip parameter with the velocity increases, the numerical results of the ordinary differential equation are obtained.

Chapter 5

MHD viscous flow over a shrinking sheet for closed form Analytical solutions

The flow prompted by a moving limit is significant in the expulsion measures in plastic and metal ventures [24] [47]. The shrinking sheet issue was additionally reached out to control law shrinking velocity or different fluids [48] [49]. A closed form analytic solution for steady MHD flow over a permeable shrinking sheet subjected to mass attractions.

5.1. Mathematical formulation

Consider a stead y, two-dimensional laminar flow over a continuously shrinking sheet in a quiescent fluid [24]. The sheet shrinking velocity is $U_w = -U_0 x$ and the wall mass transfer velocity is $v_w = v_w(x)$, which will be determined later. The *x*-axis runs along the shrinking surface in the direction opposite to the sheet motion and the *y*-axis is perpendicular to it. The governing NS equations of this problem

$$\frac{\partial u}{\partial x}+\frac{\partial v}{\partial y}=0 \tag{5.1}$$

$$u\frac{\partial u}{\partial x}+v\frac{\partial u}{\partial y}=-\frac{1}{\rho}\frac{\partial p}{\partial x}+\nu\left(\frac{\partial^2 u}{\partial x^2}+\frac{\partial^2 u}{\partial y^2}\right)-\frac{\sigma B^2}{\rho}u \tag{5.2}$$

$$u\frac{\partial v}{\partial x}+v\frac{\partial v}{\partial y}=-\frac{1}{\rho}\frac{\partial p}{\partial y}+\nu\left(\frac{\partial^2 v}{\partial x^2}+\frac{\partial^2 v}{\partial y^2}\right) \tag{5.3}$$

With the boundary conditions (BCs)

$$u(x,0)=-U_0 x,\ \ v(x,0)=v_w(x),\ \text{ and }\ u(x,\infty)=0 \tag{5.4}$$

Where u and v are the velocity components in the *x* and *y* directions respectively, *m* is the kinematic viscosity, *p* is the fluid pressure, ρ is the fluid density, and σ is the electrical conductivity of the fluid. The magnetic field with strength B is applied in the vertical direction and the induced magnetic field is neglected. This group of NS equations is valid for small magnetic Reynolds numbers. The stream function and the similarity variable can be posited in the following form,

$$\psi(x,y) = f(\eta)x\sqrt{vU_0}, \quad and \tag{5.5.a}$$

$$\eta = y\sqrt{\frac{U_0}{v}} \tag{5.5.b}$$

With these definitions, the velocities are expressed as $u = U_0 f'(\eta)$ and $v = -\sqrt{U_0 v}\, f(\eta)$. The wall mass transfer velocity becomes $v_w(x) = -\sqrt{U_0 v}\, f(0)$. The similarity equation is obtained as follows:

$$f''' + ff'' - f'^2 - M^2 f' = 0 \tag{5.6}$$

With the BCs as follows:

$$f(0) = s, \quad f'(0) = -1 \ \text{ and } \ f'(\infty) = 0 \tag{5.7}$$

Where **s** is the wall mass transfer parameter showing the strength of the mass transfer at the sheet and M is the magnetic with $M^2 = \sigma B^2/\rho U_0$. The pressure term can be obtained from Eq.(5.3) as $\frac{P}{\rho} = v\frac{\partial v}{\partial y} - \frac{v^2}{2} + \text{constant.}$ There is an analytical solution for M = 0 given by Miklavcic and Wang [50] as

$$f(\eta) = c + \frac{1}{c}e^{-cx} \tag{5.8}$$

Where and $c = f(\infty) = f''(0)$ can be found by solving $s = c + 1/c$. It is shown that there are two solutions for this equation for any $s > 2$ and there is one solution for $s = 2$. No solution exists for $s < 2$. There is also an algebraically decaying solution for M = 0 as

$$f(\eta) = \frac{6}{\eta + \sqrt{6}} \tag{5.9}$$

For $s = \sqrt{6}$

In this Letter, we will show a closed form exaction solution of Eq.(5.6) together with the BCs. Assuming the solution has a format as $f(\eta) = a + be^{-\beta\eta}$. Substituting this relation to Eq.(5.6) yields

$$b = \frac{1}{\beta} \tag{5.10}$$

$$a = s - \frac{1}{\beta} \tag{5.11}$$

$$\beta = \frac{s \pm \sqrt{s^2 - \left(4 - 4M^2\right)}}{2} \tag{5.12}$$

Then the solution reads

$$f(\eta) = s - \frac{1}{\frac{s \pm \sqrt{s^2 - \left(4 - 4M^2\right)}}{2}} + \frac{1}{\frac{s \pm \sqrt{s^2 - \left(4 - 4M^2\right)}}{2}} e^{\frac{s \pm \sqrt{s^2 - \left(4 - 4M^2\right)}}{2}\eta} \tag{5.13}$$

and

$$f'(\eta) = -e^{\frac{s \pm \sqrt{s^2 - \left(4 - 4M^2\right)}}{2}\eta} \tag{5.14}$$

5.2. Results and discussion

From the following plots we observed the velocity profiles for the different value of an exact solution at zero and with different values of M = 0.5, 1 and 2 are the rate of the analytic solution is increases.

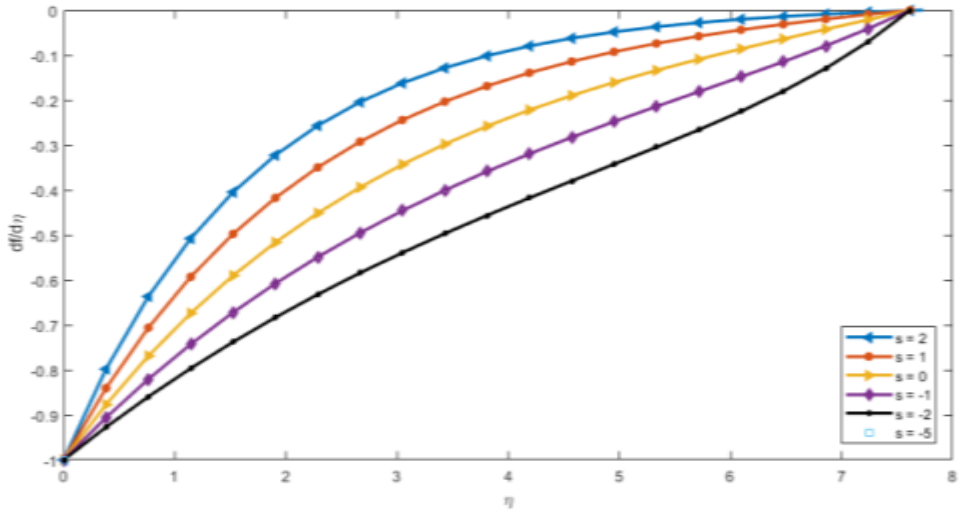

Figure 25: Velocity profiles at mass suction M = 2 under different parameters of $f'(0)$.

As figure 26, the velocity profiles at M = 2 under different initial conditions. The initial condition (s) increases as wall shear stress increases.

The rate of the analytic solution satisfies the boundary conditions. And the figures show the effect of magnetic parameters and the mass suction on the flow field.

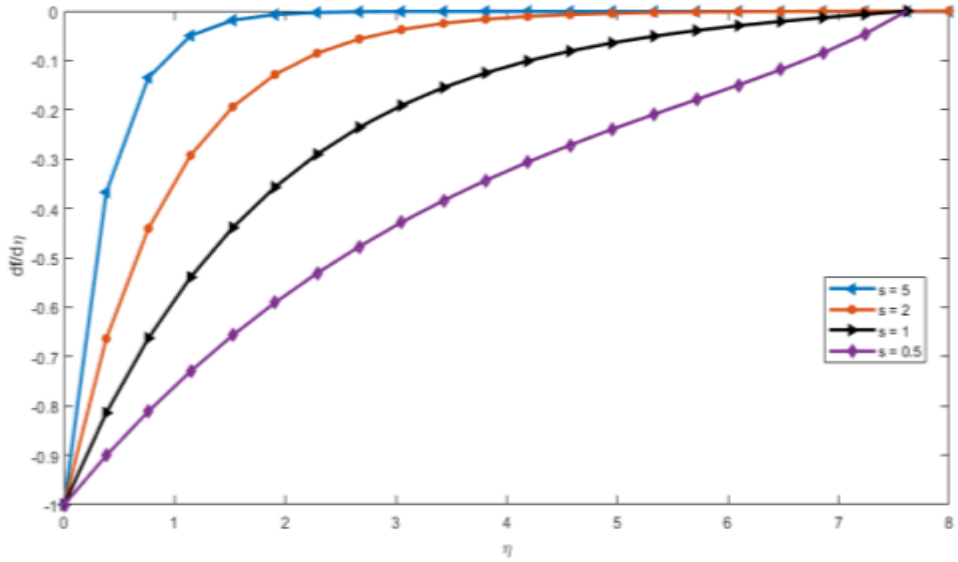

Figure 26: Velocity profiles at M = 1under different mass suction parameters.

As figure 27, the velocity profiles at M = 1 under different initial conditions. The initial condition (s) increases as wall shear stress increases.

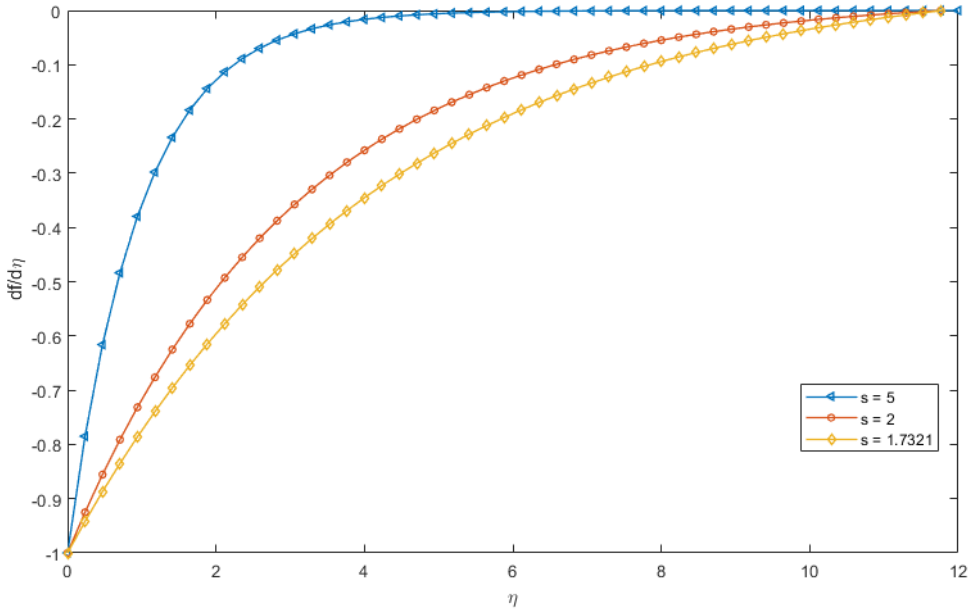

Figure 27: Velocity profiles at M = 0.5 under different mass suction parameters.

It understood that the velocity profiles are blown away from the wall for mass pressure with different values of magnetic parameters and the boundary layer thickness become thicker.

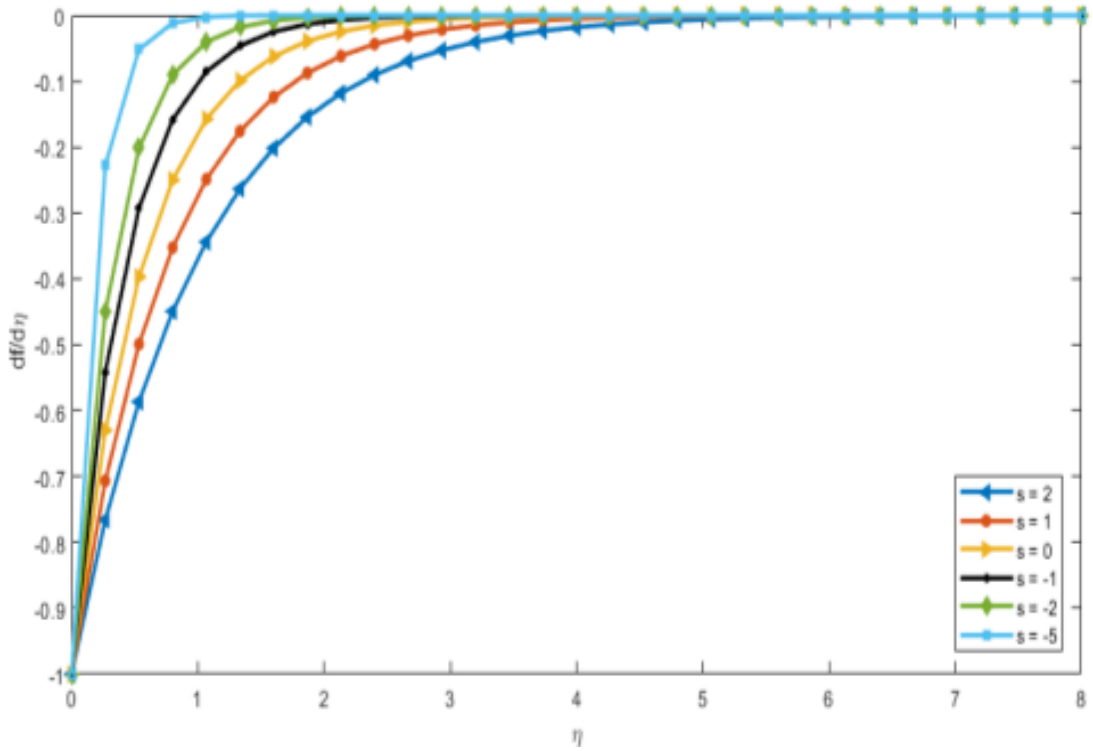

Figure 28: Analytic solution of velocity profiles at M = 2 under different mass suction parameters.

As Figures 29 and 30, the plots are the analytic solution results of the velocity profiles for a fixed magnetic value 2 and different mass transfer parameters.

The magnetohaydrodynamics flow over a shrinking sheet is also gtreatly different from the MHD flow over a stretching sheet for Newtonian fluids and for non-Newtonian fluids.

Finally, the flow of magnetohaydrodynamics over a shrinking sheet often varies significantly from the flow of MHD over a stretching sheet for Newtonian and non-Newtonian fluids [51]. The opposite value sign of the exact solution occurs only for mass suction, which implies that, s is positive. The wall shear stress increases with the increase of the mass suction and magnetic parameters for the positive branch. Nevertheless, the wall shear stress decreases with the increase of the mass suction and magnetic parameters for the negative sign branch. When M = 1, there is only one solution with $\beta = s$ and s must be greater than zero [24]. As the mass suction parameter increases, the wall shear stress for M= 1 increases. There is only one solution for M > 1, say, the positive sign branch, but there is a solution for both mass suction and mass injection $-\infty < s < \infty$, that also shows that with the mass suction parameter, the wall shear stress increases.

Chapter 6

Numerically and Analytical Analysis of MHD boundary layer flow and heat transfer along an infinite porous hot horizontal continuous moving plate

We concerned the two-dimensional magnetohyderodynamics (MHD) coupled boundary layer flow and heat transfer to wards infinity porous hot horizontal continuous moving plat [25]. The flow of an electrically conducting fluid past a continuous moving surface in a tranquil fluid has overflowing applications in many engineering processes, for example, material produced by artificial fibers, polymer expulsion, hot rolling, glass fiber, wire turning, metal turning and expulsion, cooling of metal sheet, so forth. More over the importance is the porous media system [25]. A study of the flow field and the heat transfer can be of necessary advantage from the quality of the final product [52].

6.1. Mathematical Formulation

Assume that two dimensional coupled boundary layer flows and heat transfer of a viscous conductivity of incompressible electrical fluid towards an infinity hot continuous moving plate the presence of constant section at the surface, the free stream constant U_∞ and heat generation. Let us neglect Hall-Effect and the external fluid owing polarization of charge. The plate is moving in flow direction with velocity U_w and temperature is constant, where the flow is to wards x-axis and y-axis is perpendicular to it. The transversal axis is magnetic field B_0.

The usual boundary layer approximations and the governing equations are:

$$\frac{\partial v}{\partial y} = 0 \quad \Rightarrow \quad v = -v_0 \left(\text{constant}\right), \quad v_0 > 0 \tag{5.14}$$

$$\rho\left(-v_0 \frac{\partial u}{\partial y}\right) = \mu \frac{\partial^2 u}{\partial y^2} - \sigma_e B_o^2 u \tag{5.15}$$

$$\rho C_P \left(-v_0 \frac{\partial T}{\partial y}\right) = k \frac{\partial^2 T}{\partial y^2} + \mu \left(\frac{\partial u}{\partial y}\right)^2 + Q\left(T - T_\infty\right) \tag{5.16}$$

The problem appropriate boundary conditions are given by:

$$\begin{aligned} &y=0: \quad u=\mathrm{U}_w, \quad v=-v_0, \quad T=T_w \\ &y\to\infty: \quad u\to\mathrm{U}_\infty, \quad T\to T_\infty \end{aligned} \tag{5.17}$$

Analysis

The energy and momentum equations can be change into the corresponding ordinary differential equation by using non-dimensional parameters:

$$\begin{aligned} &y=y^*\frac{v_0}{v}, \quad Ec=\frac{\mathrm{U}_\infty^2}{C_p\left(T-T_\infty\right)}, \alpha=\frac{\mathrm{U}_W}{\mathrm{U}_\infty}, \quad S=\frac{Qv^2}{kv_0^2}, \\ &\theta=\frac{T-T_w}{T_w-T_\infty}, \quad u=\frac{u}{\mathrm{U}_\infty} \end{aligned} \tag{5.18}$$

The transformed ordinary differential equations are:

$$u''+u'=Mu \tag{5.19}$$

$$\theta''+\mathrm{Pr}\,\theta'+S\theta=-Ec\,\mathrm{Pr}\left(u'\right)^2 \tag{5.20}$$

The transformed boundary conditions are:

$$u\left(0\right)=\alpha,\ \theta\left(0\right)=1\ \ and\ \ u\left(\infty\right)\to 1,\ \ \theta\left(\infty\right)\to 0. \tag{5.21}$$

Where the differentiation with respect to *y*, the Prandtl number is $\mathrm{Pr}=\mu c_p/k$, The dimensionless magnetic parameter is $M=\sigma_e B_0^2\upsilon/\rho v_0^2$, the Eckert number is $Ec=\mathrm{U}_0^2/C_p(T-T_\infty)$ and the heat sink $\left(s>0\right)$ or source $\left(s<0\right)$ is $S=Qv^2/kv_0^2$.

To solve the above equation (1) and (2) subject to the boundary condition (3), we have the analytic solution:

$$u\left(y\right)=A_1e^{n_1y}+A_2e^{n_2y} \tag{5.22}$$

$$\theta\left(y\right)=-A_3e^{2n_1y}-A_4e^{2n_2y}-A_5e^{(n_1+n_2)y}+A_6e^{n_3y}+A_7e^{n_4y} \tag{5.23}$$

Nusselt number and Skin friction

The velocity and temperature fields we can obtain the dimensionless Nusselt number Nu and Skin friction Sk, which are given by:

$$Sk = \left.\frac{\partial u}{\partial y}\right|_{y=0} = A_1 n_1 + A_2 n_2 \tag{5.24}$$

$$Nu = -\left.\frac{\partial \theta}{\partial y}\right|_{y=0} = -2A_3 n_1 - 2A_4 n_2 - A_5\left(n_1 + n_2\right) + A_6 n_3 + A_7 n_4 \tag{5.25}$$

Where the constants

$$\begin{aligned}
n_1 &= \frac{-1+\sqrt{1+4M}}{2}, \\
n_2 &= \frac{-1-\sqrt{1+4M}}{2}, \\
n_3 &= \frac{-\Pr+\sqrt{\Pr^2-4S}}{2}, \\
n_4 &= \frac{-\Pr-\sqrt{\Pr^2-4S}}{2}, \\
A_1 &= \frac{1-\alpha e^{4n_2}}{e^{4n_1}-e^{4n_2}}, \\
A_2 &= \frac{\alpha e^{4n_1}-1}{e^{4n_1}-e^{4n_2}}, \\
A_3 &= \frac{Ec\,\Pr A_1^2 n_1^2}{4n_1^2+2\Pr n_1+S}, \\
A_4 &= \frac{Ec\,\Pr A_2^2 n_2^2}{4n_2^2+2\Pr n_2+S}, \\
A_5 &= \frac{2Ec\,\Pr A_1 A_2 n_1 n_2}{\left(n_1+n_2\right)^2+\Pr\left(n_1+n_2\right)+S}, \\
A_6 &= \frac{e^{4n_4}\left(A_3+A_4+A_5+1\right)-A_3 e^{8n_1}-A_4 e^{8n_2}-A_5 e^{4(n_1+n_2)}}{e^{4n_1}-e^{4n_2}}, \\
A_7 &= 1+A_3+A_4+A_5-A_6.
\end{aligned} \tag{5.26, 5.27}$$

The analytical and numerical solutions results are presented below.

6.2. Results and Discussion

To discuss the effect of various parameters on the velocity field, thermal boundary layer, shearing stress, and coefficient of rate of heat on the wall, the numerical computation of the solution obtained in the preceding section was carried out and they are represented in the following figures.

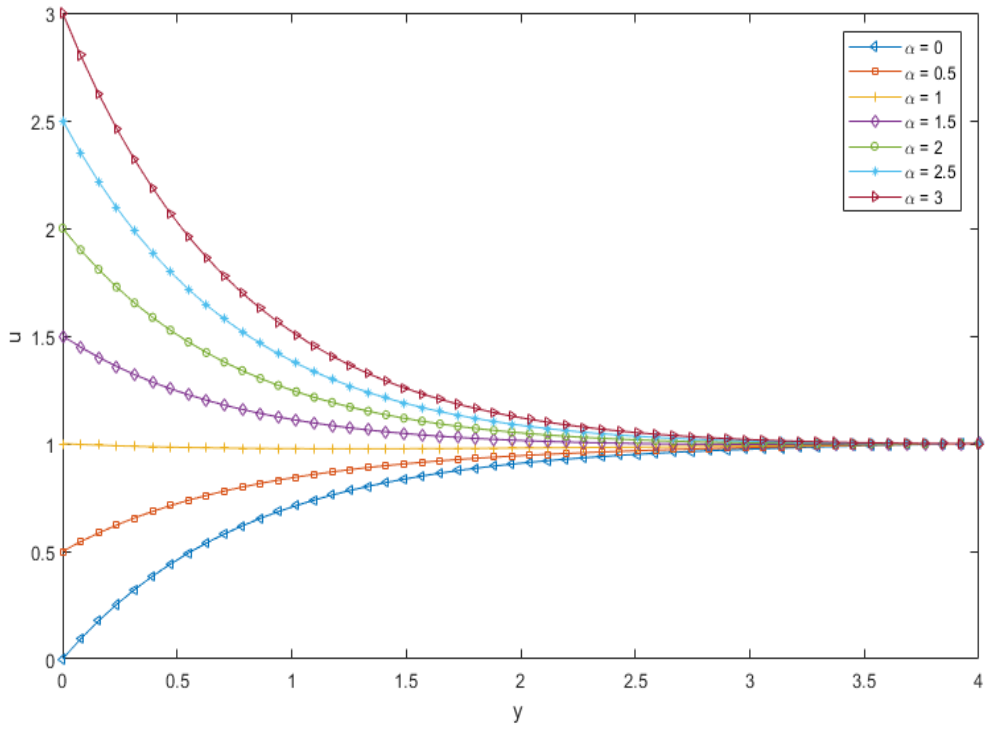

Figure 29: Effect of α on the velocity profile for M = 0, Ec = 0.01, Pr = 1 and S = 0.1.

As Figure 31, shows the effect of plate velocity α on velocity profile for a fixed values of magnetic parameter is zero, prandtl number is one and Eckert number is 0.01. From this figure we observe that the plate velocity is increases as also the velocity is increases.

The plate velocity is less than free stream velocity for $0 < \alpha < 1$, the velocity is concave down and when $\alpha > 1$ that is the plate velocity is greater than free stream velocity, the velocity is concave up [25].

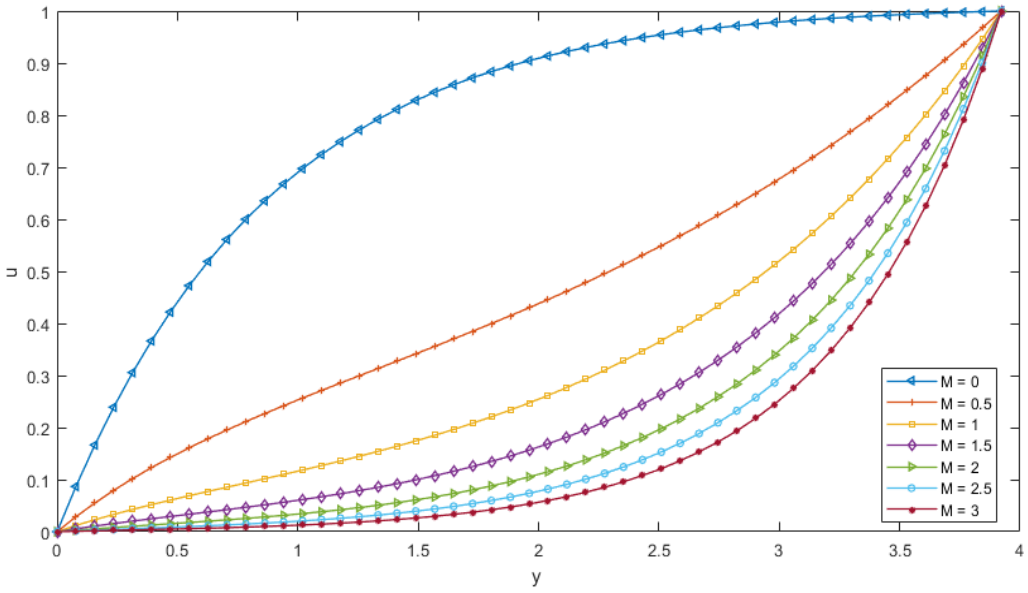

Figure 30: Effect of M on the velocity profile for $\alpha = 0$, Ec = 0.01, Pr = 1 and S = 0.1.

From Figure 32, shows the effect of magnetic parameter M on the velocity profile for the plate velocity $\alpha = 0$ and the Eckert number, Prandtl number and the source or sink values are fixed. Then the magnetic parameter M increases the velocity decreases.

We observe the application of Lorenz force. That is the electrical conductivity flow gives rise for the transverse magnetic field that is a resistance type force. The boundary layer was the slowdown motion of the fluid by this force.

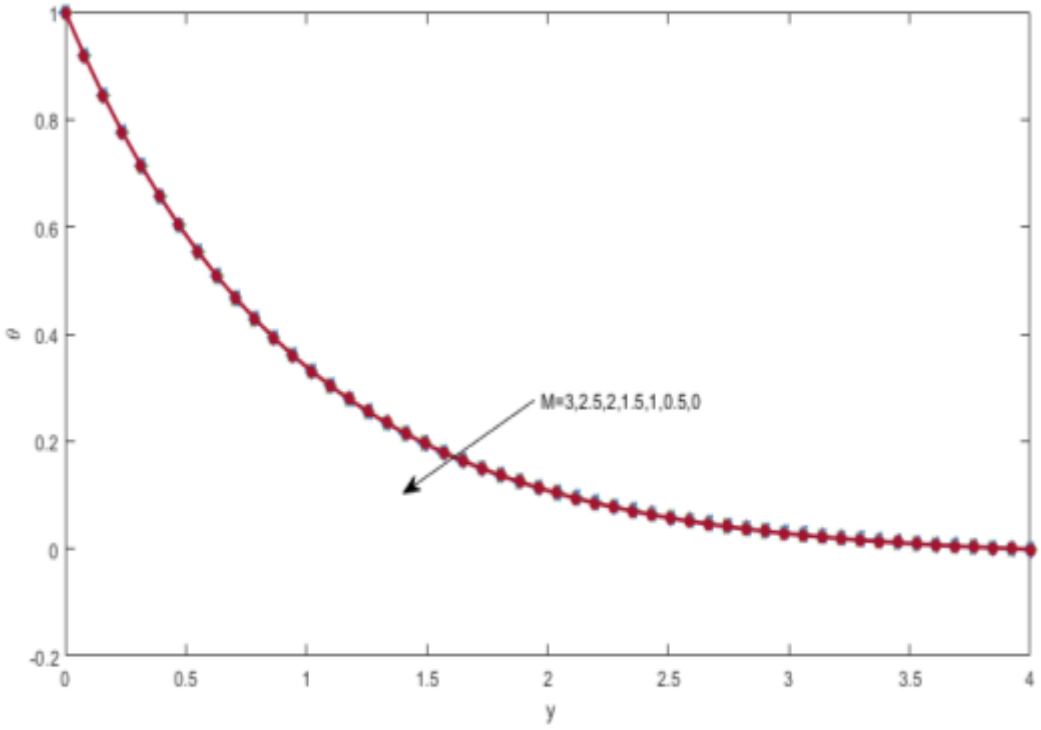

Figure 31: Effect of M on the temperature profile for α = 0.5, Ec = 0.01, Pr = 1 and S = 0.2.

From figure 33, shows the effect of magnetic parameter M on the velocity profile for the plate velocity α and the Eckert number, Prandtl number and the source or sink values are fixed. It shows the magnetic parameter has no effect on temperature.

As figure 34, the effect of Prandtl number on the velocity profile for a fixed value of plate velocity α, the Eckert number, the heat source or sink and the magnetic parameter. We observe that the prandtl number increases with in the temperature profile decreases.

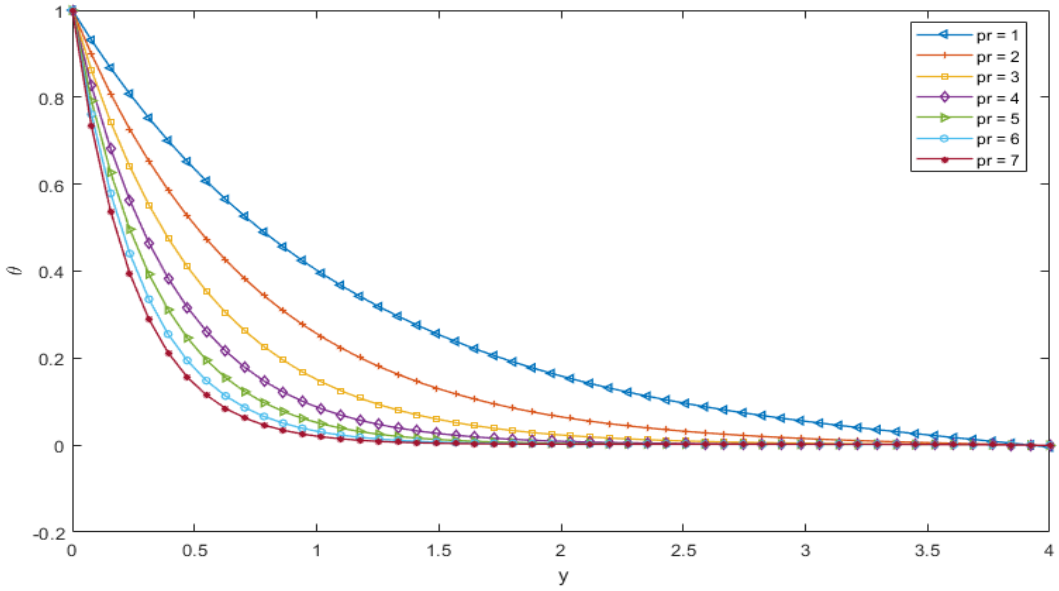

Figure 32: Effect of the prandtl number (Pr) on the temperature profile for $\alpha = 0.5$, Ec $= 0.01$, S $= 0.1$ and M $= 1$.

The viscous boundary layer is thicker than the thermal boundary layer, implying that the viscous boundary layer is thicker. Large Prandtl numbers result in thinning of the thermal boundary layer, as can be seen in this graph. Since temperature reaches zero asymptotically regardless of velocity in this case, there is no effect of Pr on the velocity field.

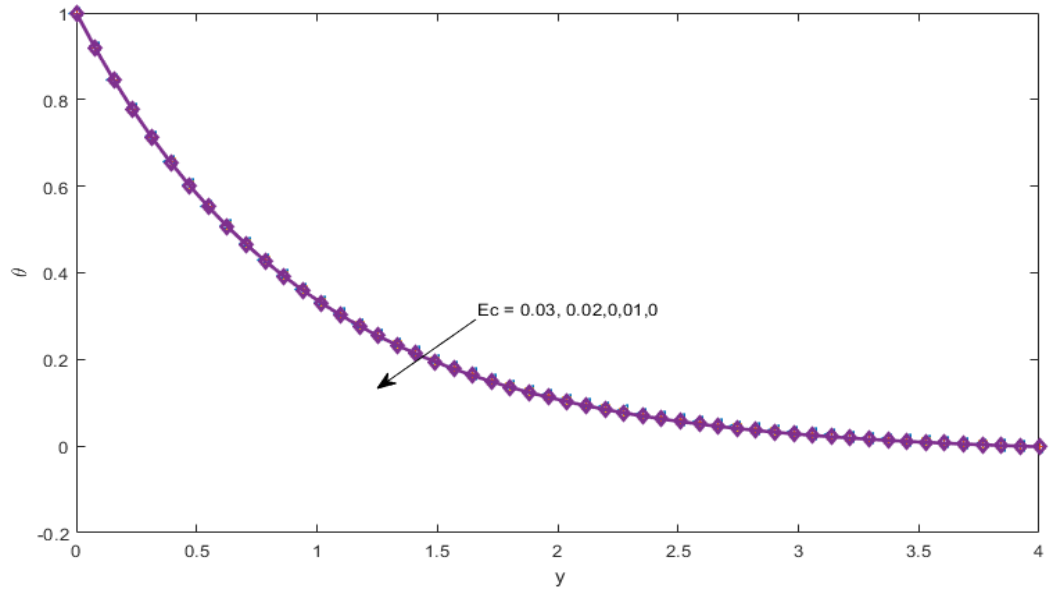

Figure 33: Effect of Eckert number on the temperature profile for fixed values of $\alpha = 0.5$, S $= 0.1$, Pr $= 1$ and M $= 1$.

As figure 35, the effect of Eckert number (Ec) on the temperature profile for different fixed values. From this figure we observe the effect of Eckert number (Ec) increases the Eckert number to enhance the temperature at a point. By physical meaning, the heat energy is stored in the field due to the frictional heating. [25]

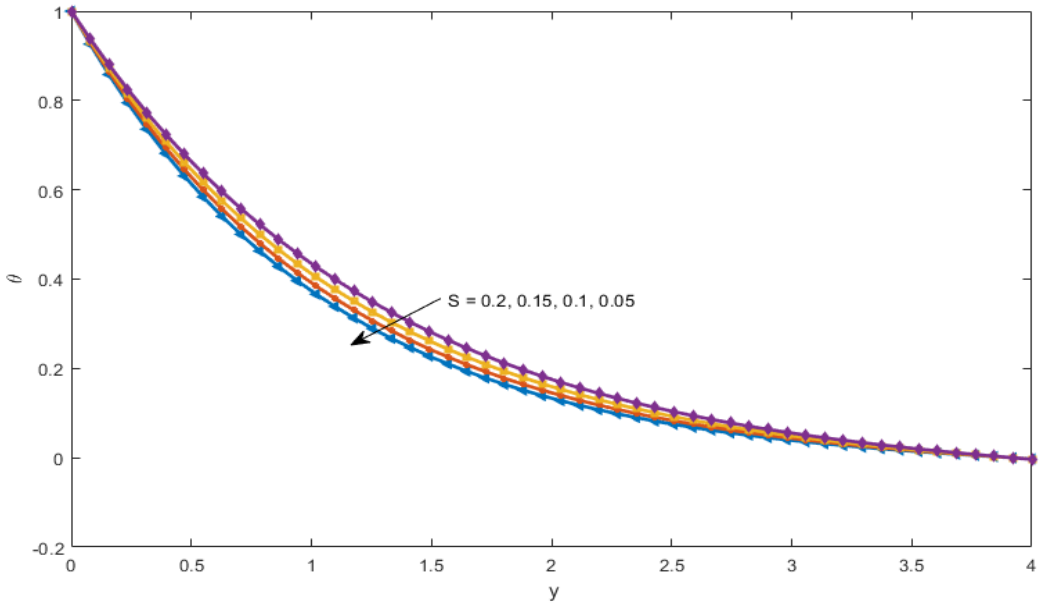

Figure 34: Effect of heat source/sink (S) parameter on the temperature profile for $\alpha = 0,\ \mathrm{Ec} = 0.01,\ \mathrm{Pr} = 1$ **and** $\mathrm{M} = 1$.

As figure 36, the effect of heat source/sink parameter for a fixed value of plate velocity α, the Eckert number, the prandtl number and the magnetic parameter. Then we observe the temperature is increase as the effect increases. This implies that, the effect of heat source/sink and the temperature are directly proportional.

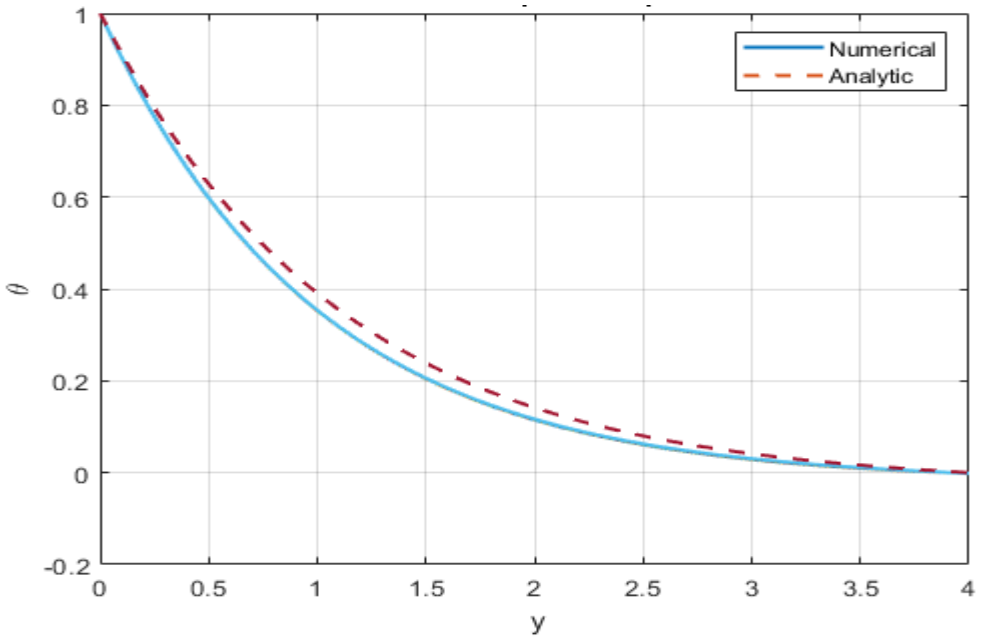

Figure 35: The Numerical and analytical solution of temperature profile

As figure 37, the numerical and the analytical solution of the temperature profile of above equation (5.20) and(5.23). From this plot we observe the numerical and that analytical solution are closed.

We have the numerical and the analytical solution so, to mesure the absolute error between the numerical and the analytical solution of the velocity profile for effect of magnetic parameter (M).

The following figures are the error analysis for two dimensions and three dimensions plots.

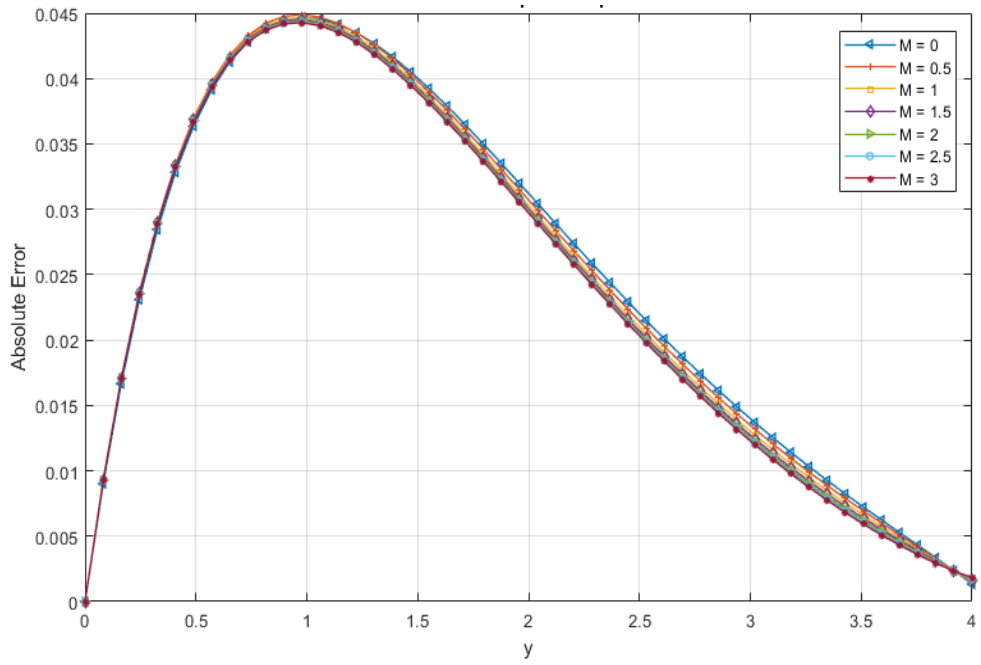

Figure 36: The absolute error of temperature profile for Effect of magnetic parameter (M) on the velocity profile for $\alpha = 0$, Ec = 0.01, Pr = 1 and S = 0.1.

From figure 38, shows the effect of magnetic parameter M on the velocity profile for the plate velocity $\alpha = 0$ and the Eckert number, Prandtl number and the source or sink values are fixed. Then we observe that the error is decreases to close to zero. That is our computation is good.

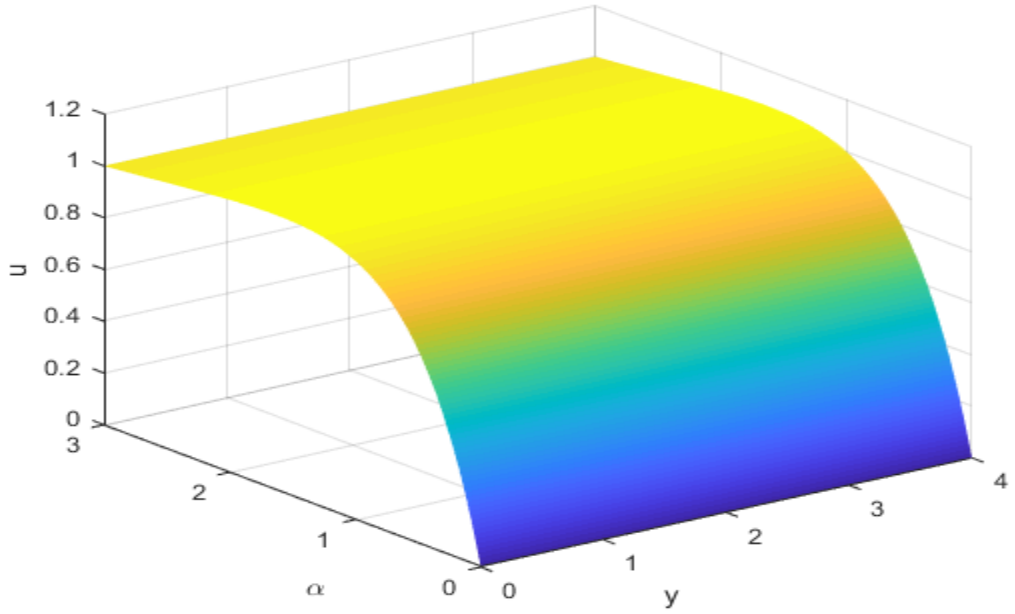

Figure 37: The 3D plot of analytic solution of velocity profile.

As figure 39, shows the effect of plate velocity α on velocity profile for a fixed values of magnetic parameter is zero, prandtl number is one and Eckert number is 0.01. From this tree dimensional figure we observe that the plate velocity is increases as also the velocity is increases.

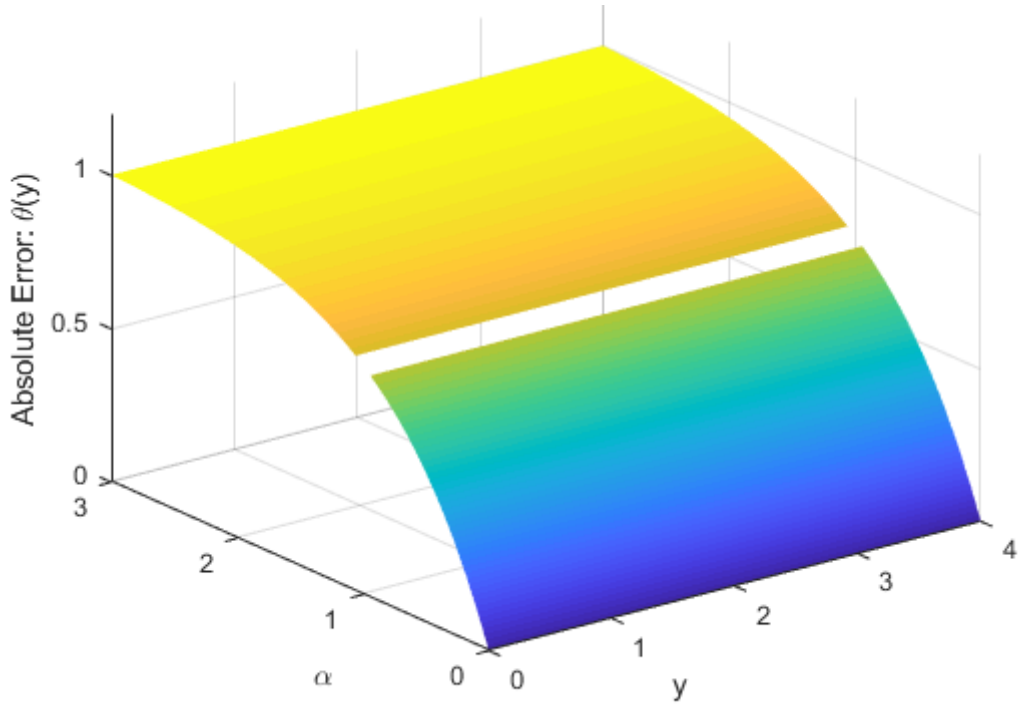

Figure 38: 3D plot of the absolute error of the numerical and analytic solution of temperature profile

From this three dimensional figure 40, the effect of the plate velocity profile α for a fixed value of the Eckert number, the Prandtl number, the heat source or sink and the magnetic parameter. We observe that the absolute error of the numerical and the analytic solution are decreases.

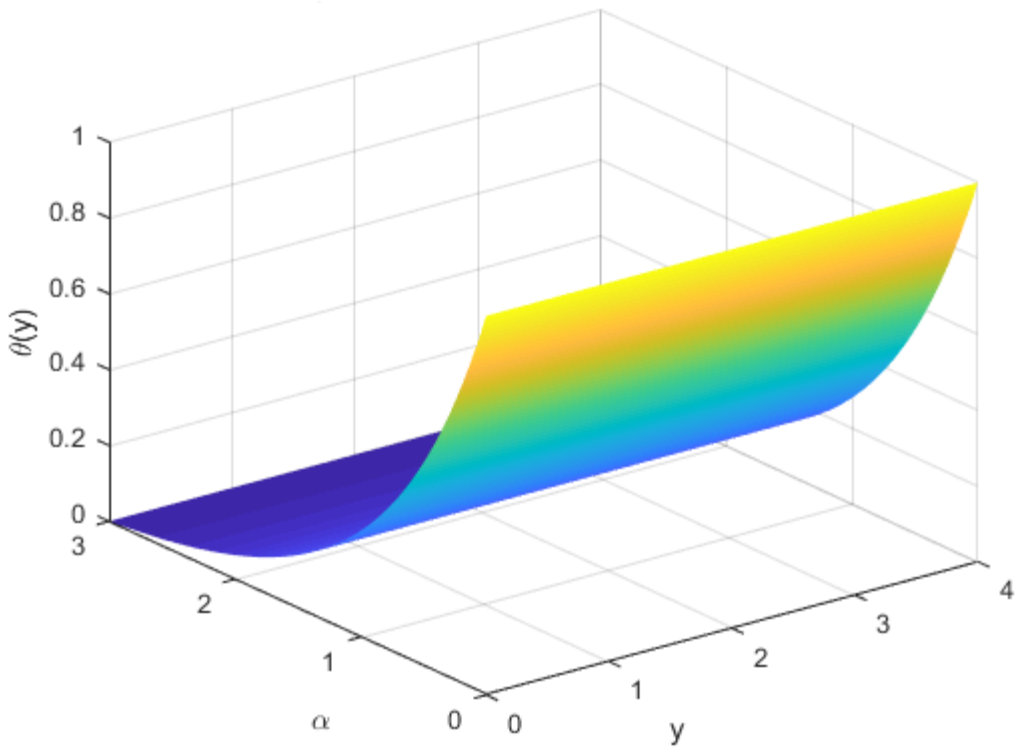

Figure 39: 3D plot for analytic solution of temperature profile

As shown figur 41, the effect of the plate velocity α for a fixed value of the Eckert number, the Prandtl number, the heat source or sink and the magnetic parameter. This plot shows the plate velocity profile decreases with in the temperature profile also increases.

As shown figur 42, the absolute errror of the effect of the plate velocity α for a fixed value of the Eckert number, the Prandtl number, the heat source or sink and the magnetic parameter. This plot shows that the absolute error is close to zero

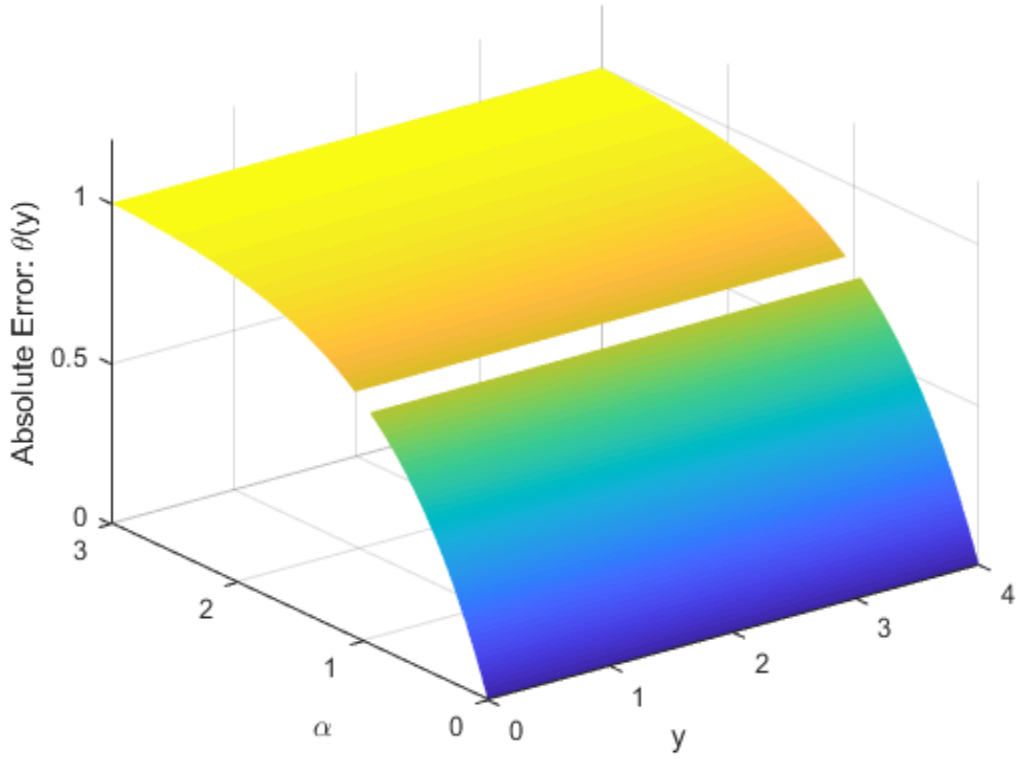

Figure 40: 3D plot for Absolute error for temperature profile

Generally, the Magnitohydrodynamic boundary layer flow and heat transfer over an infinite porous hot horizontal continuous moving plate have been mathematically modeled. Using similarity transformations, the governing ordinary differential equations are translated into ordinary differential equations. The impact of several parameters that govern the velocity and temperature profiles is graphically depicted and discussed. Parameters' effects on dimensionless velocity and temperature profiles were investigated.

Generally the major physical findings of the study are; the velocity profile in the flow region decreases as the magnetic parameters increase. As a result, we can infer that by applying a magnetic field, we can regulate the velocity field and temperature. The main velocity profiles is concave down for $0<\alpha<1$ and is concave up for $\alpha>1$. The Prandtl number has a significant impact on the boundary layer. The Prandtl number has the effect of reducing the thickness of the thermal boundary layer. The Eckert number has an important impact on the growth of the boundary layer. The heat source/sink parameter increases the thickness of the thermal boundary layer.

Chapter 7

MHD Mixed Convection Flow and Entropy Generation over an Inclined Stretching Sheet

Magnetohydrodynamic (MHD) boundary layer flow over an extending surface has imperative significance in light of its ever-expanding utilization in modern applications, for example, the creation of paper, vdish sets, link coatings, counterfeit filaments, metal turning, material shingles, manufacture of glue tapes, and metallic plates to make reference to a couple among others [53].

The flow behavior that is find the velocity profile and temperature distribution (first law investigation) in the boundary layer district was comprehend. In addition, to comprehend the vitality misfortunes during the boundary layer flow, it bodes well to play out a second law investigation. The misfortunes of vitality in the framework during the cycle are corresponding to the entropy age. Entropy creation is the proportion of irreversibility in the heat transfer issues. The investigation of entropy age inside the framework is significant as it assists with following the sources which demolish accessible energy [53]. Accordingly knowing these elements or sources one can minimize the entropy so as to hold the nature of energy [54], which is normally referred to as entropy generation minimization. At present the exploration subject of entropy generation minimization has gained unique status among researchers overall who are rethinking all energy expending, changing over and delivering frameworks and growing new methods so as to eliminate all sources that destroy the accessible work.

Regardless of the numerous investigations on the second law examination of boundary layer flows, the entropy age examination of a boundary layer flow over an inclined impermeable extending sheet under the impacts of attractive field and viscous dispersal has not been accounted for in the writing. Propelled by the previously mentioned realities, the current exploration has been embraced to play out an irreversibility investigation of MHD mixed convection flow over an inclined stretching sheet.

7.1. Mathematical Formulation

Consider the steady two dimensional boundary layer flow induced by the inclined stretching sheet having the linear velocity $u_w(x) = cx$. A magnetic field B_0 is applied normally to the stretching sheet. For boundary layer flow the continuity, momentum and energy equations take the following forms:

$$\frac{\partial u}{\partial x} + \frac{\partial \upsilon}{\partial y} = 0, \tag{6.1}$$

$$u\frac{\partial u}{\partial x} + \upsilon\frac{\partial u}{\partial y} = \nu\frac{\partial^2 u}{\partial y^2} + g\beta(T - T_\infty)Cos\alpha - \frac{\sigma B_0^2 u}{\rho}, \tag{6.2}$$

$$u\frac{\partial T}{\partial x} + \upsilon\frac{\partial T}{\partial y} = \alpha^*\frac{\partial^2 T}{\partial y^2} + \frac{\nu}{C_p}\left(\frac{\partial u}{\partial y}\right)^2 \tag{6.3}$$

In the above equation, u and υ represent velocity components in the directions of the x and y axes, T_∞ shows the free stream temperature, g denotes gravitational acceleration, α^* is the thermal diffusivity, ρ is the density of the fluid, υ is the kinematic viscosity of the fluid, B_0 depicts the imposed magnetic field, C_p represents the specific heat of the fluid at constant pressure, α is the inclination of the stretching sheet and β represents the thermal coefficient. Hear we consider the thermal expansion coefficient $\beta = mx^{-1}$ and the surface temperature of the stretching sheet of the form $T_w(x) = T_\infty + ax^2$ in order to have a self-similarity equation.

The relevant boundary conditions are:

$$u = u_w(x) = cx,\ \ \upsilon = 0,\ \ T = T_w(x) = T_\infty + ax^2 \ \text{ at } \ y = 0 \tag{6.4.a}$$

$$u \to 0,\ \ T \to 0 \ \text{ as } \ y \to \infty \tag{6.4.b}$$

In which T_w and u_w respectively represent the temperature and velocity of the stretching boundary. We look for a solution through the following transformation:

$$\eta = \sqrt{\frac{c}{\nu}}y,\ \ u = cxf',\ \ \upsilon = -\sqrt{c\nu}\,f,\ \ \theta = \frac{T - T_\infty}{T_w - T_\infty} \tag{6.5}$$

Incompressibility condition (6.1) is now automatically satisfied, whereas the other equations lead to the following expressions:

$$f'''+ ff''- f'^2+\lambda\theta Cos\alpha - M^2 f' = 0 \tag{6.6}$$

$$\frac{1}{\Pr}\theta''+ f\theta'-2f'\theta+Ecf''^2 = 0 \tag{6.7}$$

The dimensionless numbers appearing in Equations(6.6) and (6.7) are

$M = \sigma B_0^2/\rho c$ (magnetic parameter)

$\lambda = Gr/\mathrm{Re}_x^2 = g\beta(T_w - T_\infty)/u_w^2 = mga/c^2$, (thermal connective parameter)

$\Pr = \nu/\alpha^*$, (Prandtl number), $Ec = u_w^2/C_P(T_w - T_\infty) = c^2/C_P a$, (Eckert number).

While the boundary conditions, Equations (4) and (5) take the following form:

$$f(0) = 0,\ f'(0) = 1,\ \theta(0) = 1 \tag{6.8.a}$$

$$f'(\eta) \to 0,\ \theta(\eta) \to 0 \quad \text{as} \quad \eta \to \infty \tag{6.8.b}$$

The skin friction coefficient C_f and the Nusselt number Nu_x which defined as:

$$C_f = \frac{2\tau_w}{\rho u_w^2}, \tag{6.9.a}$$

$$Nu_x = \frac{xq_w}{k(T_w - T_\infty)} \tag{6.9.b}$$

Where τ_w is the shear stress and q_w is the heat flux and k is the thermal conductivity. Using variables (6.5), we obtain:

$$\mathrm{Re}_x^{1/2} C_f = f''(0),\ \ \mathrm{Re}_x^{-1/2} Nu_x = -\theta'(0) \tag{6.10}$$

Irreversibility Analysis

In the presence magnetic field, the entropy generation rate per unit volume is given by:

$$S'''_{gen} = \frac{k}{T^2}(\nabla T)^2 + \frac{\mu}{T}\Phi + \frac{1}{T}\left[(J - QV)\times(E + V\times B)\right] \tag{6.11}$$

In the above equation Φ represents the viscous dissipation function, J is the current density and $\nabla = \hat{i}\frac{\partial}{\partial x} + j\frac{\partial}{\partial y} + k\frac{\partial}{\partial z}$ is the Del operator. In the present article it is supposed that the magnitude of QV is negligible compared to the electric current density J and the electric force E has no significant effects as compared to the

magnetic force $V \times B.$ By taking these approximations and the Prandtl boundary layer approximation as well Equation (14) reduces to:

$$S_{gen}''' = \frac{k}{T^2}\left(\frac{\partial T}{\partial y}\right)^2 + \frac{\mu}{T}\left(\frac{\partial u}{\partial y}\right)^2 + \frac{1}{T}\left(\sigma B_0^2 u^2\right) \tag{6.12}$$

It is clearly seen from the above equation that there are three sources of entropy generation. The first source is the heat transfer which is due the presence of a temperature gradient in the problem, the second source is the viscous dissipation, which is due to the fluid friction, and the last source is the magnetic field which causes Joule dissipation irreversibility. The entropy generation number is the dimensionless form of volumetric entropy generation rate $\left(S_{gen}'''\right)$ and characteristic entropy generation $\left(S_0'''\right)$. Using Equation (6.5) the entropy generation given in the Equation (6.13) reduces to:

$$Ns = \frac{S_{gen}'''}{S_0'''} = \frac{\theta'^2}{\left(\theta+\Omega\right)^2} + \frac{Ec\,\mathrm{Pr}\, f''^2}{\left(\theta+\Omega\right)} + \frac{MEc\,\mathrm{Pr}\, f'^2}{\left(\theta+\Omega\right)} \tag{6.13}$$

Where $S_0''' = kc/\upsilon$ and $\Omega = T_\infty / T_w - T_\infty$ represent the characteristic entropy generation and dimensionless temperature parameter, respectively.

In many engineering problems engineers need to measure the relative importance of the source of entropy generation, and for this important measurement the Bejan number is defined as:

$$Be = \frac{\frac{k}{T^2}\left(\frac{\partial T}{\partial y}\right)^2}{\frac{\mu}{T}\left(\frac{\partial u}{\partial y}\right)^2 + \frac{1}{T}\left(\sigma B_0^2 u^2\right)} = \frac{Conductive\ \ irreversibity}{Viscous\ irreversibity + Magnetic\ irreversibity}$$

(6.14)

By using similarity variable Be takes the following form:

$$Be = \frac{\theta'^2}{\left(\theta+\Omega\right)\left(MEc\,\mathrm{Pr}\, f'^2 + Ec\,\mathrm{Pr}\, f''^2\right)} \tag{6.15}$$

7.2. Results and Discussion

In this section we present the results. As show Figure 43, the variation of temperature with different values of magnetic parameters with fixed value of several parameters. Magnetic field parameters influence on fluid temperature. It can be shown that as the value of M increases, the temperature rises. Physically, the presence of M creates a retarding force (i.e. Lorentz force) that increases fluid friction, which is what causes the temperature to rise.

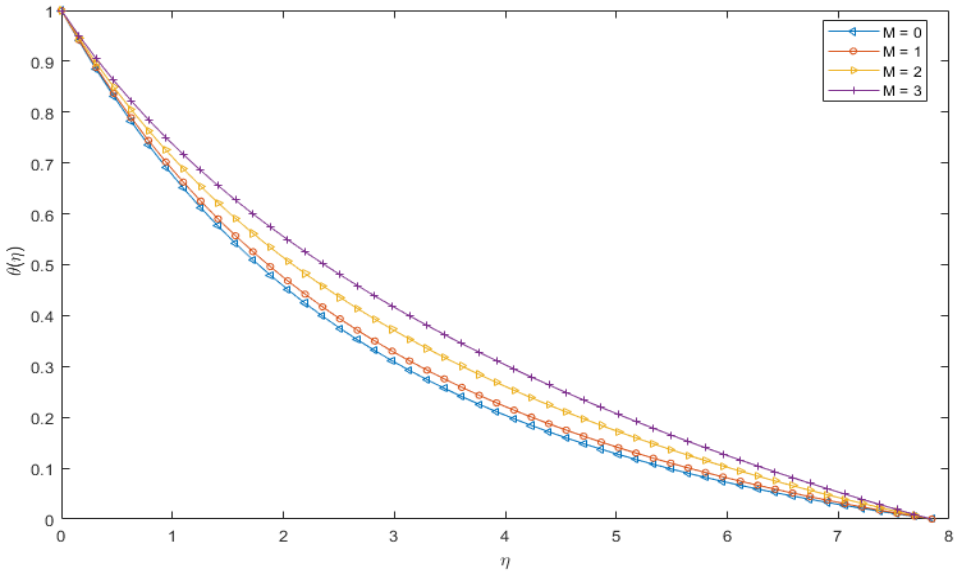

Figure 41: Variation of $\theta(\eta)$ with different value of magnetic parameter (M) and the value of the other constants are $\lambda = 1.2$, $Ec = 1$, $\alpha = \pi/4$ and $\Pr = 0.7$.

From figure 44, the plot of the variation of velocity profile with different values of magnetic parameters (M). It shows on the velocity profile, the magnetic field parameter m has an effect. It can be shown that as M is increased, the velocity decreases. This occurs because the applied transverse magnetic field produces Lorentz forces, which cause the fluid velocity to slow down.

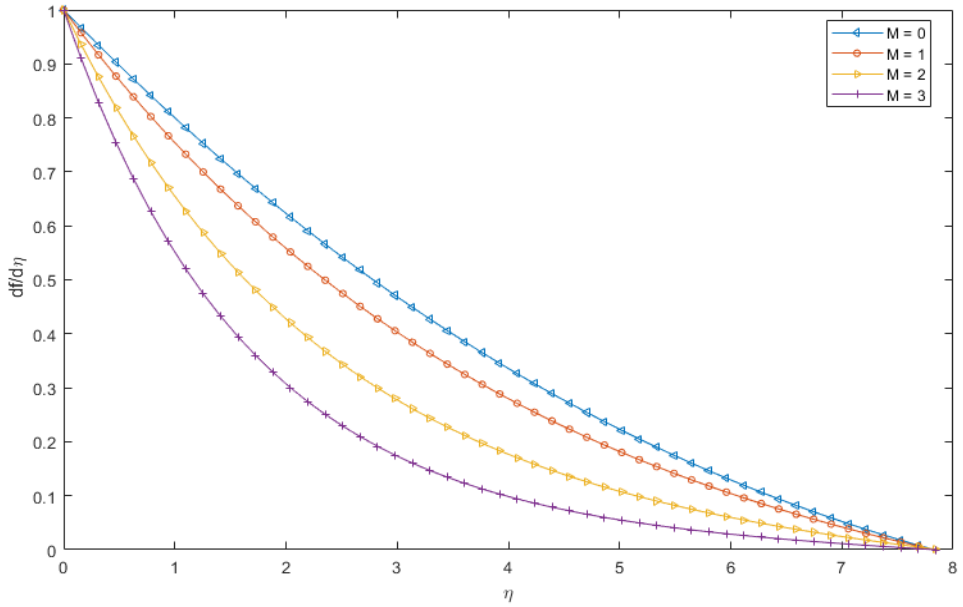

Figure 42: Variation of $f'(\eta)$ with different value of M and the value of the other constants are $\lambda = 1.2$, $Ec = 1$, $\alpha = \pi/4$ and $\Pr = 0.7$.

We summarized, the short summary of the study are; the velocity magnetic parameter M appears to have a decreasing effect on velocity, while the thermal convective parameter λ appears to have an increasing effect. As the magnetic parameter and Eckert number increase, the thickness of the thermal boundary layer increases, while the variation of the thermal convective parameter and Prandtl number has a decreasing effect. Increasing the magnetic parameter and Eckert number, increases entropy generation, while increasing the thermal convective parameter and dimensionless temperature function decreases entropy generation.

Chapter 8
Summary, Conclusion and Further Research

This chapter presents the summary, conclusion of the thesis and recommendations for further research.

8.1. Summary

The main objective of this thesis is a dynamical and numerical study of non-linear dynamics system of coupled boundary value problems for fluid mechanics and heat transfer. Our approach fully shooting-secant method is chosen for finding the numerical solutions of nonlinear dynamical coupled boundary value problems subject to specified boundary conditions. And using an eigenvalue and phase plane analysis was used for dynamical analysis of a heat transfer equations.

The thesis result, the numerical solutions and dynamical analysis of a heat transfer Equations, the analysis is improved upon and also the behavior, particularly the tip of the fin, more meticulously investigated and documented. This dynamical analysis also functions as a method of investigating the effect of the thermo-geometric parameter.

To investigated the numerical solution of boundary layer viscous flow over a wage by Falkner-Skan equations. The numerical solutions of boundary layer viscous flow over a wage by Falkner-Skan equation subject to specified initial and boundary conditions. The Runge-Kutta fourth order method used for the initial values problems arise during shooting. Finally, this thesis is successfully computing several cases of the Falkner-Skan equation. And also this problem was solved for compared with nanofluid and Newtonian fluid. Moreover the problem of required convection boundary layer flow close the stagnation point on a porous stretching/shrinking surface in a nanofluid is considered in theory.

On the other hand our aim was to find the numerical solution for the effect of velocity slip problems. Shooting-secant method is implemented to determine numerically the velocity slip parameter on boundary layer fallow with Falkner-Skan equation. Finally, which shows the increase of the slip parameter with the velocity increases, the numerical results of the ordinary differential equation are obtained.

In addition, we aimed to study to investigate the numerical solutions of MHD viscous problems. To find the numerical solutions of MHD viscous flow over a shrinking sheet we observed the different parameters effects are visible. Such as the Prandtl number has a significant impact on the boundary layer. The Prandtl number has the effect of reducing the thickness of the thermal boundary layer. The Eckert number has an important impact on the growth of the boundary layer. The heat source/sink parameter increases the thickness of the thermal boundary layer. Based on this we draw the following conclusion.

8.2. Conclusion

This thesis is a dynamical and numerical study of non-linear dynamics system of coupled boundary value problems for fluid mechanics and heat transfer. In this study, a simple and a powerful approximate method of a solution the Shooting-secant method is used for all the above mentioned seven problems and also used for chapter 2 a dynamical analysis.

In chapter 2, we investigated the solution of the energy balance for a longitudinal fin is given by an ordinary differential equation numerically by using fully shooting-secant method. We observed the solution of the numerical solution was accurate and generates numerical solutions that are stable and physically reasonable. In addition, the dynamics of the steady state of the equation with respect to the parameters was investigated with the use of phase plane analysis. During this work, the analysis in is improved upon and also the behavior, particularly the tip of the fin, more accurately investigated and documented. This dynamical analysis also functions as a method of investigating the effect of the thermo-geometric parameter.

We were studied, in chapter 3, a numerical solution of the Falkner-Skan boundary layer viscous flow over a wedge. First we were defining the Falkner-Skan equation, originally derived. Falkner and Skan (1931), is of central importance to the fluid mechanics of wall-bounded viscous flows. It is derived from the two-dimensional incompressible Navier-Stokes equations for a one-sided bounded flow using a similarity analysis and its solution describes the form of an external laminar boundary layer in the presence of an adverse or favorable stream wise pressure gradient. Although the apparent simplicity of the Falkner- Skan equation (a one-

dimensional ordinary differential equation) solving it accurately can be fraught with difficulty; these problems mainly stem from its non-linearity and third-degree order. The boundary layer theory unmistakably explains the consistent state flow more than a level plate at zero event point which is perceived as Blasius flow.

Then we found a numerical solution of the Falkner-Skan boundary layer viscous flow over a wedge was investigated including a nonslip and slip boundary condition. This problem was solved for compared with nanofluid and Newtonian fluid. Moreover the problem of required convection boundary layer flow close the stagnation point on a porous stretching/shrinking surface in a nanofluid is considered in theory.

In chapter 4, the effect of velocity slip parameter on boundary layer flow over a static wedge. The problem of the Falkner-Skan boundary layer flow past a wedge considering the velocity slips condition. For this work we compared the result with the previous work Yacob's and Muatazz Abdolhadi Bashir papers. We observed the solution of the numerical solution was accurate. We found the effect of the velocity slip for an ordinary differential equation on the Falkner-Skan boundary layer flow past a wedge has transformed. And also we observed when the slip parameter is increase the velocity also increase.

In Chapter 5, the magnetohydrodynamics viscous flow over a shrinking sheet for a closed form exact solution. The flow of magnetohaydrodynamics(MHD) over a shrinking sheet often varies significantly from the flow of MHD over a stretching sheet for Newtonian and non-Newtonian fluids. The we observed The opposite value sign of the exact solution occurs only for mass suction, which implies that, s is positive. And also as the mass suction parameter increases, the wall shear stress for M= 1 increases. There is only one solution for M > 1, say, the positive sign branch, but there is a solution for both mass suction and mass injection $-\infty < s < \infty$, that also shows that with the mass suction parameter, the wall shear stress increases.

In chapter 6, we concerned the two-dimensional magnitohydrodynamics(MHD) of the numerical and analytic solution boundary layer flow and heat transfer along an infinity porous hot horizontal continuous moving plate. The impact of several parameters that govern the velocity and temperature profiles is graphically depicted and discussed. From this work, we observed the major physical findings of the study are; the velocity profile in the flow region decreases as the magnetic parameters increase. As a result,

we can infer that by applying a magnetic field, we can regulate the velocity field and temperature. The main velocity profiles are concave down for $0<\alpha<1$ and are concave up for $\alpha>1$. The Prandtl number has a significant impact on the boundary layer. The Prandtl number has the effect of reducing the thickness of the thermal boundary layer. The Eckert number has an important impact on the growth of the boundary layer. The heat source/sink parameter increases the thickness of the thermal boundary layer.

Finally in chapter 7, magnitohydrodynamics(MHD) convectional flow and entropy generation over an inclined stretching sheet. We observed the velocity magnetic parameter M appears to have a decreasing effect on velocity, while the thermal convective parameter λ appears to have an increasing effect. As the magnetic parameter and Eckert number increase, the thickness of the thermal boundary layer increases, while the variation of the thermal convective parameter and Prandtl number has a decreasing effect. Increasing the magnetic parameter and Eckert number, increases entropy generation, while increasing the thermal convective parameter and dimensionless temperature function decreases entropy generation.

To conclude the highlights of this study, we observed Shooting-secant method is the powerful approximate method for a numerical study of non-linear dynamics system of coupled boundary value problems for mechanics. And also observed very small number difference of one of the parameters affects the systems.

8.3. Further Research

Within this section, we shall state the future areas of research in bullet point form. For boundary value problems of Non-linear dynamics system for application of mechanics, study another method such as:

- ✓ The finite element and Galerkin methods: boundary conditions for nonlinear boundary value problems included for future studies and research.
- ✓ For further study including least square, Rayleigh Ritz, moment weighted residual methods

Reference

[1] D. G. Zill and M. R. Cullen, Differntial Equations with Boundary-Value Problems, Seventh ed., 2009.

[2] W. E. Boyce, R. C. DiPrima and D. B. & Meade, Elementary Differential Equations and Boundary Value problems, Tenth ed., John Wiley & Sons, 2012.

[3] K. Gersten, Boundary-Layer Theory, Berlin: Springer, 2017.

[4] H. Schliching and K. Gersten, Boundary Layer Theory, Ninth Edition ed., vol. 121, New York, 2017.

[5] J. Schetz, Boundary Layer Analysis, Prentice Hall, 2011.

[6] F. M. White, Fluid Mechanics, McGraw-Hill, 2004.

[7] F. M. White and I. Corfield, Viscous Fluid Flow, vol. 3, New York: McGraw-Hill, 2006.

[8] G. Bar-Meir, Basics of Fluid Mechanics, Chicago: Open Textbook Library, 2006.

[9] K. Hutter and Y. Wang, Fluid and Thermodynamics, Switzerland: Springer, 2016.

[10] S. H. Strogatz, Nonlinear dynamics and chaos with student solutions manual: With applications to physics, biology, chemistry, and engineering, CRC Press, 2018.

[11] O. J. Fenuga, I. O. Abiala and S. O. Salawu, "Analysis of Thermal Boundary Layer Flow over a Vertical Plate with Electrical Conductivity and Convective Surface Boundary Conditions," *Physical Science International Journal,* vol. 17(2), pp. 1-9, 2018.

[12] O. O. Onyejekwe, *Nonlinear Ordinary Differntial Equations: Handout,* Addis Ababa, 2020.

[13] R. Bellman and K. Cooke, Differential-Difference Equations, New York & London: Academic Press, 1963.

[14] E. B. William and C. D. Richard, Elementary Differential Equations and Boundary Value Problems, Tenth ed., United States of America: John Wiley & Sons, Inc, 2012.

[15] O. O. Onyejekwe, *Qualitative Anaalysis: Handout*, Addis Ababa, 2020.

[16] Prof. Okey Oseloka Onyejekwe, *Non Linear Dynamics and Chaos Lecture Note*, Addis Ababa, 2017.

[17] Complex Systems, Introduction to the Modeling and Analysis of Complex Systems, New York: Open SUNY Textbooks, 2015.

[18] O. O. Onyejekwe, *Dynamical System: PPT*, Addis Ababa, 2020.

[19] M.A.J. Chaplin and A.M. Stuart, "A Mathematical Model for the Diffusion of Tumour Angiogenesis Factor in to the Surrounding Host Tissue," *Mathematical Medicine and Biology*, Vols. 8, No. 3, pp. 191 - 220, 1991.

[20] O. O. Onyejekwe, *Ordinary Differential Equation: PPT*, Addis Ababa, 2019.

[21] O. O. Onyejekwe, *Systems of Equation: Handout*, Addis Ababa, 2019.

[22] C. Harley, "Asymptotic and Dynamical Analyses of Heat Transfer through a Rectangular Longitudinal Fin," *Applied Mathematics*, 2013.

[23] A. B. Muatazz, M. Mustafa and A. Ilyani, "Velocity Slip Effect on Falkner-Skan Boundary Layer Flow over a Static Wedge," *Adv. studies theor. phys*, vol. 7(6), pp. 277 - 286, 2013.

[24] T. Fang and J. Zhang, "Closed-form exact solutions of MHD viscous flow over a shrinking sheet," *Communication in Nonlinear Science and Numerical Simulations*, vol. 14(7), pp. 2853-2857, 2009.

[25] A. K. Jhankal, "MHD boundary layer flow and heat transfer along an infinite porous hot horizontal continuous moving plate," *Indian Journal of Chemical Technology (IJCT)*, vol. 25(1), pp. 106-110, 2018.

[26] M. M. Keshtkar and M. Ezatabadi, "Numerical Solution for the Falkner-Skan

Boundary Layer Viscous Flow over a Wedge," *International Journal of Engineering And Science*, vol. 3(10), pp. 18-36, 2013.

[27] MathsWorks, "htt://www.mathworks.com/matlabcentral/fileexchange/65887-pplane9.," ODE software for MATLAB, Augest 2017. [Online].

[28] J. D. Hoffman, Numerical Methods for Engineers and Scientists, second Edition ed., NEWYORK: Marcel Dekker, 2001.

[29] O. O. Onyejekwe, *The Shooting Methods for the Solution of One-Dimensional BVPs*, 2020.

[30] W. John, *Mathematical Method: General Boundary Value Problems (BVPs)*, Aug, 2003.

[31] K. Atkinson, W. Han and D. Stewart, Numerical Solution of Ordinary Differential Equations, Canada: John Wiley & Sons, 2009.

[32] A. D. Kraus, A. Aziz, J. Welty and D. P. Sekulic, "Extended Surface Heat Transfer," *Appl. Mech. Rev.*, vol. 54(5), pp. B92-B92, 2001.

[33] A. Aziz and T.Y.Na, "Periodic heat transfer in fins with variable thermal parameters," *International Journal of Heat and Mass Transfer*, vol. 24(8), pp. 1397-1404, 1981.

[34] O. O. Onyejekwe, G. Tamiru, T. Amha, F. Habtamu, Y. Demiss, N. Alemseged and B. Mengistu, "Application of an Integral Numerical Technique for a Temperature-Dependent Thermal Conductivity Fin with Internal Heat Generation," *Journal of Engineering Physics and Thermophysics*, vol. 93(6), pp. 1574-1582, 2020.

[35] M. Didwania, G. Krishan and Ravikant, "Study and Analysis of Heat Transfer through Two Different Shape Fins Using CFD Tols," *Intrernational Journal of It, Engineering and Applied Sciences Research (IJIEASR)*, vol. volume 2, pp. 2319-4413, April 2013.

[36] O. O. Onyejekwe, *The Shooting method for the Solution of One-Dimensional BVPs; Handout*, Addis Ababa, 2020.

[37] G. Sobamowo, "Thermal analysis of longitudinal fin with temperarure-dependent properties and internal heat generation using Galerkin's method of weighted residual," *Applied Thermal Engineering,* vol. 99, pp. 1316-1330, 2016.

[38] R. J. Moitsheki and C. Harley, "Transient heat transfer in longitudinal fin of various profiles with temperature-dependent thermal conductivity and heat transfer coefficient," *Pramana:Journal of Physics,* vol. 77(3), pp. 519-532, 2011.

[39] C. Duque-Daza, D. Lockerby and C. Galeano, "Numerical Solution of Falkner-Skan Equation using Third-order and Higher -Order-compact Finite Difference Schemes," *Journal of the Brazilian Society of Mechanical Sciences and Engineering,* vol. 33(4), pp. 381-392, 2011.

[40] S. U. Choi and J. A. Eastman, "Enhancing thermal conductivity of fluids with nanoparticles," in *No. ANL/MSD/CP-84938; CONF-951135-29,* Argonne National Lab., IL ,United States, 1995.

[41] T. Cebeci and J. Cousteix, Modeling and Computation of Boundary-Layer Flows, Second Revised and Extended Edition ed., California: Horizons Publishing INc.. Long Beach, 2005.

[42] V. Falkner and S. Skan, "Some approximate solutions of the boundary layer equations," *The London, Edinburgh, and Dublin Philosophical Magazine and Journal of Science,* vol. 12(80), pp. 865-896, 1931.

[43] P. Summiya, "Numerical solution of the Falkner Skan Equation by using shooting techniques," *IOSR Journal of Mathematics,* vol. 10(6), pp. 78-83, 2014.

[44] B. Ganapol, "Highly Accurate Solution of the Blasius and Falkner-Skan Boundary Layer Equations via Convergence Acceleration," *arXiv preprint arXiv:1006.3888.,* 2010.

[45] M. S. Abel, P. S. Datti and N. Mahesha, "Flow and Heat Transfer in Power-Law Fluid over a Stretching Sheet with Variable Thermal Conductivity and Non-uniform Heat Source, International Journal of Heat and Mass Transfer," *International Journal of Heat and Mass Transfer,* Vols. 2(11-12), pp. 2902-2913, 2009.

[46] N. A. Yacob, A. Ishak and I. & Pop, "Falkner- Skan Problem for a Static or Moving Wedge in Nanofluids," *International Journal of Thermal Sciences,* vol. 50(2), pp. 133-139, 2011.

[47] T. Altan, S. I. Oh and G. Gegel, "Metal forming fundamentals and applications. Metals Park," *American Society of Metals*, p. 353, 1983.

[48] T. Fang, "Boundary layer flow over a shrinking sheet with power-law velocity.," *International Journal of Heat and Mass Transfer*, Vols. 51(25-26), pp. 5838-5843, 2008.

[49] M. Sajid, T. Javed and T. Hayat, "MHD rotating flow of a viscous fluid over a shrinking surface. Non-linear Dyn," *Nonlinear dynamics,* vol. 51(1), pp. 259-265, 2008.

[50] M. Miklavčič and C. Wang, "Viscous flow due to a shrinking shee," *Quarterly of Applied Mathematics,* vol. 64(2), pp. 283-290, 2006.

[51] S. Liao, "On the analytic solution of magnetohydrodynamic flows of non-Newtonian fluids over a stretching sheet," *Journal of Fluid Mechanics,* vol. 488, p. 189, 2003.

[52] O. O. Onyejekwe, Y. D. Belete and N. A. worku, "Numerical Calculations for a Boundary Layer Flow past a Moving Vertical Porous Plate with Suction/Injection and Thermal Radistion," *Applied Mathematics,* vol. 11, pp. 172-183, 2020.

[53] M. I. Afridi, M. Qasim, I. Khan, S. Shafie and S. A. Ali, "Entropy Generation in Magnetohydrodynamic Mixed Convection Flow over an Inclined Stretching Sheet," *Entropy*, vol. 19(1), p. 10, 2017.

[54] G. Webb, Magnetohydrodynamics and Fluid Dynamics: Action Principles and Conservation Laws, Springer International , 2018.

Appendix: Publications

1. **ዮሐንስ ደምስ በለጠ፡** “የባሕረ ሐሳብ ትምህርት ለዘመን አቆጣጠር፤ ለከዋክብት እና ለአየር ትንበያ ጥናት መጽሐፈ ሄኖክ መነሻ”፡ *Journal of Ethiopia church studies*: A.A ፡ ኤ.ቤ.ጥ.መ፣ ቁ.፮ (ነሐሴ ፳፻፲)
2. Okey Oseloka Onyejekwe, **Yohannes Demiss** and Nahom Alemseged Worku: “Numerical Calculations for a boundary Layer Flow past a Moving Vertical Porous Plate with Suction/Injection and Thermal Raiation”: *Applied Mathematics*, 2020, 11, 172-183.

3. Okey Oseloka Onyejekwe, Beruk Minale, Fikru Habtamu, Tesfaye Amha, Genet Tamiru, Betlhem Mengistu, **Yohannes Demiss** and Nahom Alemseged Worku: “ Numerical Discrete-Domain Integral Formulations for Generalized Burger-Fisher Equations”, *Applied Mathematics*, 2020, 11, 137-145

4. O. O. Onyejekwe, G. Tamiru, T, Amha, F. Habtamu, **Y. Demiss** ,A. Worku and B. Mengistu: “APPLICATION OF INTEGRAL NUMERICAL TECHNIQUE FOE A TEMPERATURE-DEPENDENT THERMAL CONDUCTIVITY FIN WITH INTERNAL HEAT GENERATION.” *Journal of Engineering physics and Thermophysics*, Vol 93, N0 6, November, 2020.